

THE DOWNWARD CONTINUATION TO THE EARTH'S SURFACE OF TRUNCATED
SPHERICAL AND ELLIPSOIDAL HARMONIC SERIES OF THE GRAVITY AND
HEIGHT ANOMALIES

Christopher Jekeli

The Ohio State University
Research Foundation
1958 Neil Avenue
Columbus, Ohio 43210

December, 1981

Scientific Report No. 11

Approved for public release; distribution unlimited

AIR FORCE GEOPHYSICS LABORATORY
AIR FORCE SYSTEMS COMMAND
UNITED STATES AIR FORCE
HANSCOM AFB, MASSACHUSETTS 01731

Foreword

This report was prepared by Christopher Jekeli, Graduate Research Associate, Department of Geodetic Science & Surveying, The Ohio State University, under Air Force Contract No. F19628-79-C-0027, The Ohio State University Research Foundation Project No. 711664, Project Supervisor Richard H. Rapp. The contract covering this research is administered by the Air Force Geophysics Laboratory, Hanscom Air Force Base, Massachusetts, with Mr. George Hadgigeorge, Contract Monitor.

ACKNOWLEDGEMENTS

In the first place, my utmost gratitude and appreciation goes to my adviser and mentor, Dr. Richard H. Rapp, for his enthusiastic involvement and continual expert guidance during the course of this work and throughout my five years at the Department of Geodetic Science. Also, I was very fortunate to have at my ready disposal any of his data sets, as well as his and Dr. Ivan I. Mueller's vast personal libraries; for this I am indeed thankful.

To the entire faculty, staff, and students, past and present, I am indebted for providing a congenial and friendly atmosphere in which I could pursue my studies and which made my graduate years particularly pleasant and memorable. I would especially like to thank my fellow Ph.D. candidates and friends Kostas Katsambalos, Erricos Pavlis, John Hannah, Lenny Krieg, and Yehuda Bock in this respect, who, while occupied with their own dissertations, were always ready to listen to my problems and offer helpful advice.

The clarifications on certain mathematical aspects by Professors John T. Scheick and Stefan Drobot of The Ohio State University Mathematics Department and Dr. M.S. Petrovskaya of the Institute for Theoretical Astronomy, Leningrad, were also greatly appreciated.

In addition to Dr. Rapp, Drs. D. P. Hajela and P. Nevai deserve special thanks for serving on the reading committee and providing many constructive comments.

Finally, I wish to thank Susan L. Carroll for the excellent typing of the mostly difficult equations.

More than three-fourths of the required computer time was generously provided by the Instruction and Research Computer Center of The Ohio State University.

TABLE OF CONTENTS

	page
Abstract	ii
Foreword	iii
LIST OF TABLES	vii
LIST OF FIGURES	ix
1. Introduction	1
1.1 The Problem and Background	2
1.2 Other Problems and Methods of Downward Continuation.	9
1.3 Preliminaries and Definitions	12
2. The Downward Continuation of Spherical Harmonic Series	18
2.1 Simple Mass Distributions	19
2.2 The Volumetric Density Model	30
2.2.1 The Derivation of the Error Series	30
2.2.2 The Interpretation of the Error Series	43
2.2.3 The Description of the Earth Model	47
2.2.4 The Numerical Analysis	51
2.3 The Density Layer Model	55
2.3.1 The Derivation of the Error Series	55
2.3.2 The Description of the Model	65
2.3.3 The Equations for the Numerical Analysis	69
2.3.4 The Numerical Results of the Error Analysis	79
3. The Ellipsoidal Harmonic Series.	92
3.1 The Transformation from Spherical to Ellipsoidal Harmonic Coefficients.	96
3.2 The Ellipsoidal Series of the Gravity and Height Anomalies	106
3.3 The Derivation of the Error Series	107
3.4 The Results of the Numerical Analysis	113

	Page
4. Corrections to the Spherical Approximation	118
5. Summary, Conclusion, Recommendation	126
LIST OF REFERENCES	130

APPENDIXES

A. Divergence and Convergence Conjectures. . . .	136
B. Series Expansions for the Serrated Ellipsoid. .	138

LIST OF TABLES

Table	Page
1: The Region of the surface model in which the downward continuation errors are computed	80
2: Accuracy of series (2.152) (without the linear term), series (2.153) (without the quadratic term), and series (2.148) versus the number of included terms.	83
3: RMS downward continuation error of spherical harmonic series of gravity anomaly and RMS gravity anomaly evaluated (first 300 terms) at the points of Table 1 and at the indicated subregions. Maximum absolute values for each region and sub-region are given parenthetically.	86
4: RMS downward continuation error of spherical harmonic series of height anomaly and RMS height anomaly evaluated (first 300 terms) at the points of Table 1 and at the indicated subregions. Maximum absolute values for each region and sub-region are given parenthetically.	87
5: RMS downward continuation error of gravity anomaly and height anomaly spherical harmonic series in steps of 30 degrees: n=30,60,....,300, based on those points of Table 1 for which t=100 m.	88
6: RMS downward continuation error of spherical harmonic series of mean gravity anomaly and RMS mean gravity anomaly evaluated (first 300 terms) at the points of Table 1 and at the indicated subregions. Maximum absolute values for each region and subregion are given parenthetically.	90

- 7: RMS downward continuation error of spherical harmonic series of mean height anomaly and RMS mean height anomaly evaluated (first 300 terms) at the points of Table 1 and at the indicated subregions. Maximum absolute values for each region and subregion are given parenthetically. 91
- 8: RMS downward continuation error of ellipsoidal harmonic series of gravity anomaly in regions of Table 1 (latitude ranges refer to reduced latitude) at points on the ellipsoid $u = 6356800$ m ($R = 521854.4492$ m) and above the surface model no more than 100 m. Maximum absolute values for each region are given parenthetically. 116

LIST OF FIGURES

Figure	Page
1: Bounding sphere versus bounding ellipsoid	8
2: Equatorial disk density distribution	20
3: Serrated homogeneous ellipsoid density distribution	25
4: Partial sums of spherical harmonic series of Δg , T for equatorial disk and serrated ellipsoid density distributions (Figures 2 and 3) minus corresponding true values evaluated at $r_p=6377200$ m, $\theta_p=77^\circ 5$	28
5: Partial sums of spherical harmonic series of Δg , T for equatorial disk and serrated ellipsoid density distributions (Figures 2 and 3) minus corresponding true values evaluated at $r_p=6357200$ m, $\theta_p=7^\circ 5$	29
6: Differences between partial sums of inner and outer spherical harmonic series of Δg , T for equatorial disk and serrated ellipsoid density distributions evaluated at $r_p=6377200$ m, $\theta_p=77^\circ 5$	31
7: Differences between partial sums of inner and outer spherical harmonic series of Δg , T for equatorial disk and serrated ellipsoid density distributions evaluated at $r_p=6357200$ m, $\theta_p=7^\circ 5$	32
8: Partial sums of spherical harmonic series of Δg derived from 180 degree field plus random harmonic coefficients to degree 1500, and evaluated at $\theta_p=\lambda_p=10^\circ$, $r_p=6356, 6372, 6388,$ 6404 km; the surface of convergence is a sphere of radius 6378 km	33
9: Sphere of computation versus bounding sphere.	35
10: The volumetric density model (density values are in units of g/cm^3).	48

11: Topographical profile of southern Africa ($\theta_p = 102^\circ 5'$, $-12^\circ 5' \leq \lambda \leq 90^\circ 0'$) and values of partial sums of downward continuation error in gravity anomaly (volumetric density model): $\bar{n} = 16, 36, 180$.	52
12: Partial sums of downward continuation error in Δg (volumetric density model) for points 1 and 4 of Figure 11 and $0 \leq \bar{n} \leq 180$.	53
13: Degree variances of equivalent rock topography used to define model of earth's surface.	70
14: Comparison of Topographical profiles $\phi = 22^\circ 5'$, $0^\circ \leq \lambda \leq 90^\circ$, based on 5° , 1° , and 0.6 mean elevations and geoid undulations (0.6 mean elevations/undulations include random harmonics for $101 \leq n \leq 300$).	71
15: Subregions over which RMS downward continuation errors are computed.	81
16: Degree variances of gravity anomaly on bounding sphere.	84
17: Schematic illustration of the points contributing to the computed RMS downward continuation error.	93
18: Ellipsoidal coordinates (u, δ, λ) versus spherical coordinates (r, θ, λ) of the point P.	93
19: Partial sums of ellipsoidal harmonic series of Δg for equatorial disk and serrated ellipsoid density distributions (Figures 2 and 3) minus corresponding true values evaluated at $r_p = 6357200$, $\theta_p = 7^\circ 5'$.	114
20: The deflection of the vertical.	121
21: The normal directional derivative.	121

1. Introduction

Recent years have seen a quantum jump in the continuing efforts to improve and expand our knowledge of the earth's gravity field. It is marked by the transition from terrestrial measurements, limited essentially to land areas, to measurements in outer space which are used to ascertain the global gravity field. The foremost instrument advancing this effort has been the satellite borne altimeter, enabling a direct measurement of an equipotential surface, the geoid, over much of the oceanic surface of the earth. Further strides will undoubtedly be made by the planned GRAVSAT mission (see the report by the National Research Council, 1979) utilizing the measurements of satellite-to-satellite tracking and achieving coverage over the entire globe. Looking ahead into the not so distant future, satellite borne gradiometers will provide even greater detail and accuracy. While the obvious advantage of measuring the earth's gravity field at satellite altitudes is global accessibility within a relatively short period of time, the fundamental difficulty is the translation or "downward continuation" of the data to the earth's surface where they are most needed. In principle, several procedures to achieve this translation exist; all rely to some extent on a simplifying assumption such as a perfectly spherical, or a flat, earth. On account of the enormous amount of data that satellite missions provide, the number of methods to simultaneously process the entire data set is reduced considerably. The method of harmonic analysis of the gravitational potential will come under close examination in this paper. Its feasibility from the computational standpoint cannot be easily challenged, even for extremely dense data coverage. However, far from being a panacea, it is also associated with several problems. Aside from an instability in the propagation of noise, the most nagging question is one of correct theory. It is the latter which will be studied here, not by delving into areas of pure theory, but rather on a numerical basis, which, it is felt, will provide some value to the scientist who must eventually make use of the data.

1.1 The Problem and Background

From classical potential theory, we know that the (Newtonian) potential due to attracting masses is an harmonic function in free space. That is, its second derivatives are continuous and it satisfies Laplace's equation; moreover, it is regular at infinity (Günter, 1967, p.25). Kellogg (1953, p.220) shows that an harmonic function is also analytic in its region of harmonicity (cf. Cauchy Riemann equations in the theory of complex variables). The solution to the exterior Dirichlet boundary value problem states that given values of the potential everywhere on a known surface enclosing the masses it is determined uniquely in the space exterior to that surface. Applied to earth orbiting satellites, the known surface is the sphere that contains the satellite orbits. Because the potential is also analytic in the region between the earth's surface and the orbital sphere (we remove the atmosphere, see below), by the uniqueness of analytic continuation, the potential function outside the orbital sphere represents the potential in the entire region above the earth's surface, i.e. in the largest region wherein the actual potential is analytic.

For an irregular density distribution such as the earth's, a closed form of the potential in space cannot be found. Instead, it is often represented as a series, in one form or another; however, any series is associated with a particular region of convergence and cannot converge to the true potential in the total space. Since we are dealing with exterior potentials, the region of convergence is an exterior region that contains the point of infinity, and it is separated from the region of divergence (the interior region) by the so-called surface of convergence. In general, the region of convergence may, or may not, contain the maximum region of analyticity of the potential, nor is the surface of convergence necessarily a sphere. These facts were convincingly demonstrated by Krarup (1969) and Moritz (1978); see below. In many cases, it is possible to derive a series which converges to the potential in the region where the outer series diverges; we call this the inner series.

Owing to the near spherical shape of the terrestrial body, the most familiar series is the spherical harmonic series. Kellogg (1953, p.143) showed that the spherical harmonic series converges uniformly to the potential outside any sphere containing all the attracting masses and centered at the origin of the coordinate system. Strictly, this theorem finds no application in our physical world since it guarantees convergence only outside the sphere enclosing the

entire universe. Within our limited scope of terrestrial and near-earth applications, however, the masses outside our solar system have negligible gravitational effect. Moreover, we may simply redefine the exterior gravitational field of the earth with appropriate corrections so as to exclude the effects of an atmosphere and, say, of the sun and the moon. The latter and possibly other extra-terrestrial bodies are mathematically moved to infinity (where they have no gravitational influence) by subtracting the corresponding tidal potential. The atmosphere is most conveniently embedded (conceptually) inside the earth such that the center of mass remains undisturbed (Moritz, 1974); of course, the resulting change in the earth's exterior gravity field must be accounted for when comparing terrestrial data with data downward continued from satellite altitudes. Positioning the origin of our coordinate system approximately at the earth's center of mass, we therefore have guaranteed convergence of the spherical harmonic series of the potential outside the sphere whose radius equals the farthest distance of the earth's surface from the earth's center; this is the top of the Chimborazo Mountain, in central Ecuador (latitude $-1^{\circ}4'$), with a radial distance of about 6384403 m (Sjöberg, 1977).

A more general result was rigorously proved by Krarup (1969, chapter 3), namely that the spherical harmonic expansion converges everywhere on and outside the smallest sphere (called the limit sphere) that contains all singularities of the potential and its analytic continuation. Thus, the proof that the potential series converges everywhere at the earth's surface would be complete if the potential could be analytically continued down to the so-called Bjerhammar sphere (the sphere that is entirely enclosed within the earth). Kellogg (1953, p.197) comments that the potential function representing the potential of an analytic density distribution bounded by an analytic surface can be continued analytically across the surface. Of course, in view of Poisson's equation, the actual potential is not represented by this function at points of nonzero density; indeed, its discontinuous second derivatives preclude its being analytic on the surface. The possibility of analytically continuing the geopotential inside the irregular masses of the earth seems very doubtful, for as Krarup points out, if it were possible for some given mass distribution, the mere addition of a mass point ("grain of sand") above the limit sphere introduces a singularity in the potential function at this point and thereby destroys the analyticity of the continuation. Therefore, given that the series for the potential converges with certainty only outside the bounding sphere, the question arises whether there exists any justification for

using the series at or near the surface of the earth.

Claims of both proof and disproof of series convergence at the earth's surface appear in the geodetic literature; none is logically sound. The proof by Arnold (1978) of convergence everywhere on the surface is patently flawed, as is Morrison's (1970) conjecture of divergence everywhere (see Appendix A). The "grain of sand" example was used by Moritz (1980, p.64) to argue on the instability of the property of convergence, implying that, in the strictest sense, the size and shape of the surface of convergence, if it is not the bounding sphere, is not well defined. Any further theoretical advances on the behavior of spherical harmonic series near the surface of an attracting body will come by studying density distributions bounded by surfaces, both of which are mathematically regular by some measure. A study which approaches this type of analysis is the one by Kholshchevnikov (1977), who finds upper bounds for the decay rate of spherical harmonics, on the bounding sphere, with respect to the degree n for variously structured bodies. These upper bounds are generally proportional to (fixed) negative powers of n , depending on the measure of regularity of the density and bounding surface. Such decay rates are insufficiently strong to yield convergence below the bounding sphere; yet as they are only upper bounds, convergence cannot hereby be excluded.

While the precise convergence surface for series corresponding to arbitrary density distributions bounded by arbitrary surfaces has eluded theorists, several fundamental, as well as interesting, results have been established. Krarup (1969) examined the potential resulting from a Kelvin transformation of the potential of a uniform mass distribution on a straight line. Using this example, he disproved the intuitive notion that the surface which separates regions of convergence and divergence is always a sphere. A general theory regarding the shape of the surface of convergence for special spherical harmonic series was developed by Ecker (1972). He proved that a sphere is the surface of convergence for rotationally symmetric potentials (i.e. series of zonal harmonics only), while a torus defines the surface of convergence for a series of only tesseral harmonics (Krarup's example). Other surfaces of convergence lying between these two extremes result for series of only those sectorials whose degree n and order m satisfy the relation $m = \ell n$, ℓ being predefined and $0 \leq \ell \leq 1$. The case $\ell = 0$ represents the series of zonals, and Ecker proved the following result:

Theorem: A series of spherical harmonics $\sum_{n=0}^{\infty} \left(\frac{1}{r}\right)^n a_n P_n(\cos\theta)$

converges everywhere outside the sphere of radius ρ , where

$$\rho = \lim_{n \rightarrow \infty} \sup^n \sqrt{|a_n|}$$

and diverges almost everywhere inside this sphere.

Here, r, θ are the polar coordinates, radius and colatitude, and P_n denotes the Legendre polynomial of n -th degree. The qualification "almost everywhere" for divergence is included to allow convergence on sets of measure zero (regions having no volume) inside the convergence sphere (e.g. any series of odd zonals converges for every $r > 0$ at the equator, since $P_{2n+1}(0) = 0$). The radius of convergence for the by now classic example of a homogeneous oblate ellipsoid of revolution (Jung, 1956, p.543; Moritz, 1980, p.52) is found, using the above theorem, to be $\rho = E$, the focal distance of the ellipsoid, showing also that the surface of convergence may not bound the generating masses (i.e., in this case the potential function can be analytically continued to the sphere of radius E but, of course, does not represent the potential inside the ellipsoid).

The question of convergence or divergence of the potential at the earth's surface may be circumvented by the Runge-Krarup theorem (Krarup, 1969; Moritz, 1980, p.67). Briefly, this theorem, already known to Walsh (1929, p.535) for the inner potential, states that a function harmonic outside the earth's surface may be approximated arbitrarily well in its region of harmonicity by a function which is harmonic outside a given sphere totally inside the earth. Obviously, the spherical harmonic series of an harmonic function converges everywhere outside any sphere contained entirely in its region of harmonicity, in particular on the earth's surface if this sphere is embedded entirely within the earth. It should be noted that the Runge-Krarup theorem is an existence theorem; it guarantees only the existence of an approximating function and does not provide the method to find it. Furthermore, nothing is said about the closeness of corresponding individual terms of the two series for the actual and approximating potentials. The approximation is arbitrarily accurate only in the limit, i.e. for the total sum (however, one can expect that, because of the near sphericity of the earth's surface, the corresponding lower degree terms of the two series do not differ substantially). We may also note that the theorem holds for any exterior potential no matter how badly its series diverges below the bounding sphere, so that the application of the theorem is not contingent on the instability of the convergence surface of the actual potential series.

The fact that the Runge-Krarup theorem says nothing about the accuracy of individual terms of the potential series is very restrictive on the possible use of the theorem to the practicing geodesist. Hence, for example, Sjöberg's (1979) statement that "the coefficients of the approximating potential ... can be selected arbitrarily close to the coefficients of the external potential ... to any desired degree" is somewhat misleading if not inaccurate. For the closer the coefficients of the approximating potential are chosen to those of the actual potential, the further is the postponement of the arbitrary closeness of the approximating series to the true potential. However, for the example of a point mass situated on the equator of an oblate spheroid (so that the ensuing potential series diverges in the polar regions), Sjöberg shows that in this case, the postponement is not unduly exacerbated if the first 300 or 400 terms of the actual divergent series are used for the corresponding terms of the approximating potential. Moritz's statement (Moritz, 1980, p.66) based on the Runge-Krarup theorem that the earth's potential, for practical purposes, can always be considered as a "convergent potential" is similarly misleading. This statement should not be interpreted as claiming convergence, for all practical purposes, of the actual series of the potential on and outside the earth's surface. Instead it is a statement on the practical equivalence of the potential and an approximating series that converges on and above the surface. Term for term, especially at high degrees, the approximating series and the actual series must be quite different since the former converges while the latter possibly diverges near the earth's surface. Therefore, the Runge-Krarup theorem can not be invoked to justify the use of a portion of the series of the actual potential at the earth's surface.

Until now the discussion has centered on the convergence of a spherical harmonic series, where the use of spherical coordinates is motivated by the near spherical shape of the earth's surface. But to a second approximation, the surface of the earth is an ellipsoid, or more precisely an oblate spheroid, an ellipsoid whose equatorial axes are equal (i.e. it is a surface of revolution) and whose poles are flattened. The question arises whether the use of different coordinates such as ellipsoidal coordinates has a significant bearing on the problem of convergence at the earth's surface. The ellipsoidal coordinates for which the general triaxial ellipsoid is a coordinate surface (a surface defined by the fixed value of one coordinate, in this case one of the semi-axes) are rather more difficult to work with than spherical coordinates, but expansions of the potential and the gravity anomaly have been formulated in

terms of the orthogonal lamé functions, see (Hobson, 1965, pp 473-475; Walter, 1970; and Savrov, 1974). Because the deviations between best fitting triaxial and biaxial ellipsoids are of the same order of magnitude as geoid undulations, the triaxial ellipsoid has generally been abandoned as an approximation to the earth's surface. Thus, the coordinate system to be considered is the spheroidal system (Hobson, 1965, p.421, see also chapter 3) in which the expansion of the potential is in terms of familiar Legendre functions. Though not widely used in practice, these coordinates have received considerable attention in geodesy, in particular, by Jung (1956) and Hotine (1969). The term "spheroid" in the geodetic vocabulary conventionally denotes an equipotential surface of some normal (reference) potential. On the other hand, the term "ellipsoid" usually implies oblate spheroid; hence it will also be used here to mean exclusively an ellipsoid of revolution flattened at the poles.

Imposing rotational symmetry with respect to one of the ellipsoidal coordinates, namely the longitude, in this case yields ellipsoidal harmonic functions whose structure differs from their spherical counterparts only in the dependence on the distance from the origin. Due to the corresponding similarity to spherical harmonic expansions we have theorems, such as,

1. the ellipsoidal harmonic series of the potential converges uniformly everywhere outside the ellipsoid that bounds the generating masses; and
2. there exists an ellipsoidal harmonic series which converges uniformly above the "Bjerhammar ellipsoid" and approximates the potential outside the earth's surface with arbitrary accuracy.

The proof of the first statement follows immediately from the uniform convergence of the ellipsoidal series for the reciprocal distance (equation (3.27); cf. Kellogg, 1953, p.143, and see also Hobson, 1965, pp.430-433). The second statement is merely a corollary to the Runge-Krarup theorem since the Bjerhammar sphere enters only to relate the theorem to spherical harmonic expansions and can easily be replaced by the Bjerhammar ellipsoid. Other corresponding theorems with respect to the "limit ellipsoid" or to the convergence surface of a series of ellipsoidal zonals undoubtedly exist, but may require more exacting proofs.

Unfortunately, the transition to ellipsoidal coordinates does not solve the problem of series convergence at the earth's surface since its distance from the bounding

ellipsoid can still be 6 to 7 km (for the bounding sphere it is as much as 25 km). However, we recognize that the convergence problem is a manifestation of the choice of coordinate system, for the ellipsoidal series will converge to the potential in regions where convergence of the spherical series is doubtful (e.g. the polar areas). Also, because the equatorial radius of the bounding ellipsoid could exceed the radius of the bounding sphere, the spherical series will converge in regions where the ellipsoidal series may not, see Fig. 1. The dependence of

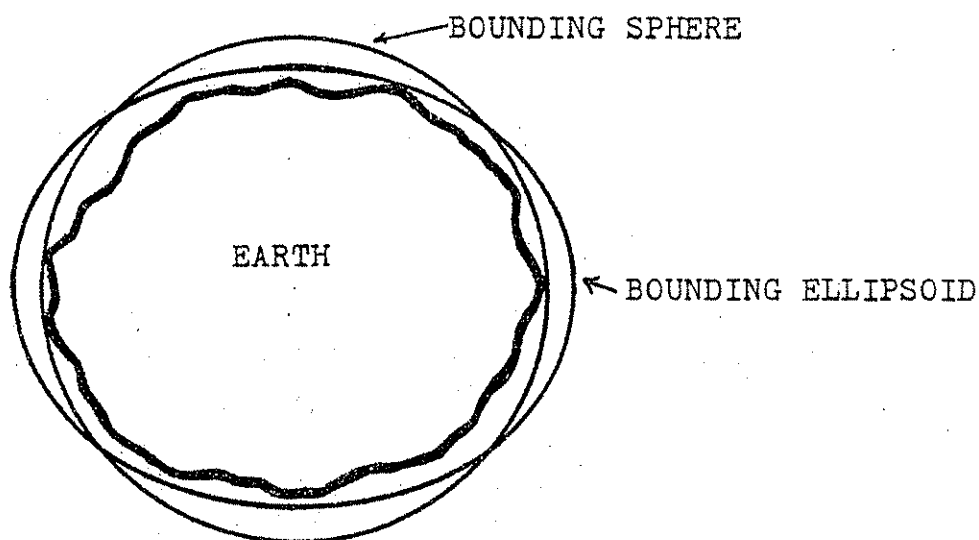


Figure 1: Bounding sphere versus bounding ellipsoid.

the region of convergence on the coordinate system is even more directly illustrated by simply changing the coordinate origin, at which the bounding sphere is (always) centered. Therefore, the smallest bounding sphere is obtained if the origin of the system of spherical coordinates coincides with the geometrical center of the earth. The feasibility of a choice of coordinates other than ellipsoidal coordinates that guarantees convergence of the corresponding series significantly closer to the earth's surface seems unlikely since the next approximation to the surface is a considerably more complex geometric figure. This is an upward continuation of the telluroid, or some smoothed version of it. The telluroid (Heiskanen and Moritz, 1967, p.292) is the surface of points at which the normal potential equals the gravity potential at the corresponding points on the earth's surface, where correspondence is established if the telluroid and surface points lie on the same (normal) plumb line in the normal gravity field. The telluroid imitates the earth's surface quite closely since their difference, the height anomaly, varies as smoothly as the geoid undulation with average values of 30 m. However, the corresponding coordinate system (in which the bounding telluroid is a coordinate surface) will be too abstruse to work with.

The essence of this paper addresses the question of whether the probable divergent character, at the earth's surface, of the spherical harmonic expansion of the disturbing potential (and gravity anomaly) eliminates it from the repertoire of viable methods of downward continuation. In light of the foregoing summary of the theoretical viewpoints on convergence and divergence of the earth's potential series, the analysis will be based on the assumption that the series definitely diverges below the bounding sphere. Although divergence has not been proved, this premise is certainly reasonable, if only as the worst-case situation.

1.2 Other Problems and Methods of Downward Continuation

The question of divergence or convergence at the earth's surface will never impede our computational abilities in practical situations. That is, with a finite number of measurements of the potential we can determine only a finite number of coefficients of the harmonic series, and any finite sum of spherical harmonics converges, indeed is analytic, everywhere except at the origin of the coordinate system. Yet, if the total infinite series of the potential does diverge at the earth's surface, then the more

coefficients we determine the greater will be the effect of this divergent character on the partial sums. The question of convergence, however, is then better posed as a question of representation.

Since the partial sum, whether in the space above or below the bounding sphere, is thus only an estimate of the true potential, the question of representation belongs to a much larger class of problems, namely the problem of approximation. As with most areas in physical geodesy, our limited accessibility to the gravity field, i.e. limited to discrete and noisy measurements, automatically renders our problem "ill-posed." An ill-posed problem, according to Thikonov and Arsenin (1977), is a problem that either has no solution, has more than one solution, or its solution is unstable with respect to the given data. Our inability to measure the gravity field in space beyond a certain degree of detail means that there exists an infinite number of solutions, all differing in the detail which we were not able to discern, but all satisfying our measurements. Therefore, the solution is not unique. But as easily as this problem is recognized, it is as quickly eliminated by requiring a solution for a gravity field concordant in detail with the measurements. That a solution always exists is guaranteed by the fact that any finite sum of spherical harmonics, which in fact satisfy Laplace's equation and are regular at infinity, represents a potential.

The instability of the solution arises because the harmonic coefficients obtained from the measurements at satellite altitude are not errorless. This is expertly shown by Rummel et al. (1979) for the case that the measurement noise is white noise. White noise affects all harmonics of the measured signal equally so that the infinite sum of the effects is unbounded. Since the discreteness of the measurements places a limit on the number of harmonic coefficients that can be determined, the downward continuation of the error, while not causing unbounded error in the solution, nevertheless produces an amplification of the error. The error in the n -th degree harmonic coefficient is amplified by the approximate ratio $(r/R)^n$ in the process of downward continuation (see section 1.3), where R is the radius of the earth and r is the radius of the satellite orbit. For minimal satellite altitudes of 150 km, this ratio increases to over 1000 at $n=300$, which means that the 300-th degree coefficient of the gravity anomaly at altitude must be known to μgal (10^{-8} m/s^2) accuracy in order to recover mgal (10^{-5} m/s^2) accuracy at the earth's surface. This demonstrates that the problem of downward continuation belongs to the class of ill-posed problems.

The foremost method to solve the ill-posed problem is to impose constraints on the desired solution, as for example, searching for a smoothed version of the true solution. Another example is the method of collocation which generates a solution whose norm in the space of solutions is minimum. While solving the nonuniqueness problem, collocation can still be an unstable process, sometimes even requiring the presence of noise in the data to stabilize, or regularize, the solution. Equivalently, one can simply introduce a regularizing factor which has the same effect as noise in that it filters the higher frequencies of the solution (Rummel et al. 1979). A serious difficulty with the usual collocation is the sheer volume of the computations, increasing with the cube of the number of the data. However, with specially gridded data which are then amenable to very efficient computational algorithms, Colombo (1979) demonstrates the applicability for highly detailed global solutions of the gravity field.

Aside from collocation, other frequently discussed, more deterministic, methods of downward continuation rely in one way or another on the inverse of the solution to a boundary-value problem, either Poisson's integral (first boundary-value problem) or the Pizzetti-Stokes formula (third boundary-value problem); both formulated on the supposition of a spherical earth. When regarded as formulas relating the sought after sources that produce the observed data, i.e. as formulas for the inverse problem, they become Fredholm integral equations of the first kind. Their solution is usually found by successive approximations, but because it is unstable, the iterations may not converge. Assuming a spherical earth, the Stokes "integral equation" is readily solved, yielding the inverse Stokes equation (Molodenskii et al., 1962, p.50). Most treatises on applications of downward continuation were predicated on airborne measurements of gravity and made use of the Poisson integral, but only for local determinations; see for example the works by Schwarz (1973) and Moritz (1966a).

Finally, we note a method of downward continuation that is founded on the usual technique for analytic continuation. Because the potential of the earth (without atmosphere) is analytic everywhere above its surface, the downward continuation from the bounding sphere is theoretically achievable using a Taylor series expansion. That is, given the potential on the bounding sphere (as a series), we know also its derivatives. Hence, the Taylor expansion about a point on the the bounding sphere can be evaluated anywhere within the sphere that excludes all singularities of the potential; i.e. the sphere that is centered at the expansion point and just touches the earth's surface. This method was

briefly developed by Hotine (1969, pp. 172-173), but its applicability seems uncertain. Continuations of 3 to 25 km using Taylor series require fairly accurate evaluations of the (radial) derivatives of the potential. However, with only a finite number of harmonic terms in the series, the derivatives, particularly of higher (>1) order, will suffer considerably from the truncation effect, as well as random errors in the high degree coefficients.

1.3 Preliminaries and Definitions

There are certainly many additional aspects to the problem of using satellite derived data for terrestrial applications. In the first place, the potential will not be observed directly. The measurements at the satellite altitude will consist of either satellite to satellite Doppler tracking data or gradiometry data. The former provides velocity differences, hence potential differences, between two satellites (see Hajela, 1978; Rummel, 1980; Schwarz, 1972), while the latter yields linear combinations of components of the gravitational gradient tensor (see Reed, 1973; Rummel, 1979). Secondly, for global coverage, the satellites must follow near polar orbits thereby creating a nonuniform data set with heavy concentrations at the poles. In order to perform a spherical harmonic analysis, the data must exist on a sphere (see below), but the satellite orbits cannot be exactly circular (the satellite moves in a noncentral force field). Finally, the earth's potential field is not stationary in inertial space. It completes one full rotation every 24 hours on an axis that wobbles due to precession and nutation, as well as polar motion. Therefore, the raw data must undergo considerable preprocessing in order to obtain uniform or specially gridded coverage on a sphere that is fixed in the earth's gravitational field. These preparations in the determination of the final product are beyond the scope of the following analysis, since they depend primarily on the type of satellite mission. Furthermore, it is assumed that the potential is available for downward continuation in the form of a (finite) spherical harmonic series. We note that the analysis of spherically distributed discrete data is corrupted by aliasing, the influence of the higher frequency content of the data on the desired harmonic coefficients. This effect can be minimized by using optimal estimation techniques (see Colombo, 1978).

The downward continuation error in the present context refers to a deterministic error, as opposed to a random, or probabilistic error. Given the potential, defined everywhere in space, and its series representation in a

region of convergence, one can define this error precisely as the difference between the truncated series continued beyond the region of convergence and the true value of the potential. This definition has the disadvantage in that it includes a type of truncation, or omission, error, i.e. the neglect of higher degree information, which has nothing to do with series divergence. The alternative definition, as the difference between truncated inner and outer series, however, seems even less agreeable, since the inner series, in our case, is not the spectral representation of the potential. Consequently, corresponding terms of the two series are not comparable.

At present we lack the resources (primarily a sufficiently accurate series of the potential determined in outer space to high degree) to conduct an analysis of the downward continuation with actual data. The natural alternative is to devise an earth model with a complexity that adequately takes into account the anticipated advances in determining series expansions in space. Ideally, the potential of this model should be known exactly on the model surface and be expandable in a series that diverges below the bounding sphere. Instead of exact values on the surface, an inner series may suffice if it can be expanded to a high degree.

From the mathematical standpoint, the spherical polar coordinates r, θ, λ lend themselves most conveniently to formulations on a global scale. With respect to the Cartesian system of coordinates x, y, z , r is the radial distance from the origin, θ is the polar angle measured from the z -axis, and λ is the angle (longitude) measured counterclockwise in the xy -plane from the x -axis:

$$\begin{aligned} x &= r \sin\theta \cos\lambda \\ y &= r \sin\theta \sin\lambda \\ z &= r \cos\theta \end{aligned} \tag{1.1}$$

In geodesy, the second coordinate is often the latitude, but then is usually the coordinate in an ellipsoidal system of coordinates. All derivations in section 2 are performed in the above spherical coordinate system.

The solutions to Laplace's equation (which is satisfied by the potential in free space) are the solid spherical harmonic functions of degree n and order m :

$$r^n \bar{Y}_{nm}(\theta, \lambda), r^{-(n+1)} \bar{Y}_{nm}(\theta, \lambda), n \geq 0, -n \leq m \leq n \tag{1.2}$$

the first when the region of harmonicity contains the origin, and the second when it contains infinity. The \bar{Y}_{nm} are known as surface spherical harmonics and are defined by

$$\bar{Y}_{nm}(\theta, \lambda) = \bar{P}_{n|m|}(\cos\theta) \begin{cases} \cos m\lambda & m \geq 0 \\ \sin|m|\lambda & m < 0 \end{cases} \quad (1.3)$$

This departs from the more conventional definition adopted by mathematicians (see Cushing, 1975, p.158) where the inconvenience of separate definitions for negative and nonnegative orders is avoided by using the exponential function $e^{im\lambda}$ instead of the sinusoids; however, (1.3) is more customary in physical geodesy. The \bar{P}_{nm} are the associated Legendre functions, normalized such that the integral of the square of surface harmonics over the unit sphere is 4π . Furthermore, the functions \bar{Y}_{nm} are orthogonal, i.e.

$$\frac{1}{4\pi} \iint_{\sigma} \bar{Y}_{nm}(\theta, \lambda) \bar{Y}_{pq}(\theta, \lambda) d\sigma = \begin{cases} 1 & n=p \text{ and } m=q \\ 0 & n \neq p \text{ or } m \neq q \end{cases} \quad (1.4)$$

where $d\sigma = \sin\theta d\theta d\lambda$ and σ represents the unit sphere; and they form a complete set of basis functions. This means that any continuous function $F(\theta, \lambda)$ defined on the unit sphere, that is, for $0 \leq \theta \leq \pi$ and $0 \leq \lambda \leq 2\pi$, can be uniquely expressed as a uniformly convergent series of spherical harmonics:

$$F(\theta, \lambda) = \sum_{n=0}^{\infty} \sum_{m=-n}^n f_{nm} \bar{Y}_{nm}(\theta, \lambda) \quad (1.5)$$

where (by multiplying both sides by \bar{Y}_{nm} , integrating over σ , and noting (1.4))

$$f_{nm} = \frac{1}{4\pi} \iint_{\sigma} F(\theta, \lambda) \bar{Y}_{nm}(\theta, \lambda) d\sigma \quad (1.6)$$

The condition that F be continuous can be relaxed to F being

Lebesgue integrable, but then the series (1.5) does not always converge to F . The operation (1.6), resulting in the coefficients f_{nm} , is known as the Legendre transform and the coefficients constitute the (Legendre) spectrum of F . In view of (1.2), the extension of an harmonic function into (the exterior) space is

$$F(r, \theta, \lambda) = \sum_{n=0}^{\infty} \sum_{m=-n}^n \left(\frac{R}{r}\right)^{n+1} f_{nm} \bar{Y}_{nm}(\theta, \lambda) \quad (1.7)$$

where R defines the radius of the sphere on which F has the spectrum $\{f_{nm}\}$ (see equation (1.6)). If the spectrum of F is determined in space, then "downward continuation" simply means a decrease in the variable r . Also, the spectra of F on two different spheres, of radii R_1 and R_2 , are related by

$$f_{nm}^{(1)} = \left(\frac{R_2}{R_1}\right)^{n+1} f_{nm}^{(2)} \quad (1.8)$$

provided that the series converges on each sphere. It is obvious from (1.6) that the definition of Legendre spectrum is not restricted to functions defined on a sphere. The surface can assume any shape as long as to each coordinate pair (θ, λ) there corresponds a unique point of the surface, and vice versa. Of course, if a function is defined in three dimensions, then its spectra with respect to a sphere and some other (nonspherical) surface are not comparable.

This introduction to spherical harmonics concludes with a statement of a very useful formula, the addition theorem for Legendre polynomials:

$$P_n(\cos \psi) = \frac{1}{2n+1} \sum_{m=-n}^n \bar{Y}_{nm}(\theta, \lambda) \bar{Y}_{nm}(\theta', \lambda') \quad (1.9)$$

where ψ is the central angle between points (θ, λ) and (θ', λ') on the unit sphere, and where the P_n are the familiar Legendre polynomials.

We follow Hobson (1965, pp.89-90) in the definition of the associated Legendre functions. For any complex μ not on the real line segment $[-1, 1]$,

$$P_n^m(\mu) = (\mu^2 - 1)^{\frac{1}{2}m} \frac{d^m}{d\mu^m} P_n(\mu) \quad (1.10)$$

$$Q_n^m(\mu) = (\mu^2 - 1)^{\frac{1}{2}m} \frac{d^m}{d\mu^m} Q_n(\mu)$$

where the Q_n^m , Q_n are the Legendre functions of the second kind. The Legendre functions with real arguments $\mu = \cos \theta \in [-1, 1]$ are then defined by

$$P_n^m(\cos \theta) = (\pm i)^m P_n^m(\cos \theta \pm 0 i) \quad (1.11)$$

$$= (\pm i)^m \lim_{\nu \rightarrow 0} P_n^m(\cos \theta \pm \nu i)$$

The right side of (1.11) is the limit through the complex plane onto the line segment $[-1, 1]$ and is found to be

$$P_n^m(\cos \theta \pm 0 i) = (\pm i)^m \sin^m \theta \frac{d^m}{d(\cos \theta)^m} P_n(\cos \theta) \quad (1.12)$$

and similarly for Q_n^m , so that

$$\begin{aligned} P_n^m(\cos \theta) &= (-1)^m \sin^m \theta \frac{d^m}{d(\cos \theta)^m} P_n(\cos \theta) \\ Q_n^m(\cos \theta) &= (-1)^m \sin^m \theta \frac{d^m}{d(\cos \theta)^m} Q_n(\cos \theta) \end{aligned} \quad (1.13)$$

Definitions (1.10) and (1.13) hold for any n, m , but we consider only those functions for which n, m are nonnegative integers with $0 \leq m \leq n$. Finally, we apply the required normalization:

$$\bar{P}_{nm}(\mu) = (-1)^m \sqrt{\frac{(2n+1)(n-m)!}{\epsilon_m(n+m)!}} P_n^m(\mu), \text{ for all } \mu \quad (1.14)$$

$$\bar{Q}_{nm}(\mu) = (-1)^m \sqrt{\frac{(2n+1)(n-m)!}{\epsilon_m(n+m)!}} Q_n^m(\mu), \text{ for all } \mu$$

where

$$\epsilon_m = \begin{cases} 1, & m = 0 \\ \frac{1}{2}, & m \neq 0 \end{cases} \quad (1.15)$$

2. The Downward Continuation of Spherical Harmonic Series

Although the problem of convergence and divergence has generally been recognized, more attention has been paid to the theoretical concerns than to a numerical analysis of the situation in practice. A passing, conjectural, comment by Cook (1967) suggests that the effect of divergence on the n -th degree coefficient is on the order of J_n^3 for the potential and J_n^2 for the gravity anomaly, where J_n is the n -th degree zonal harmonic coefficient. The notable works in this area are those of Levallois (1972) and Sjöberg (1977). Their numerical results derive from the postulated effect, on the series expansion, of the masses between the bounding sphere and the sphere of computation. With several approximations, Levallois estimated these effects over much of the earth's surface for expansions of the geoid undulation up to degree 200. He obtained errors of a few tens of centimeters with the exceptional meter in equatorial regions, even for low degree expansions; several meters in the midlatitudes, generally for all degrees of truncation; and up to 16 m in polar regions for the high degree expansion. Sjöberg's analysis is restricted to expansions up to degree 16 and 24, but enlarged to include the errors in gravity anomalies. His results show errors as large as 0.5 to 5 m depending on the complexity of the earth model, as well as the point of computation. Downward continuation errors in gravity anomalies were found to be extraordinarily large, in some instances on the order of the anomalies themselves (up to 30 mgal).

These results for the gravity anomaly are unacceptable as we have only to compare the GEM9 harmonic coefficients (derived solely from observations of satellite orbit perturbations, Lerch et al., 1977) and coefficients derived from terrestrial data. Rapp (1978) found an RMS (root mean square) difference in the two expansions (up to degree 20) of 7.0 mgal. He also computed an RMS difference of 9.1 m in the expansions of the geoid undulation, rather high, but more likely due to measurement errors than the divergence of the series.

An appraisal of this method of estimating the downward continuation error, given in section 2.2.4, suggests that it is an unsuitable method on account of the simplistic density

hypothesis of the intervening masses. Also an attempt is made to explain the irreconcilable downward continuation errors of the gravity anomaly, mentioned above. In section 2.3 we embark on a similar course to ascertain the effects of series divergence, but now with a firmer control on the generation of the earth's disturbing potential. Results from a subsequent numerical analysis agree generally with expectations based on the discussions of the following section.

2.1 Simple Mass Distributions

A study of potential series corresponding to simple mass distributions will illuminate some of the broader aspects of the harmonic series behavior of the earth's potential. In order to draw definite conclusions on the partial sums of the series, the mass distribution should be sufficiently elementary so that 1) the surface separating regions of convergence and divergence is well defined, 2) the series for either region is calculable to arbitrarily high degree, and 3) although it is not essential, a closed formula of the potential is available to check the numerical computations.

The following "experimental mass distributions" are not designed to simulate the earth's distribution of mass; hence, any of the specific quantitative results obviously do not hold for the earth. Infinite series will be developed for both the potential and the gravity anomaly since they are associated with different rates of convergence.

In the usual spherical coordinate system (1.1), consider an infinitesimally thin layer of uniform density distributed in the form of a circular disk on the equatorial plane $\theta = 90^\circ$ and centered at the origin (see Fig. 2). The constant density is χ and the radius is denoted a . For any point P , the potential due to the attracting mass is

$$V_p = V(r_p, \theta_p, \lambda_p) = \kappa \chi \int_{r=0}^a \int_{\lambda=0}^{2\pi} \frac{r \, d\lambda \, dr}{l} \quad (2.1)$$

where κ is the constant of gravitation, and

$$l = \sqrt{r_p^2 + r^2 - 2rr_p \cos\psi} ; \quad \cos\psi = \sin\theta_p \cos(\lambda - \lambda_p) \quad (2.2)$$

Because of rotational symmetry, we may choose $\lambda_p = 0$. The

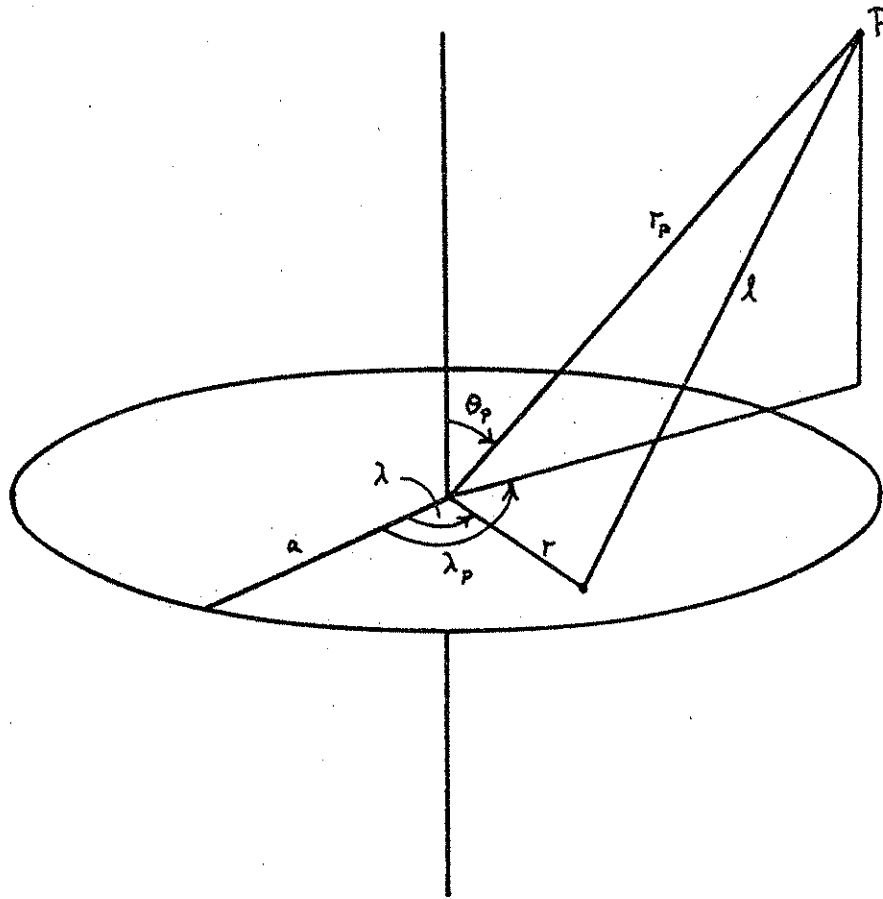


Figure 2: Equatorial disk density distribution.

integration with respect to r is easily performed:

$$V_p = \kappa \chi \int_0^{2\pi} [\ell_a - r_p + r_p \cos\psi \ln \frac{\ell_a + a - r_p \cos\psi}{r_p - r_p \cos\psi}] d\lambda \quad (2.3)$$

where

$$\ell_a = \sqrt{a^2 + r_p^2 - 2ar_p \cos\psi} \quad (2.4)$$

As reference, we choose the potential of the entire mass concentrated at the coordinate origin:

$$U_p = \frac{\kappa \pi a^2 \chi}{r_p} \quad (2.5)$$

Hence the disturbing potential is

$$\begin{aligned} T_p &= V_p - U_p \\ &= 2\kappa \chi \int_0^{\pi} [\ell_a - r_p + r_p \cos\psi \ln \frac{\ell_a + a - r_p \cos\psi}{r_p - r_p \cos\psi}] d\lambda - \frac{\kappa \pi a^2 \chi}{r_p} \end{aligned} \quad (2.6)$$

where because of symmetry, the integrals over the intervals $(0, \pi)$ and $(\pi, 2\pi)$ are identical.

The series expansions of V are obtained by substituting into the integral (2.1) the uniformly convergent series for the reciprocal distance:

$$\ell^{-1} = \sum_{n=0}^{\infty} \frac{r_p^n}{r^{n+1}} P_n(\cos\psi) \quad , \quad r_p > r \quad (2.7)$$

for the outer series, and

$$\ell^{-1} = \sum_{n=0}^{\infty} \frac{r_p^n}{r^{n+1}} P_n(\cos\psi) \quad , \quad r_p < r \quad (2.8)$$

for the inner series. We find for $r_p > a$

$$V_p = \kappa \chi \sum_{n=0}^{\infty} \frac{r_p}{n+2} \left(\frac{a}{r_p}\right)^{n+2} \int_0^{2\pi} P_n(\cos\psi) d\lambda \quad (2.9)$$

Now the addition theorem (1.9) provides the integrals of P_n :

$$\begin{aligned} \int_0^{2\pi} P_n(\cos\psi) d\lambda &= \frac{1}{2n+1} \sum_{m=-n}^n \bar{Y}_{nm}(\theta_p, 0) \int_0^{2\pi} \bar{Y}_{nm}(\tfrac{1}{2}\pi, \lambda) d\lambda \\ &= \frac{2\pi}{2n+1} \bar{P}_{n0}(\cos\theta_p) \bar{P}_{n0}(0) \end{aligned} \quad (2.10)$$

since

$$\int_0^{2\pi} \bar{Y}_{nm}(\tfrac{1}{2}\pi, \lambda) d\lambda = 0, \quad m \neq 0 \quad (2.11)$$

Now

$$P_n(0) = \begin{cases} 0 & , \quad n \text{ is odd} \\ \frac{(-1)^{\frac{1}{2}n} 1 \cdot 3 \cdot 5 \cdots (n-1)}{2^{\frac{1}{2}n} (\frac{n}{2})!} & , \quad n \text{ is even} \end{cases} \quad (2.12)$$

and the series expansion for V becomes

$$V_p = 2\pi \kappa \chi a \sum_{n=0}^{\infty} \left(\frac{a}{r_p}\right)^{2n+1} \mu_n P_{2n}(\cos\theta_p) \quad (2.13)$$

where

$$\mu_n = \frac{1}{2n+2} P_{2n}(0); \quad \mu_{n+1} = -\frac{n+\frac{1}{2}}{n+1} \mu_n, \quad n \geq 0; \quad \mu_0 = \frac{1}{2} \quad (2.14)$$

The disturbing potential is simply

$$T_p = 2\pi \kappa \chi a \sum_{n=1}^{\infty} \left(\frac{a}{r_p}\right)^{2n+1} \mu_n P_{2n}(\cos \theta_p), \quad r_p > a \quad (2.15)$$

For points inside the bounding sphere, we decompose the integral (2.1) into the two parts for which the series (2.7) and (2.8) respectively converge:

$$\begin{aligned} V_p &= \kappa \chi \int_0^{2\pi} \left[\int_0^{r_p} \sum_{n=0}^{\infty} \left(\frac{r}{r_p}\right)^{n+1} P_n(\cos \psi) dr + \right. \\ &\quad \left. + \int_{r_p}^a \sum_{n=0}^{\infty} \left(\frac{r_p}{r}\right)^n P_n(\cos \psi) dr \right] d\lambda \\ &= \kappa \chi r_p \sum_{\substack{n=0 \\ n \neq 1}}^{\infty} \int_0^{2\pi} \left[\frac{1}{n+2} - \frac{1}{n-1} \left(\left(\frac{r_p}{a}\right)^{n-1} - 1 \right) \right] P_n(\cos \psi) d\lambda + \\ &\quad + \kappa \chi r_p \int_0^{2\pi} \left[\frac{1}{3} + \ln \frac{a}{r_p} \right] \cos \psi d\lambda \end{aligned} \quad (2.16)$$

The last term vanishes; and with (2.10) and (2.12) we obtain

$$V_p = 2\pi \kappa \chi r_p \sum_{n=0}^{\infty} \left[\frac{4n+1}{2n-1} - \frac{2n+2}{2n-1} \left(\frac{r_p}{a}\right)^{2n-1} \right] \mu_n P_{2n}(\cos \theta_p) \quad (2.17)$$

The disturbing potential, with respect to the reference potential (2.5), is

$$\begin{aligned} T_p &= 2\pi \kappa \chi r_p \sum_{n=0}^{\infty} \left[\frac{4n+1}{2n-1} - \frac{2n+2}{2n-1} \left(\frac{r_p}{a}\right)^{2n-1} \right] \mu_n P_{2n}(\cos \theta_p) - \\ &\quad \frac{\kappa \pi a^2 \chi}{r_p}, \quad r_p < a \end{aligned} \quad (2.18)$$

That this series converges for $r_p < a$ is obvious once we recognize that $\mu_n = O(n^{-3/2})$ since $P_{2n}(\cos \theta) = O(n^{-1/2})$.

For the present purposes, we may adopt the following definition of the gravity anomaly (Heiskanen and Moritz, 1967, p.89):

$$\Delta g = - \frac{\partial T}{\partial r} - \frac{2}{r} T \quad (2.19)$$

Applying (2.19) to (2.6) and omitting the tedious derivations, the closed form for the anomaly is found to be

$$\begin{aligned} \Delta g_p = & 6\pi\kappa\chi + \frac{\pi\kappa\chi a^2}{r_p^2} - 2\kappa\chi \int_0^\pi [3 \cos \psi \ln \frac{a+l_a-r_p \cos \psi}{r_p-r_p \cos \psi} + \\ & + \frac{3r_p^2+2a^2-5r_p a \cos \psi}{r_p l_a} + \frac{r_p}{l_a} \frac{r_p \cos \psi - (a+l_a) \cos^2 \psi}{a+l_a-r_p \cos \psi}] d\lambda \quad (2.20) \end{aligned}$$

Because surface layers generate potentials whose derivatives are discontinuous as they cross the surface, expression (2.20) is valid anywhere except on the disk.

The definition (2.19) applied to the series for the disturbing potential, (2.15) and (2.18), yields the outer and inner series for the gravity anomaly:

$$\Delta g_p = 2\pi\kappa\chi \sum_{n=1}^{\infty} (2n-1) \mu_n \left(\frac{a}{r_p}\right)^{2n+2} P_{2n}(\cos \theta_p), \quad r_p > a \quad (2.21)$$

$$\begin{aligned} \Delta g_p = & 2\pi\kappa\chi \sum_{n=0}^{\infty} \left[\frac{(2n+2)^2}{2n-1} \left(\frac{r_p}{a}\right)^{2n-1} - 3\frac{4n+1}{2n-1} \right] \mu_n P_{2n}(\cos \theta_p) + \\ & + \pi\kappa\chi \left(\frac{a}{r_p}\right)^2, \quad r_p < a \quad (2.22) \end{aligned}$$

The term by term differentiation of the series (2.15) and (2.18) is permitted since the series of radial derivatives is uniformly convergent with respect to r_p .

Another simple mass distribution, which approaches that of the earth, is a homogeneous ellipsoid. In order to evaluate the coefficients of the series expansions exactly and, more importantly, so that the bounding sphere is the surface of convergence, the ellipsoidal surface is broken into latitudinal bands of constant curvature, each 5° wide, giving it a serrated appearance (see Fig. 3). The potential at a point P due to the smooth ellipsoid is given by

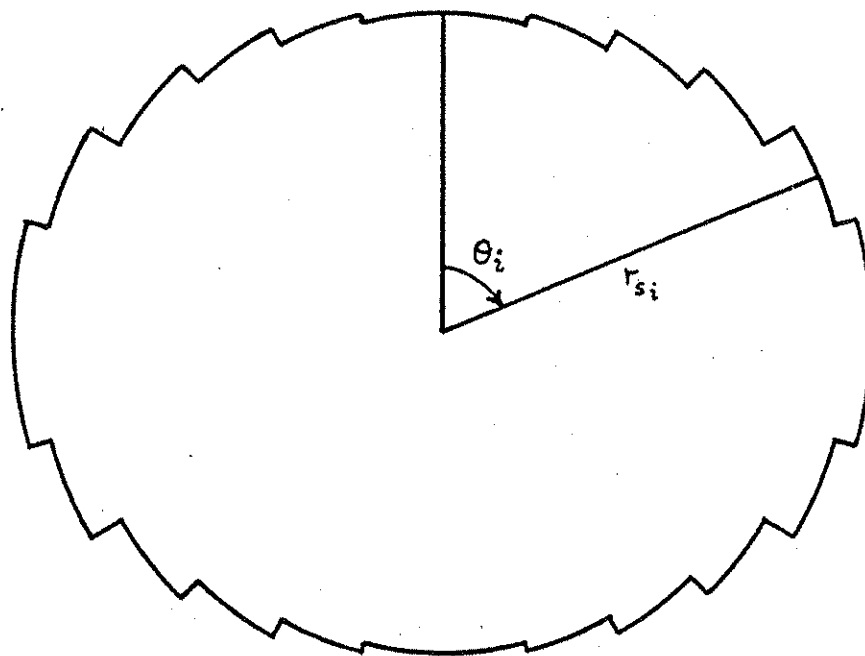


Figure 3: Serrated homogeneous ellipsoid density distribution.

$$V_p = \kappa \chi \iint_{\sigma} \int_0^{r_s} \frac{1}{l} r^2 dr d\sigma \quad (2.23)$$

where σ denotes the unit sphere, $d\sigma = \sin\theta d\theta d\lambda$, and where $r_s = r_s(\theta)$ is the radial distance to the ellipsoid surface. With the introduction of the serrations,

$$V_p = \kappa \chi \sum_{i=0}^{2N-1} \int_0^{2\pi} \int_{\theta_i}^{\theta_{i+1}} \int_0^{r_{si}} \frac{r^2 dr}{l} \sin\theta d\theta d\lambda \quad (2.24)$$

where $\theta_i = i\Delta\theta$, $i=0, \dots, 2N-1$, $N=90/\Delta\theta$, and $r_{si} = r_s(\theta_i)$. Only the inner integral can be evaluated in closed form, thus precluding the computation of exact values of the potential and gravity anomaly. The derivations of the series are completely analogous to those of the equatorial disk and are relegated to Appendix B. The final results are given by equations (B.7), (B.8) for the potential and (B.9), (B.10) for the gravity anomaly.

For the numerical tests, the equatorial disk was given a radius of $a=6378140$ m and a uniform density of $\chi=3 \times 10^5$ g/cm³. Similarly, $a=6378140$ m was chosen as the equatorial radius of the homogeneous ellipsoid. The centers of the latitudinal bands, each $\Delta\theta = 5^\circ$ wide, lie on an ellipsoid with a flattening of $f=1/298.257$; and therefore, the corresponding radii of these bands are computed according to

$$r_{si} = \frac{a}{\sqrt{1+e'^2 \cos^2 \theta_{i+\frac{1}{2}}}} \quad (2.25)$$

where $i=1, \dots, 17$, and $e'^2 = 1/(1-f)^2 - 1$. The homogeneous density of the ellipsoid was equated with the average density of the earth, $\chi = 5.5$ g/cm³; and $\kappa = 66.7 \times 10^{-9}$ cm/(g.s²) was adopted as the constant of gravitation.

The differences between the resulting partial sums of the series (2.15), (2.21), (B.7), and (B.9), as functions of the truncation degree, and the corresponding true values are shown in Fig. 4 for $r_p=6377200$ m, $\theta_p=77^\circ.5$ (near the equator) and in Fig. 5 for $r_p=6357200$ m, $\theta_p=7^\circ.5$ (near the pole). Both points of evaluation (r_p, θ_p) were selected below the sphere of convergence, so that each of the series must diverge in the limit. (Using Ecker's theorem (see section 1.1), it is possible to prove that the bounding

sphere of the equatorial disk is also the surface of convergence. A simple proof of the divergence inside the bounding sphere of the serrated ellipsoid was not found, but it is verified by Figures 4 and 5.) The partial sums, being in any case discrete functions, were evaluated in steps of 20 (Fig. 4) and 300 (Fig. 5) degrees and connected by straight lines for clarity, but thereby also smoothing their strong oscillatory behavior. The true values (not shown) of the potential and gravity anomaly were provided by formulas (2.6) and (2.20) for the equatorial disk and by the inner series (B.8) and (B.10) for the homogeneous ellipsoid (truncated at $n=\bar{n}=30000$). In the figures, the value immediately above each zero, related only to it, indicates roughly the range of the oscillations over the given domain of truncation degrees.

A study of these graphs reveals several interesting aspects of harmonic series divergence. The most obvious conclusion is that the more distant the point of evaluation is from the sphere of convergence, the more severe is the divergence of the series. The series near the pole shows definite signs of divergence around $\bar{n}=1200$ to 1800, while the series near the equator had to be summed to $\bar{n} > 15000$, and higher for the potential, in order to detect a significant divergence pattern. Also, for low \bar{n} , the deviations from the true values actually decrease with increasing truncation degree before they start their eventual, unbounded, increase. This is particularly the case for the potential, even in the worse situation at the pole. The distinction between truncation error and downward continuation error (due to divergence, see section 1.3) thereby becomes exceedingly nebulous for the lower degree sums. Whether a comparison of these partial sums with those of the inner series gives a better indication of the downward continuation error is questionable for lower degree expansions, since this type of comparison is associated with other interpretive problems, as discussed in section 2.2.2. The difference between inner and outer partial sums, shown in Figures 6 and 7 for the same two points as above, does indicate that some of the truncation effect is common to both. This is particularly the case for the equatorial disk, less so for the ill behaved series of the ellipsoid. Connected with the overall delay in divergence is the difference in behavior between the potential and anomaly series. Since most of the power of the potential is concentrated in the lower degree harmonics, the divergent character of the series is apparent somewhat later than for the anomaly, its power being spread more to the higher degree terms (i.e. it is essentially the derivative of the potential). These conclusions hold equally for both density distributions, but are clearly more vividly depicted for the

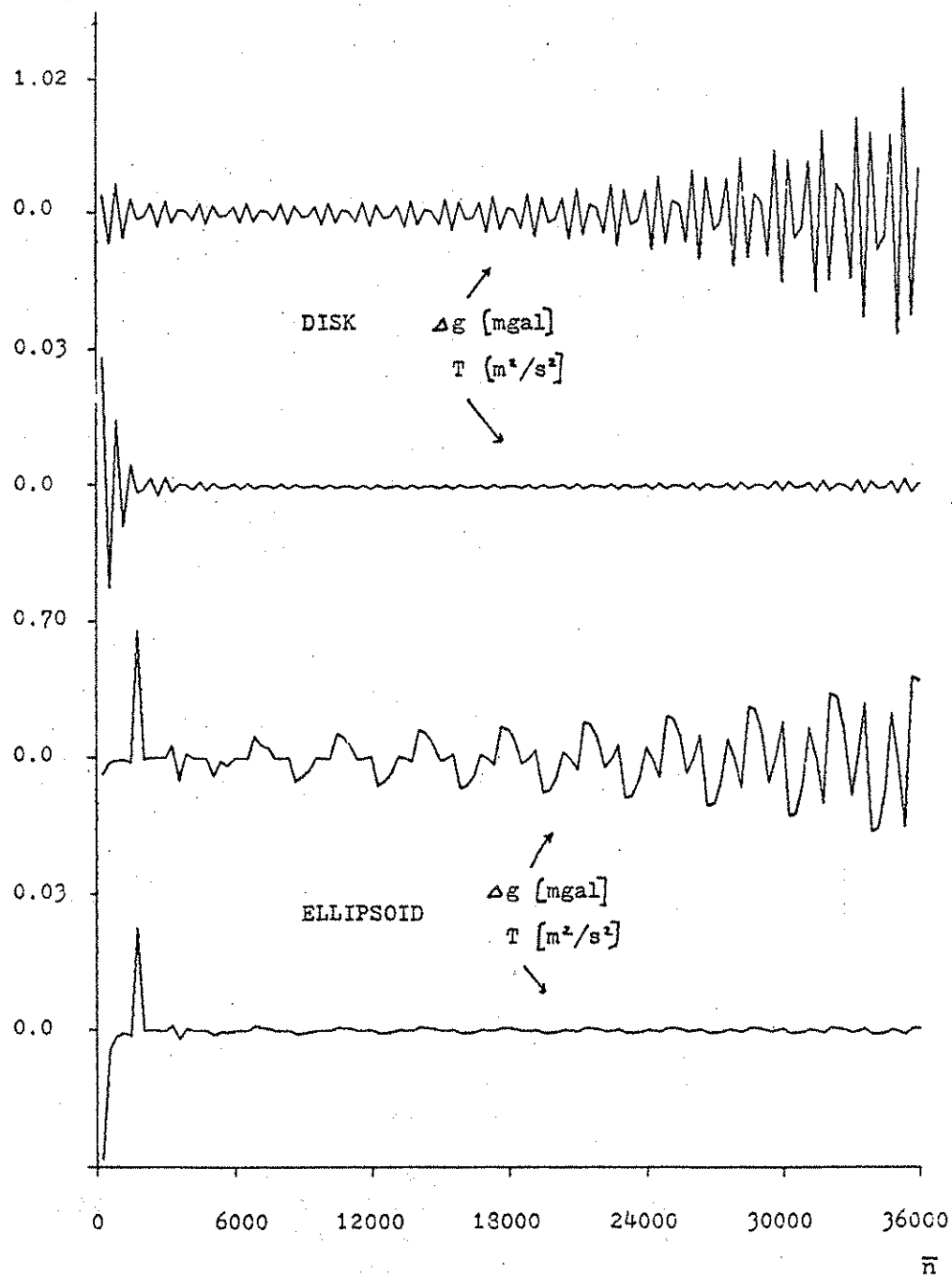


Figure 4: Partial sums of spherical harmonic series of Δg , T for equatorial disk and serrated ellipsoid density distributions (Figures 2 and 3) minus corresponding true values evaluated at $r_p=6377200$ m, $\theta_p=77.5^\circ$.

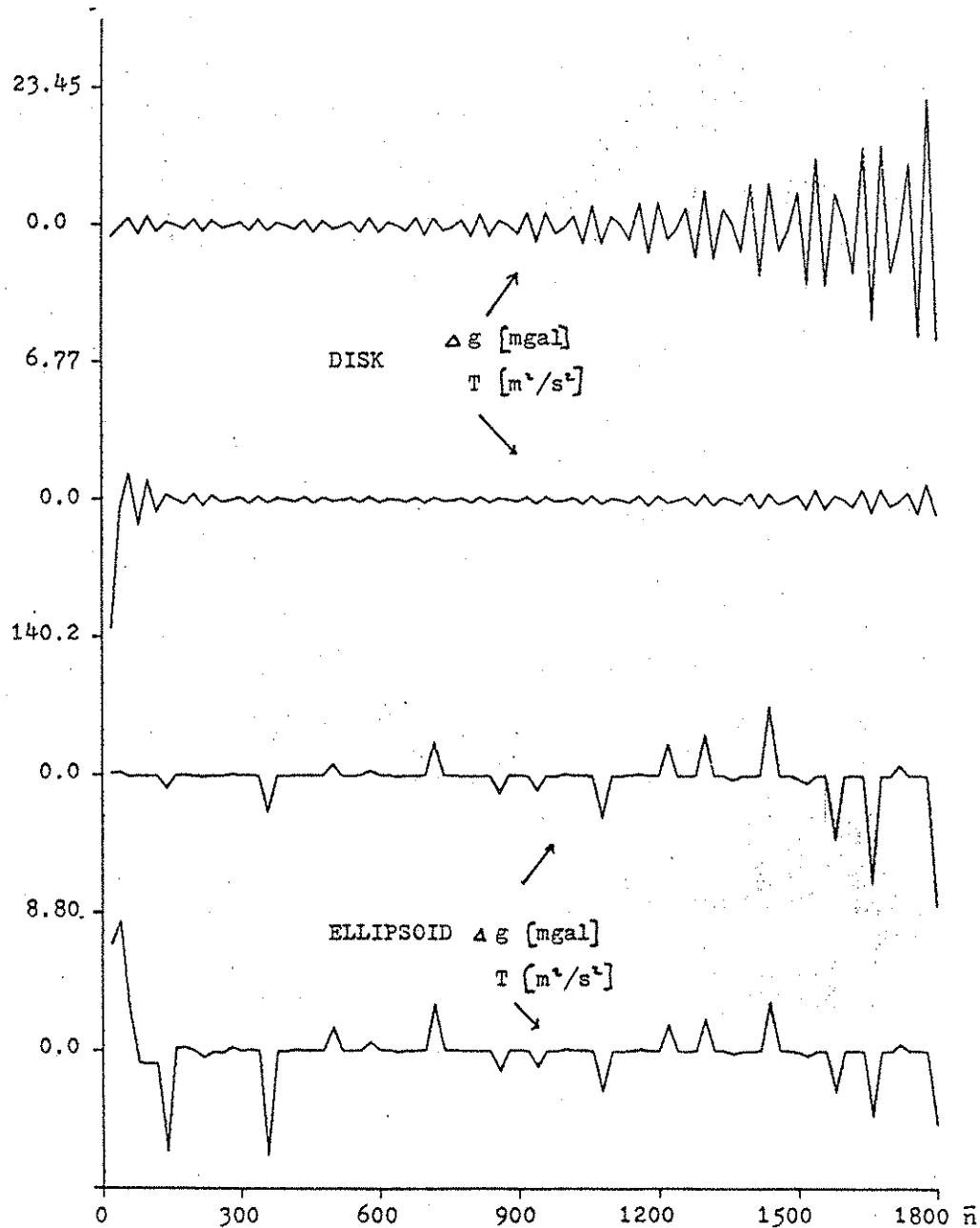


Figure 5: Partial sums of spherical harmonic series of Δg , T for equatorial disk and serrated ellipsoid density distributions (Figures 2 and 3) minus corresponding true values evaluated at $r_p = 6357200$ m, $\theta_p = 7^\circ 5'$.

equatorial disk. The spikes in the graphs corresponding to the homogeneous ellipsoid are undoubtedly due to the salience of the bounding surface.

The conspicuous oscillatory character of the partial sums is evidently attributable to the symmetry and homogeneity of the density distributions. However, some type of irregular oscillation of a full spherical harmonic series should not be excluded. Figure 8 shows the partial sums of a gravity anomaly series derived from the (180,180) harmonic coefficient solution of the earth's gravity field (Rapp, 1978) and random higher-degree coefficients that were scaled to decay according to the Tscherning/Rapp degree variance model (for more details, see section 2.3.2). The sums were evaluated (using an equation such as (2.50)) up to degree 1500 at a colatitude of 10° (near the pole) for various radial distances. Unfortunately, because of inevitable constraints in computer storage, and also time, such computations are feasible only for polar latitudes where the (normalized) Legendre functions of high order are virtually zero and can be safely neglected. On the other hand, since the true value of the anomaly below the convergence sphere cannot be known, this graph is almost useless for quantitative assessments of the downward continuation error. The intent of Fig. 8 is to illustrate the tendency for oscillation of a divergent series, as well as the very moderate effect of divergence for degrees of truncation less than 300.

2.2 The Volumetric Density Model

2.2.1 The Derivation of the Error Series

The masses of the earth generate a potential whose gradient is the attractive force field postulated by Newton. It can be shown that this Newtonian potential at a point P is the sum of all attracting masses, each divided by its distance from the attracted point P. Formulated for a nondiscrete mass distribution, the potential V_p is

$$V_p = \kappa \iiint_{\Omega} \frac{\mu}{r} d\Omega \quad (2.26)$$

κ is Newton's gravitational constant, Ω is the (three-dimensional) volume containing the mass distribution; μ is the density function; $d\Omega$ is an element of volume, so that

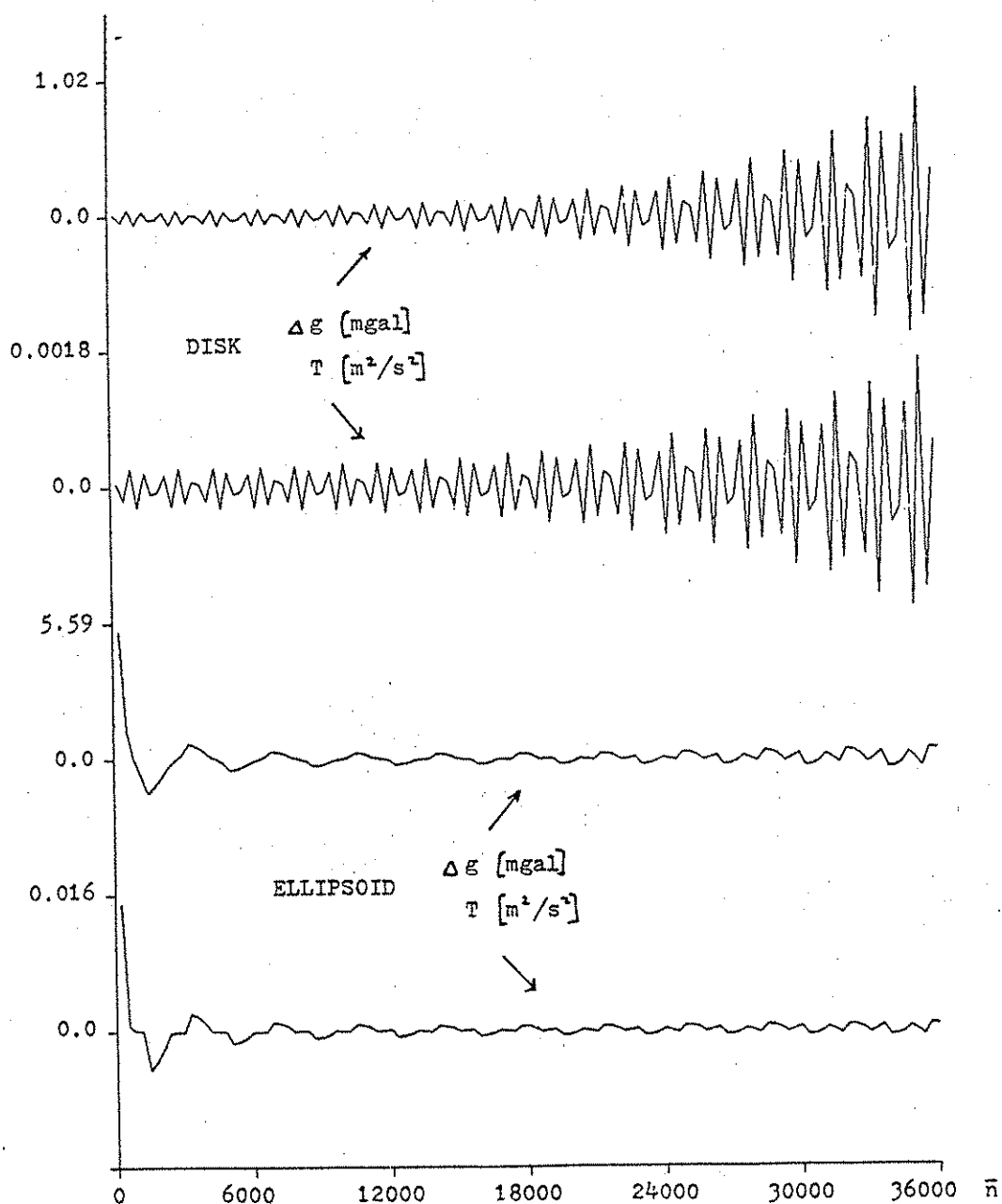


Figure 6: Differences between partial sums of inner and outer spherical harmonic series of Δg , T for equatorial disk and serrated ellipsoid density distributions evaluated at $r_p = 6377200$ m, $\theta_p = 77^\circ.5$.

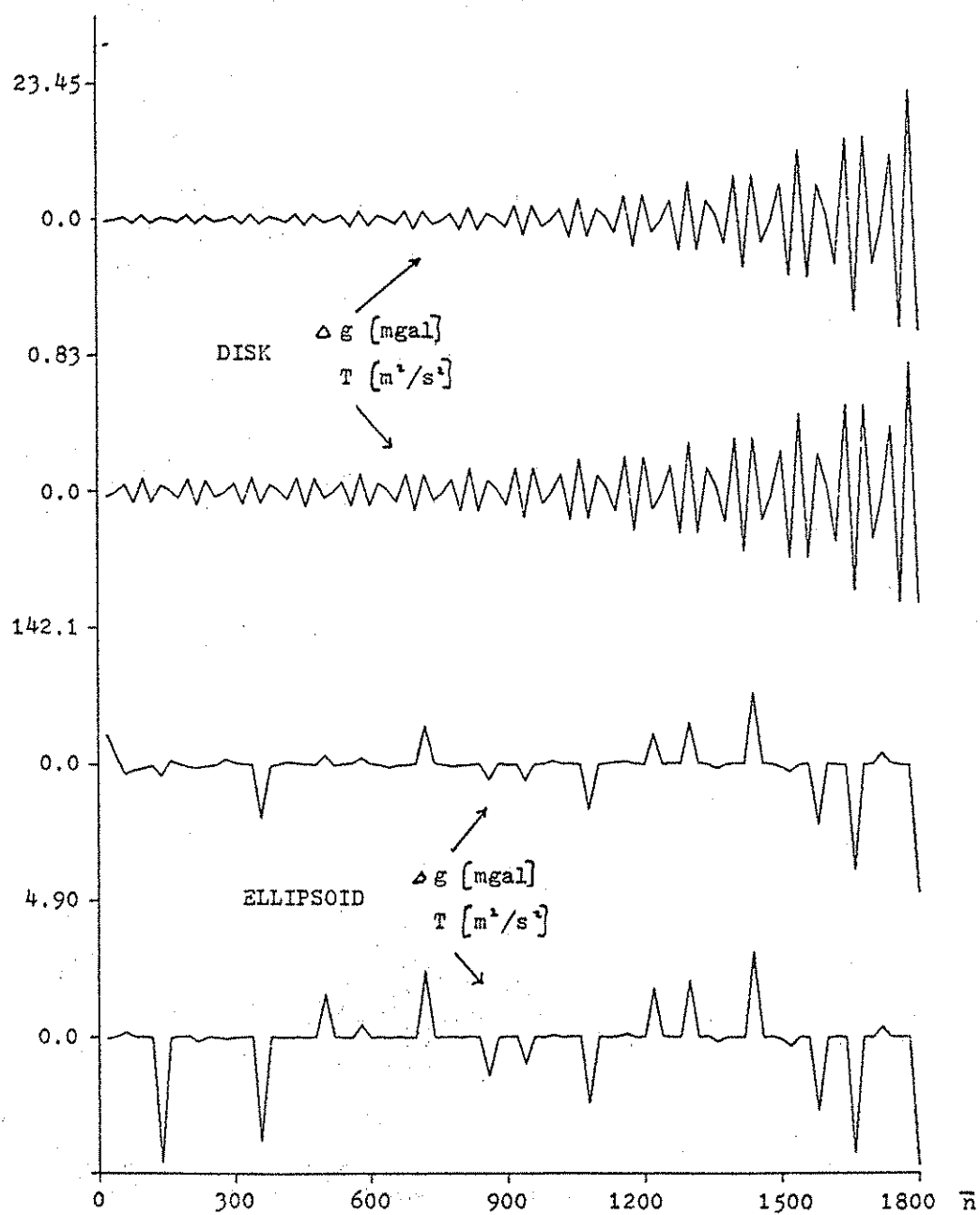


Figure 7: Differences between partial sums of inner and outer spherical harmonic series of Δg , T for equatorial disk and serrated ellipsoid density distributions evaluated at $r_p = 6357200 \text{ m}$, $\theta_p = 7.5^\circ$.

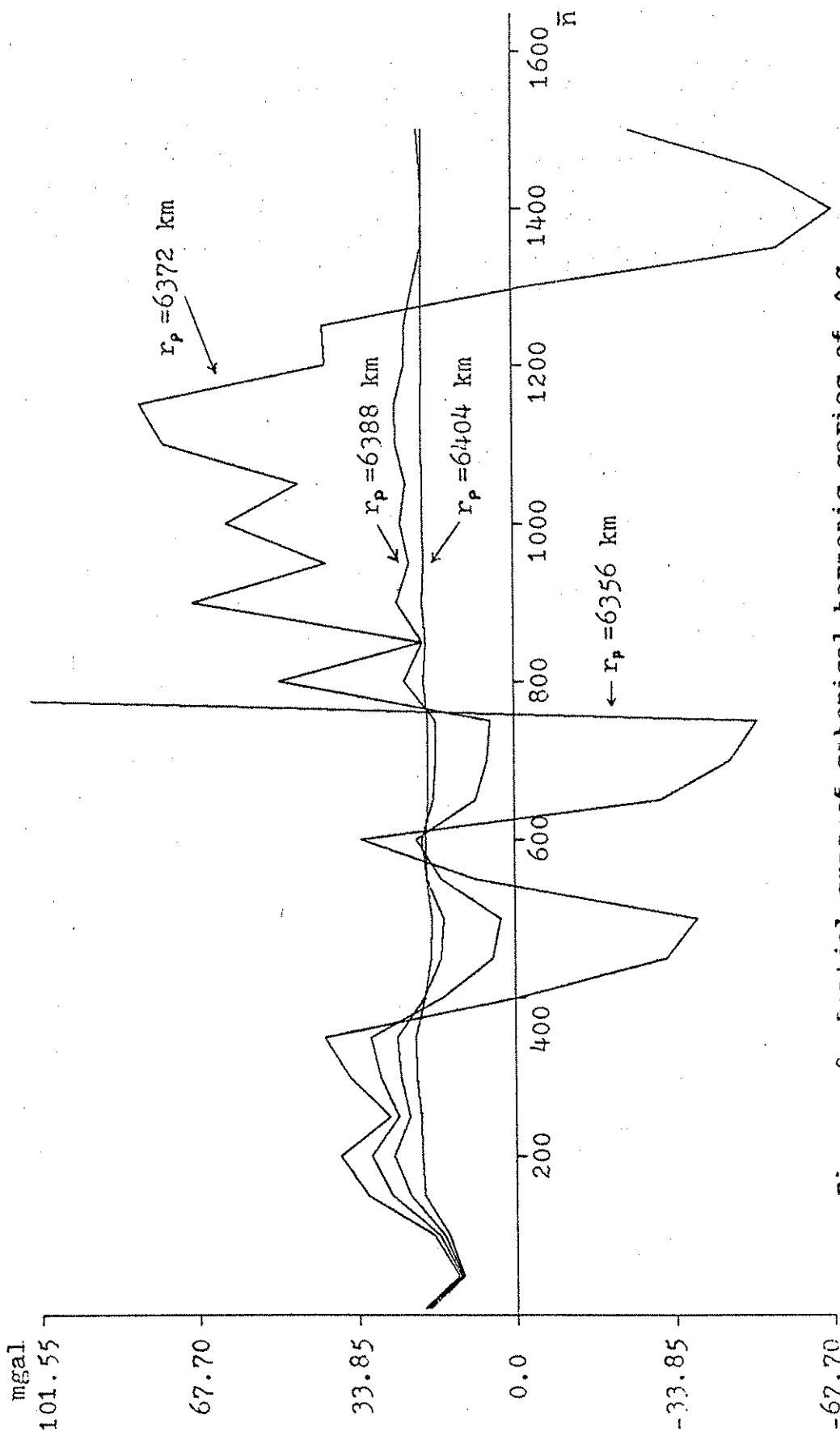


Figure 8: Partial sums of spherical harmonic series of Δg derived from 180 degree field plus random harmonic coefficients to degree 1500, and evaluated at $\theta_p = \lambda_p = 10^\circ$, $r_p = 6356, 6372, 6388, 6404$ km; the surface of convergence is a sphere of radius 6378 km.

the elemental mass is $\mu d\Omega$; and ℓ is the distance between the attracted point P and the attracting mass $\mu d\Omega$. The only restriction on the density μ , formulated in the context of modern potential theory, is that it be Lebesgue integrable (Wermer, 1974); hence discontinuity of μ on a set of measure zero is permitted, but the total mass must be finite. Without significant loss of generality we will adhere to the classic requirement of piecewise continuity and boundedness. The integral expression above for V is valid anywhere in space (i.e. it can be shown that it converges to the potential everywhere, even where the integrand is singular ($\ell=0$), see (Kellogg, 1953, p.151)). Our interest lies only on and outside the surface that bounds all generating masses, viz. the earth's surface.

The expansion of V into a series of spherical harmonic functions can be founded directly on its being a solution of Laplace's equation. Alternatively, to give a physical meaning to the ensuing coefficients of the series, the potential $1/\ell$ (generated by a point of mass $1/\kappa$) is first expanded as a spherical harmonic series (equation (2.7)). Upon the substitution of (2.7) into (2.26), the integration may be performed term by term to yield

$$V_p = \frac{\kappa}{r_p} \sum_{n=0}^{\infty} \iiint_{\Omega} \mu(r, \theta, \lambda) \left(\frac{r}{r_p}\right)^n P_n(\cos \psi) d\Omega \quad (2.27)$$

The validity of this expression is guaranteed only for points outside the bounding sphere S_b (see Fig. 9). In (2.27) r is the radius to the volume element $d\Omega = r^2 \sin \theta \, d\theta \, d\lambda \, dr$, and $\cos \psi$ is now

$$\cos \psi = \cos \theta \cos \theta_p + \sin \theta \sin \theta_p \cos(\lambda - \lambda_p) \quad (2.28)$$

The potential at a surface point P below the bounding sphere can also be represented as a convergent series by considering separately those regions for which the series (2.7) and (2.8) are respectively convergent:

$$V_p = \frac{\kappa}{r_p} \sum_{n=0}^{\infty} \iint_{\sigma} \left[\int_0^{\bar{r}} \mu \left(\frac{r}{r_p}\right)^n r^2 \, dr + \int_{\bar{r}}^{r_s} \mu \left(\frac{r_p}{r}\right)^{n+1} r^2 \, dr \right] \cdot P_n(\cos \psi) d\sigma \quad (2.29)$$

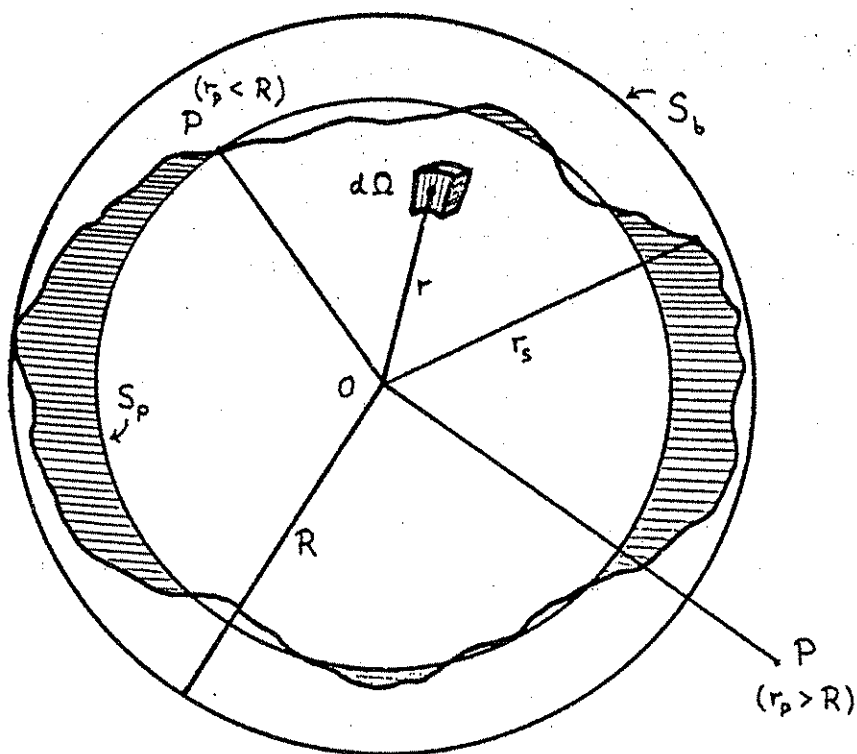


Figure 9: Sphere of computation versus bounding sphere.

where σ denotes the unit sphere, $d\sigma = \sin\theta d\theta d\lambda$, r_s is the radial distance to the earth's surface, and $\bar{r} = \min(r_s, r_p)$. Note that r_s is a function of (θ, λ) , as is \bar{r} which denotes the radius either to the sphere of computation or to the earth's surface, whichever is less.

Using the addition theorem for the Legendre polynomials (1.9), the potential V_p , for points above the bounding sphere, can be expanded as follows:

$$\begin{aligned} V_p &= \frac{\kappa}{r_p} \sum_{n=0}^{\infty} \iiint_{\Omega} \mu \left(\frac{r}{r_p} \right)^n \frac{1}{2n+1} \sum_{m=-n}^n \bar{Y}_{nm}(\theta, \lambda) d\Omega \bar{Y}_{nm}(\theta_p, \lambda_p) \\ &= \sum_{n=0}^{\infty} \sum_{m=-n}^n \left(\frac{R}{r_p} \right)^{n+1} v_{nm} \bar{Y}_{nm}(\theta_p, \lambda_p) \end{aligned} \quad (2.30)$$

where

$$v_{nm} = \frac{\kappa}{R(2n+1)} \iiint_{\Omega} \mu \left(\frac{r}{R} \right)^n \bar{Y}_{nm}(\theta, \lambda) d\Omega \quad (2.31)$$

and where R is the radius of the bounding sphere S_b . Similarly, the expansion of the potential at P inside S_b is

$$V_p = \sum_{n=0}^{\infty} \sum_{m=-n}^n \tilde{v}_{nm}(r_p) \bar{Y}_{nm}(\theta_p, \lambda_p) \quad (2.32)$$

where

$$\tilde{v}_{nm}(r_p) = \frac{\kappa}{r_p(2n+1)} \iiint_{\sigma} \left[\int_0^{\bar{r}} \mu \frac{r^{n+2}}{r_p^n} dr + \int_{\bar{r}}^{r_s} \mu \frac{r_p^{n+1}}{r^{n-1}} dr \right] \bar{Y}_{nm}(\theta, \lambda) d\sigma \quad (2.33)$$

$$\bar{Y}_{nm}(\theta, \lambda) d\sigma$$

The "coefficients" \tilde{v}_{nm} are functions of r_p ; note that for $r_p > R$

$$\tilde{v}_{nm}(r_p) = \left(\frac{R}{r_p} \right)^{n+1} v_{nm} \quad (2.34)$$

Hence, the expression (2.32) is valid in all of the exterior space. We note also that the series (2.32) for $r_p < R$ is not a series of solid spherical harmonics, nor is it an analytic representation of V everywhere above the sphere of radius r_p , because the potential has discontinuous second derivatives on and inside the earth's surface.

In current practice the expression (2.30) for V_p (truncated at $n=\bar{n}$) is used anywhere above the earth's surface (even inside S_0). The difference between the computed potential (equation (2.30) with ∞ replaced by \bar{n}) and the true potential (2.32) is the total error of computation:

$$\begin{aligned} \varepsilon(\hat{V}_p) &= \hat{V}_p - V_p \\ &= \sum_{n=0}^{\bar{n}} \sum_{m=-n}^n \left[\left(\frac{R}{r_p} \right)^{n+1} v_{nm} - \tilde{v}_{nm}(r_p) \right] \bar{Y}_{nm}(\theta_p, \lambda_p) \\ &\quad - \sum_{n=\bar{n}+1}^{\infty} \sum_{m=-n}^n \tilde{v}_{nm}(r_p) \bar{Y}_{nm}(\theta_p, \lambda_p) \end{aligned} \quad (2.35)$$

$\varepsilon(\hat{V}_p)$ here is called the downward continuation error. Most authors identify only the first term as the downward continuation error, in which case the second term, representing the neglect of more detailed information, can be called the truncation error. However, for reasons to be elucidated below, the first definition is to be preferred and will be adhered to in all subsequent discussions. Now, the coefficients of the error series (2.35) for $0 \leq n \leq \bar{n}$ are given explicitly by

$$\begin{aligned} a_{nm}(r_p) &= \left(\frac{R}{r_p} \right)^{n+1} v_{nm} - \tilde{v}_{nm}(r_p) \\ &= \frac{\kappa}{r_p(2n+1)} \iint_{\sigma} \left[\int_0^{r_s} \mu \frac{r^{n+2}}{r_p^n} dr - \int_0^{\bar{r}} \mu \frac{r^{n+2}}{r_p^n} dr \right. \\ &\quad \left. - \int_{\bar{r}}^{r_s} \mu \frac{r^{n+1}}{r^{n-1}} dr \right] \bar{Y}_{nm}(\theta, \lambda) d\sigma \end{aligned} \quad (2.36)$$

The first and second terms differ by an integral of the

density in the shaded portion of Figure 9; therefore

$$a_{nm}(r_p) = \frac{\kappa r_p}{2n+1} \iint_{\sigma} \int_{\bar{r}}^{r_s} \mu \left[\left(\frac{r}{r_p} \right)^{n+2} - \left(\frac{r_p}{r} \right)^{n-1} \right] dr \quad (2.37)$$

$$\bar{Y}_{nm}(\theta, \lambda) d\sigma$$

A similar derivation can be found in (Sjöberg, 1977; Cook, 1967).

In the strictest sense, the computation of the coefficients $a_{nm}(r_p)$, $0 \leq n \leq \bar{n}$, requires a knowledge of the density of the masses between the computation sphere S_p and the earth's surface; to assess the truncation error, we need estimates of the coefficient functions $\tilde{v}_{nm}(r_p)$ (or the density function of the whole earth).

Because the earth is nearly ellipsoidal in shape and its internal density, on a large scale, exhibits approximately ellipsoidal symmetry, the earth's gravity potential, as a matter of convenience, is described with respect to the potential of a rotating equipotential reference ellipsoid, which accounts for the coarse features of the gravity field. How this reference potential, designated U , is chosen is irrelevant for the problem at hand provided it can be calculated precisely either in closed form or as a convergent series anywhere on and above the earth's surface. To simplify subsequent definitions, we also stipulate that the potential on the ellipsoid equals the geoidal potential. U includes the centrifugal potential arising from the earth's rotation, which therefore does not contribute to the disturbing potential. An expression for U is found in (Heiskanen and Moritz, 1967, p.67). If \bar{U} denotes the gravitational potential of the rotating ellipsoid (i.e. without the explicit centrifugal part), then the disturbing potential is given by

$$T_p = V_p - \bar{U}_p \quad (2.38)$$

since the centrifugal potential has been omitted in V . By expanding the normal potential in a series, we have from (2.30)

$$T_p = \sum_{n=0}^{\infty} \sum_{m=-n}^n \left(\frac{R}{r_p} \right)^{n+1} t_{nm} \bar{Y}_{nm}(\theta_p, \lambda_p) \quad (2.39)$$

where t_{nm} is the difference between v_{nm} and the corresponding coefficients of \bar{U} . Since \bar{U}_p is supposed to be known everywhere, the error in downward continuing a truncated spherical harmonic series of T is

$$\varepsilon(\hat{T}_p) = \varepsilon(\hat{V}_p) \quad (2.40)$$

where $\varepsilon(\hat{V}_p)$ is given by (2.35).

The most ubiquitous quantity in physical geodesy is the gravity anomaly, simply because the force of gravity is most readily observed. It is defined (when there is no mass external to the geoid) by

$$\Delta g = g|_{\text{geoid}} - \gamma|_{\text{ellipsoid}} \quad (2.41)$$

where g is the magnitude of the earth's gravity vector on the geoid and γ is the magnitude of the gradient of U on the reference ellipsoid (see *ibid.* p. 83). This definition is easily generalized to gravity anomalies in the external space of the earth, where geoid and ellipsoid are replaced by geopotential and spheropotential surface, the potential of both surfaces, in their respective fields, being identical. Approximating γ by the gravity of a homogeneous ball and the normal gradients by radial derivatives then yields

$$\Delta g_p = -\frac{\partial T_p}{\partial r_p} - \frac{2}{r_p} T_p \quad (2.42)$$

For a quantitative analysis of these approximations, see section 4.

The corresponding spherical harmonic series of Δg may be found as follows. Substituting the radial derivative of the reciprocal distance ℓ^{-1} (see (2.2)),

$$\frac{\partial}{\partial r_p} \ell^{-1} = \frac{-r_p + r \cos \psi}{\ell^3} \quad (2.43)$$

into (2.26) yields

$$\frac{\partial V_p}{\partial r_p} = \kappa \iiint_{\Omega} \mu \frac{\partial}{\partial r_p} \left(\frac{1}{\ell} \right) d\Omega =$$

$$= - \kappa \iiint_{\Omega} \mu \frac{r_p - r \cos \psi}{\ell^3} d\Omega \quad (2.44)$$

Thus, combining (2.26), (2.38), and (2.42), the gravity anomaly for any point P becomes

$$\Delta g_p = \kappa \iiint_{\Omega} \mu \left[\frac{r_p - r \cos \psi}{\ell^3} - \frac{2}{r_p \ell} \right] d\Omega + \frac{\partial \bar{U}_p}{\partial r_p} + \frac{2}{r_p} \bar{U}_p \quad (2.45)$$

Differentiating (2.7) with respect to r_p results in

$$\frac{r^2(r \cos \psi - r_p)}{\ell^3} = - \sum_{n=0}^{\infty} (n+1) \left(\frac{r}{r_p}\right)^{n+2} P_n(\cos \psi), \quad r_p > r \quad (2.46)$$

Similarly for $r_p < r$, differentiation of (2.8) with respect to r_p gives

$$\frac{r_p^2(r_p - r \cos \psi)}{\ell^3} = - \sum_{n=1}^{\infty} n \left(\frac{r_p}{r}\right)^{n+1} P_n(\cos \psi), \quad r_p < r \quad (2.47)$$

Substituting the above series, as well as (2.7) and (2.8) into (2.45):

$$\begin{aligned} \Delta g_p = & \kappa \sum_{n=0}^{\infty} \left[\iiint_{\Omega_1} \mu(n-1) \frac{r^n}{r_p^{n+2}} P_n(\cos \psi) d\Omega + \right. \\ & \left. - \iiint_{\Omega_2} \mu(n+2) \frac{r_p^{n-1}}{r^{n+1}} P_n(\cos \psi) d\Omega \right] - G_p \end{aligned} \quad (2.48)$$

where

$$\Omega_1 = \{(r, \theta, \lambda) / r_p > r\}, \quad \Omega_2 = \{(r, \theta, \lambda) / r_p < r\} \quad (2.49)$$

and where $G_p = -\partial \bar{U} / \partial r_p - 2\bar{U}/r_p$. We note that for points P above the bounding sphere, the set Ω_2 is empty and $\Omega_1 = \Omega$;

then with the addition formula (1.9) we obtain the familiar series expansion

$$\begin{aligned}\Delta g_p &= \sum_{n=0}^{\infty} \sum_{m=-n}^n \frac{n-1}{R} \left(\frac{R}{r_p}\right)^{n+2} v_{nm} \bar{Y}_{nm}(\theta_p, \lambda_p) - G_p \\ &= \sum_{n=0}^{\infty} \sum_{m=-n}^n \left(\frac{R}{r_p}\right)^{n+2} g_{nm} \bar{Y}_{nm}(\theta_p, \lambda_p)\end{aligned}\quad (2.50)$$

by absorbing the expansion of G_p , so that

$$g_{nm} = \frac{n-1}{R} t_{nm} \quad (2.51)$$

The error in using a truncated version of this series for points on the earth's surface (i.e. below the bounding sphere) is therefore the difference between equation (2.50) (∞ replaced by \bar{n}) and the true expansion (2.48):

$$\begin{aligned}\epsilon(\Delta \hat{g}_p) &= \kappa \sum_{n=0}^{\bar{n}} \iint_{\sigma} \left[(n-1) \int_{\bar{r}}^{r_s} \mu \left(\frac{r}{r_p}\right)^{n+2} dr \right. \\ &\quad \left. + (n+2) \int_{\bar{r}}^{r_s} \mu \left(\frac{r_p}{r}\right)^{n-1} dr \right] P_n(\cos \psi) d\sigma \\ &\quad - \kappa \sum_{n=\bar{n}+1}^{\infty} \iint_{\sigma} \left[(n-1) \int_0^{\bar{r}} \mu \left(\frac{r}{r_p}\right)^{n+2} dr \right. \\ &\quad \left. - (n+2) \int_{\bar{r}}^{r_s} \mu \left(\frac{r_p}{r}\right)^{n-1} dr \right] P_n(\cos \psi) d\sigma\end{aligned}\quad (2.52)$$

Then with the addition theorem,

$$\begin{aligned}\epsilon(\Delta \hat{g}_p) &= \sum_{n=0}^{\bar{n}} \sum_{m=-n}^n d_{nm}(r_p) \bar{Y}_{nm}(\theta_p, \lambda_p) \\ &\quad + \sum_{n=\bar{n}+1}^{\infty} \sum_{m=-n}^n d'_{nm}(r_p) \bar{Y}_{nm}(\theta_p, \lambda_p)\end{aligned}\quad (2.53)$$

where

$$d_{nm}(r_p) = \frac{\kappa}{2n+1} \iint_{\sigma} \int_{\bar{r}}^{r_s} \left[(n-1) \left(\frac{r}{r_p} \right)^{n+2} + (n+2) \left(\frac{r_p}{r} \right)^{n-1} \right] \mu dr \quad (2.54)$$

$$\bar{Y}_{nm}(\theta, \lambda) d\sigma$$

and

$$d'_{nm}(r_p) = - \left(\frac{R}{r_p} \right)^{n+2} \frac{n-1}{R} v_{nm} + d_{nm}(r_p) \quad (2.55)$$

(2.55) can also be verified by adding and subtracting the density integral over the region Ω_1 . We note that for $r_p > R$, $d_{nm}(r_p) = 0$ and the remaining error is simply one of truncation.

Similarly, the geoid undulation (or more generally, the height anomaly, i.e. the separation between geopotential and spheropotential surfaces at the same potential) is given by Bruns' formula (Heiskanen and Moritz, 1967, p.85):

$$\zeta_p = \frac{T_p}{\gamma_Q} \quad (2.56)$$

where γ_Q is the normal gravity at the point Q, being the normal projection of P onto the spheropotential surface. γ_Q is conventionally approximated by its average value on the reference ellipsoid. Here, we use a common alternative, namely the gravity, at P, associated with an homogeneous ball: $\gamma_Q \approx \kappa M / r_p^2$ (M = the total mass of the earth); see section 4. We then have

$$\zeta_p \approx \frac{r_p^2 T_p}{\kappa M} \quad (2.57)$$

and for points P above the bounding sphere

$$\zeta_p = \sum_{n=0}^{\infty} \sum_{m=-n}^n \left(\frac{R}{r_p} \right)^{n-1} z_{nm} \bar{Y}_{nm}(\theta_p, \lambda_p) \quad (2.58)$$

where

$$z_{nm} = \frac{R^2}{\kappa M} t_{nm} \quad (2.59)$$

Using only the terms up to degree n to represent the height anomaly at the earth's surface results in an error given by

$$\varepsilon(\hat{\zeta}_p) = \frac{R^2}{\kappa M} \varepsilon(\hat{T}_p) \quad (2.60)$$

where $\varepsilon(\hat{T}_p)$ is given by (2.40).

2.2.2 The Interpretation of the Error Series

The proper understanding of any numerical computations of errors such as (2.35) or (2.53) comes only with the correct interpretation of the true series expansion, such as (2.32) or (2.48). Consider, for example, the potential series (2.32); the same arguments obviously hold for the gravity anomaly. Recalling that R is the radius of the bounding sphere S_b , the potential in the space exterior to S_b is given by the uniformly convergent series (2.30). The coefficients v_{nm} have either of the following interpretations. First, they are density integrals, as given by (2.31). Secondly, they constitute the spectrum of V on the bounding sphere S_b (cf. (1.6)):

$$v_{nm} = \frac{1}{4\pi} \iint_{\sigma} V(R, \theta, \lambda) \bar{Y}_{nm}(\theta, \lambda) d\sigma \quad (2.61)$$

The expansion of the potential in spherical harmonics at points below the bounding sphere is achieved by considering separately the two domains in which the inner and outer series of solid harmonics converge. The resulting "coefficients" $\tilde{v}_{nm}(r_p)$ are more correctly functions of r_p and in the first place are density integrals (equation (2.33)). The \tilde{v}_{nm} do not describe the spectrum of the potential on the earth's surface. That is, the potential spectrum of constant coefficients obtained from surface values, as suggested by (1.6), and the functions $\tilde{v}_{nm}(r_p)$ are clearly not identical. Instead, because the series (2.32) converges everywhere to the potential V , even inside the earth's body (Kellogg, 1953, p.151), the functions $\tilde{v}_{nm}(R_p)$ for constant $r_p = R_p$ represent the spectrum of the potential

on the sphere of radius R_p , whether inside or outside the earth's body; that is,

$$\tilde{v}_{nm}(R_p) = \frac{1}{4\pi} \iint_{\sigma} V(R_p, \theta, \lambda) \bar{Y}_{nm}(\theta, \lambda) d\sigma \quad (2.62)$$

The term by term evaluation of the downward continuation error, as given by equation (2.37), therefore does not produce negative corrections to the spectrum of the potential on the surface. We are forced to identify the downward continuation error with the entire sum of error components and on a point by point basis.

Obviously, evaluations of the infinite sum are beyond our computational ability. Moreover, the finiteness of the number of harmonic coefficients of the potential determined in space necessarily limits our efforts to estimating mean values of the potential or gravity anomaly, and not point values. This requires a modification in the formulation of the downward continuation error. Consider first functions defined on a sphere and define an (isotropic) averaging operator by

$$\bar{F}(\bar{\theta}, \bar{\lambda}) = \iint_{\sigma_c} B(\psi) F(\theta, \lambda) d\sigma \quad (2.63)$$

where \bar{F} denotes the average of a function F over the circular cap $\sigma_c = \{(\theta, \lambda) / 0 \leq \psi \leq \psi_0\}$ and weighted by the kernel $B(\psi)$. ψ is the angle between the center of the cap $(\bar{\theta}, \bar{\lambda})$ and the point of the integration (θ, λ) . Meissl (1971, p.26) shows that if the kernel's (one dimensional) spectrum is $\{\sqrt{2n+1} \beta_n / 4\pi\}$ and the spectrum of F is $\{f_{nm}\}$, then

$$\bar{f}_{nm} = \beta_n f_{nm} \quad (2.64)$$

are the spectral components of the average of F , that is, \bar{F} . In the terminology of spectral theory, the coefficients β_n are also known as the frequency response of the averaging operator (2.63).

Applying this result in the present context, let \hat{V} denote a truncated version of the general series (2.32),

valid anywhere on or outside the earth's surface:

$$\hat{V}_p = \sum_{n=0}^{\bar{n}} \sum_{m=-n}^n \tilde{v}_{nm}(r_p) \bar{Y}_{nm}(\theta_p, \lambda_p) \quad (2.65)$$

For constant $r_p = R_p$, this may be interpreted as a weighted average of V over the sphere of radius R_p , where the frequency response is unity for $0 \leq n \leq \bar{n}$ and zero for higher degrees. It is impossible to devise such a perfect response for the usual average that is limited to values within a cap. We consider instead the average

$$\bar{V}_p = \sum_{n=0}^{\infty} \sum_{m=-n}^n \beta_n v_{nm}(r_p) \bar{Y}_{nm}(\theta_p, \lambda_p) \quad (2.66)$$

where the weights have been chosen so that the frequency response is

$$\beta_n \approx 0, \quad n > \bar{n} \quad (2.67)$$

a value to which it tapers smoothly from a value of 1 at $n=0$. As an average on the sphere of radius r_p , it is clear that values of V coincide with values of the potential averaged over an area of the earth's surface only if that area coincides with the spherical cap. This is never the case exactly, but it is a reasonable approximation if the cap is small. The size of the cap for the average (2.66) is essentially determined by the desired "cut-off frequency" \bar{n} . Therefore, if the potential as determined outside the bounding sphere is first averaged over a spherical cap, or equivalently, its spectrum is multiplied by a particular frequency response function, and the truncated series is evaluated at the earth's surface:

$$\hat{\bar{V}}_p = \sum_{n=0}^{\bar{n}} \sum_{m=-n}^n \left(\frac{R}{r_p}\right)^{n+1} \beta_n v_{nm} \bar{Y}_{nm}(\theta_p, \lambda_p) \quad (2.68)$$

then the downward continuation error of the average potential \bar{V} is (cf. (2.35) and (2.36))

$$\varepsilon(\hat{V}_p) = \sum_{n=0}^{\bar{n}} \sum_{m=-n}^n \beta_n a_{nm}(r_p) \bar{Y}_{nm}(\theta_p, \lambda_p) \quad (2.69)$$

A similar result holds for mean gravity anomalies, as well as mean height anomalies:

$$\varepsilon(\hat{\Delta g}_p) = \sum_{n=0}^{\bar{n}} \sum_{m=-n}^n \beta_n d_{nm}(r_p) \bar{Y}_{nm}(\theta_p, \lambda_p) \quad (2.70)$$

$$\varepsilon(\hat{\zeta}_p) = \frac{r_p^2}{\kappa M} \sum_{n=0}^{\bar{n}} \sum_{m=-n}^n \beta_n a_{nm}(r_p) \bar{Y}_{nm}(\theta_p, \lambda_p) \quad (2.71)$$

where $d_{nm}(r_p)$ is given by (2.54) and in each case the frequency response β_n is assumed to vanish for $n > \bar{n}$ (equation (2.67)).

An operator which filters higher degree harmonics nearly perfectly is the Gaussian filter, its name deriving from the shape of the weighting function $w_G(\psi)$, defined by

$$B_G(\psi) = \frac{w_G(\psi)}{\iint_{\sigma} w_G(\psi) d\sigma} \quad (2.72)$$

where

$$\begin{aligned} w_G(\psi) &= e^{-a(1-\cos\psi)} \\ &\approx e^{-\frac{1}{2}a\psi^2}, \text{ for small } \psi \end{aligned} \quad (2.73)$$

If we define $w_G(\psi)=0$ for $\psi > \psi_c$, then the frequency response is given by (see Jekeli, 1981)

$$\beta_{G_0} = 1, \quad \beta_{G_1} = \frac{1-y_0 e^{-a(1-y_0)}}{1-e^{-a(1-y_0)}} - \frac{1}{a}$$

and

$$\beta_{G_{n+1}} = -\frac{2n+1}{a} \beta_{G_n} + \beta_{G_{n-1}} + \frac{e^{-a(1-y_0)}}{1-e^{-a(1-y_0)}} \cdot \quad (2.74)$$

$$\cdot [P_{n-1}(y_0) - P_{n+1}(y_0)] , n > 0$$

where $y_0 = \cos \gamma_0$. The parameter "a" specifies the amount of smoothing. If we desire $\beta_{\bar{n}} = f_0$ (e.g. $f_0 = 0.05$ implies that only 5% of the \bar{n} -th degree harmonic coefficient contributes to the average), then an approximate formula for "a" is

$$a \approx \frac{\bar{n}^2}{2 \ln(1/f_0)} \quad (2.75)$$

2.2.3 The Description of the Earth Model

To evaluate the density integrals of the downward continuation error requires a simplification of the earth's surface, as well as the volumetric density. In the simplifying scheme adopted here, the volume between the sphere of computation and the earth's surface is partitioned into (three-dimensional) blocks that are delimited on the sides by $\theta = \text{constant}$, $\lambda = \text{constant}$ and on the top and bottom faces by $r_s = \text{constant}$, $r_p = \text{constant}$. Within each block the density is assumed to vary only as a step function in the radial direction and be otherwise constant. The required lithospheric (crustal and upper mantle) densities, as well as the corresponding depths are taken from (Bowford, 1971, p.457) and illustrated in Fig. 10. With these assumptions, the coefficients $d_{nm}(r_p)$ of the downward continuation error of the gravity anomaly (2.54) reduce to

$$d_{nm}(r_p) = \frac{K}{r_p^2(2n+1)} \sum_i G_n(r_p, \theta_i, \lambda_i) \iint_{\Delta\sigma_i} \bar{Y}_{nm}(\theta, \lambda) d\sigma \quad (2.76)$$

where

$$G_n(r_p, \theta_i, \lambda_i) = \begin{cases} \int_{r_p}^{r_{si}} \left[(n-1) \left(\frac{r}{r_p} \right)^n + (n+2) \left(\frac{r_p}{r} \right)^{n+1} \right] r^2 dr , & r_{si} > r_p \\ 0 , & r_{si} \leq r_p \end{cases} \quad (2.77)$$

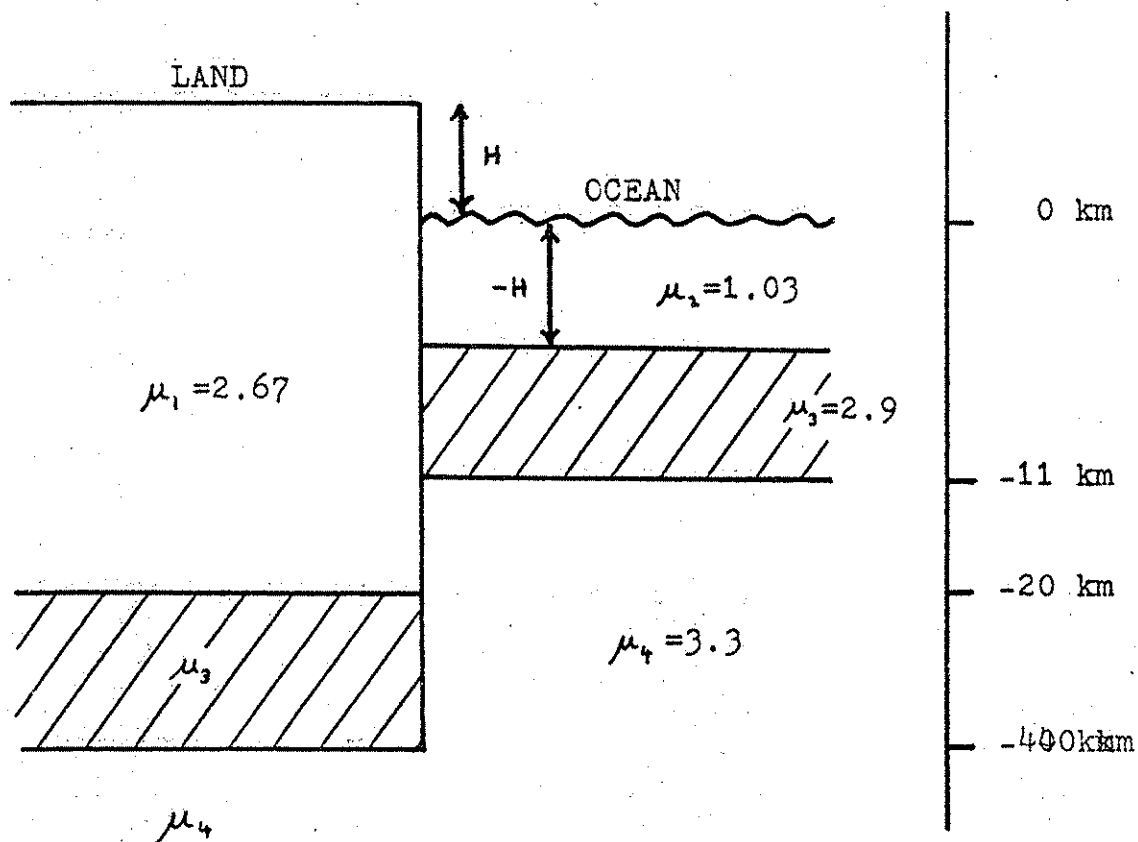


Figure 10: The volumetric density model (density values are in units of g/cm^3).

Defining for $r_b > r_a$

$$F_n(r_a, r_b) = \int_{r_a}^{r_b} \left[(n-1) \left(\frac{r}{r_p} \right)^n + (n+2) \left(\frac{r_p}{r} \right)^{n+1} \right] r^2 dr, \quad n \geq 0$$

$$= \begin{cases} \frac{n-1}{n+3} r_p^3 \left[\left(\frac{r_b}{r_p} \right)^{n+3} - \left(\frac{r_a}{r_p} \right)^{n+3} \right] - \frac{n+2}{n-2} r_p^3 \left[\left(\frac{r_p}{r_b} \right)^{n-2} - \left(\frac{r_p}{r_a} \right)^{n-2} \right], & n \geq 0, n \neq 2 \\ \frac{1}{5} r_p^3 \left[\left(\frac{r_b}{r_p} \right)^5 - \left(\frac{r_a}{r_p} \right)^5 \right] + 4r_p^3 \ln \frac{r_b}{r_a}, & n = 2 \end{cases} \quad (2.78)$$

the functions G_n are given by the following linear combinations (see Fig. 10)

$$\begin{aligned} H_i \geq 0, \quad r_p < r_1: G_n &= \mu_4 F_n(r_p, r_1) + \mu_3 F_n(r_1, r_2) + \mu_1 F_n(r_2, r_{Si}) \\ H_i \geq 0, \quad r_1 \leq r_p < r_2: G_n &= \mu_3 F_n(r_p, r_2) + \mu_1 F_n(r_2, r_{Si}) \\ H_i \geq 0, \quad r_2 \leq r_p < r_{Si}: G_n &= \mu_1 F_n(r_p, r_{Si}) \\ H_i < 0, \quad r_p < r_3: G_n &= \mu_4 F_n(r_p, r_3) + \mu_3 F_n(r_3, r_4) + \mu_2 F_n(r_4, r_{Si}) \\ H_i < 0, \quad r_3 \leq r_p < r_4: G_n &= \mu_3 F_n(r_p, r_4) + \mu_2 F_n(r_4, r_{Si}) \\ H_i < 0, \quad r_4 \leq r_p < r_{Si}: G_n &= \mu_2 F_n(r_p, r_{Si}) \end{aligned} \quad (2.79)$$

If ρ denotes the geocentric distance to the surface of a reference ellipsoid, then the radii are computed as follows

$$r_{Si} = \begin{cases} \rho_i + N_i + H_i, & H_i > 0 \\ \rho_i + N_i, & H_i \leq 0 \end{cases}$$

$$\begin{aligned}
 r_1 &= r_{Si} - H_i - 40 \text{ km} \\
 r_2 &= r_1 + 20 \text{ km} \\
 r_3 &= r_{Si} - 11 \text{ km} \\
 r_4 &= r_{Si} + H_i
 \end{aligned}
 \left. \vphantom{\begin{aligned} r_1 \\ r_2 \\ r_3 \\ r_4 \end{aligned}} \right\} \begin{aligned} &H_i \geq 0 \\ &H_i < 0 \end{aligned} \quad (2.80)$$

where N_i is the geoid undulation and

$$\rho_i = \frac{a}{\sqrt{1 + e'^2 \cos^2 \theta_i}} \quad (2.81)$$

a is the semimajor axis of the ellipsoid and e' is the second eccentricity, related to the flattening f by $e'^2 = 1/(1-f)^2 - 1$. The surface of the earth was divided into latitudinal bands each 5° wide, and each band was further subdivided into blocks having approximately the area of a $5^\circ \times 5^\circ$ block at the equator (Hajela, 1975). The elevation data that Sjöberg (1977) used provided values of H_i (on land or sea, see Fig. 10) at the center points (θ_i, λ_i) of these blocks. Finally, the undulation N_i was computed from the GEM10B harmonic coefficients (complete to degree and order 36, Lerch et al., 1978):

$$N_i = \bar{R} \sum_{n=2}^{36} \sum_{m=-n}^n \bar{z}_{nm} \bar{Y}_{nm}(\theta_i, \lambda_i) \quad (2.82)$$

where \bar{R} is the mean radius of the earth ($\bar{R}=6371$ km).

The modeling of the density as above does not conform to any established theory of isostasy. Since gravimetric evidence indicates that the mass excesses and deficiencies near the earth's surface are to some extent isostatically compensated deeper within, a model which incorporates this idea may be more authentic. Adopting the Airy-Heiskanen theory of isostasy (Heiskanen and Moritz, 1967, pp.135-6) with an assumed crustal thickness of $D=30$ km changes the density model only in the way the radii r_1, \dots, r_4 are computed (changing also μ_4 to 3.27 g/cm^3):

$$\begin{aligned}
 r_1 &= r_2 = r_{Si} - D - 5.45 H_i, & H_i > 0 \\
 r_3 &= r_{Si} - D - 2.73 H_i \\
 r_4 &= r_{Si} + H_i
 \end{aligned}
 \left. \vphantom{\begin{aligned} r_1 \\ r_3 \\ r_4 \end{aligned}} \right\} H_i \leq 0 \quad (2.83)$$

2.2.4 The Numerical Analysis

We consider only evaluations of the downward continuation error in gravity anomalies because they support most vividly the subsequent conclusions. The dependence of the error (2.53) on the radial distance r , necessitates a point by point evaluation. A dense grid of computed values over the entire earth is prohibited by the excessive computer time that would be required. Therefore, in order to estimate the downward continuation error, we must restrict ourselves to a judicious selection of points, which should be governed by our objective to detect the influence, not only of the earth's ellipticity, but also its topography. For example, consider a single profile in longitude across southern Africa ($\theta_0 = 102.5, -2.5 \leq \lambda, \leq 79.5$). Figure 11 shows the earth's shape in this profile as defined by the 5° mean elevations and the GEM10B geoid. For each of six points along the profile the first term in (2.53) was calculated with $\bar{n}=16, 36, \text{ and } 180$. Fig. 11 shows that, as a supposed downward continuation error, its values for low truncation degrees are inordinately, in fact unbelievably, large (see the introduction to chapter 2). As \bar{n} increases, this "error" generally decreases but not monotonically as shown in the Fig. 12 of partial sums. The summation to degree 180 is not strictly legitimate for an earth that is sampled on a 5° equal area grid of a total of 1654 values. That is, 1654 bits of information on the gravity field determine a maximum number of $1654 \approx (39+1)^2$ coefficients in its spectral harmonic representation (see also Shebalin, 1980). Therefore, the computed terms for degrees greater than 39 in no way reflect the earth's true gravity field, but the error terms to degree 180 are included to illustrate their general trend. Of course, in the evaluation of the error according to equation (2.53), we have totally neglected the higher degree contribution from $\bar{n}+1$ to infinity because it is unknown for this model.

From the few numerical results presented in Figures 11 and 12 and on the basis of the experiments described in section 2.1, as well as the discussion in section 2.2.2, the following inescapable conclusion is asserted. The errors depicted here, instead of showing the divergent character of the series, may rather be a reflection of the implicit choice of model for the earth's gravity field at the earth's surface. In the first place, Figures 4 and 5 of section 2.1 strongly suggest that the divergence is not manifest for low values of the truncation degree, especially near the equator. If we accept this, then the first part of equation (2.53), i.e. that being evaluated here, must be the difference between two entirely incompatible partial sums. In fact, the downward continued sum represents what could be

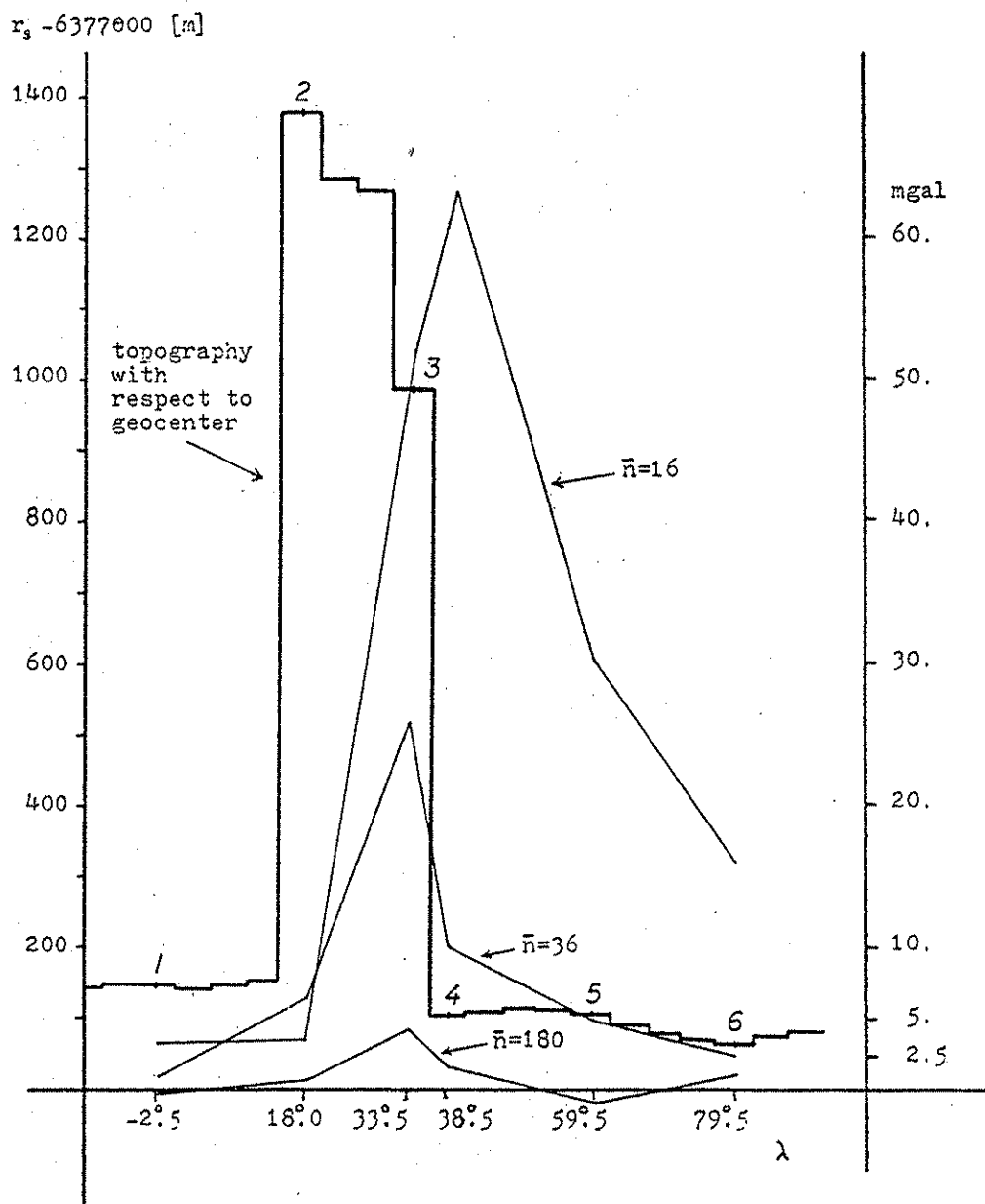


Figure 11: Topographical profile of southern Africa ($\theta_p = 102^{\circ}.5$, $-12^{\circ}.5 \leq \lambda_p \leq 90^{\circ}.0$) and values of partial sums of downward continuation error in gravity anomaly (volumetric density model): $\bar{n}=16, 36, 180$.

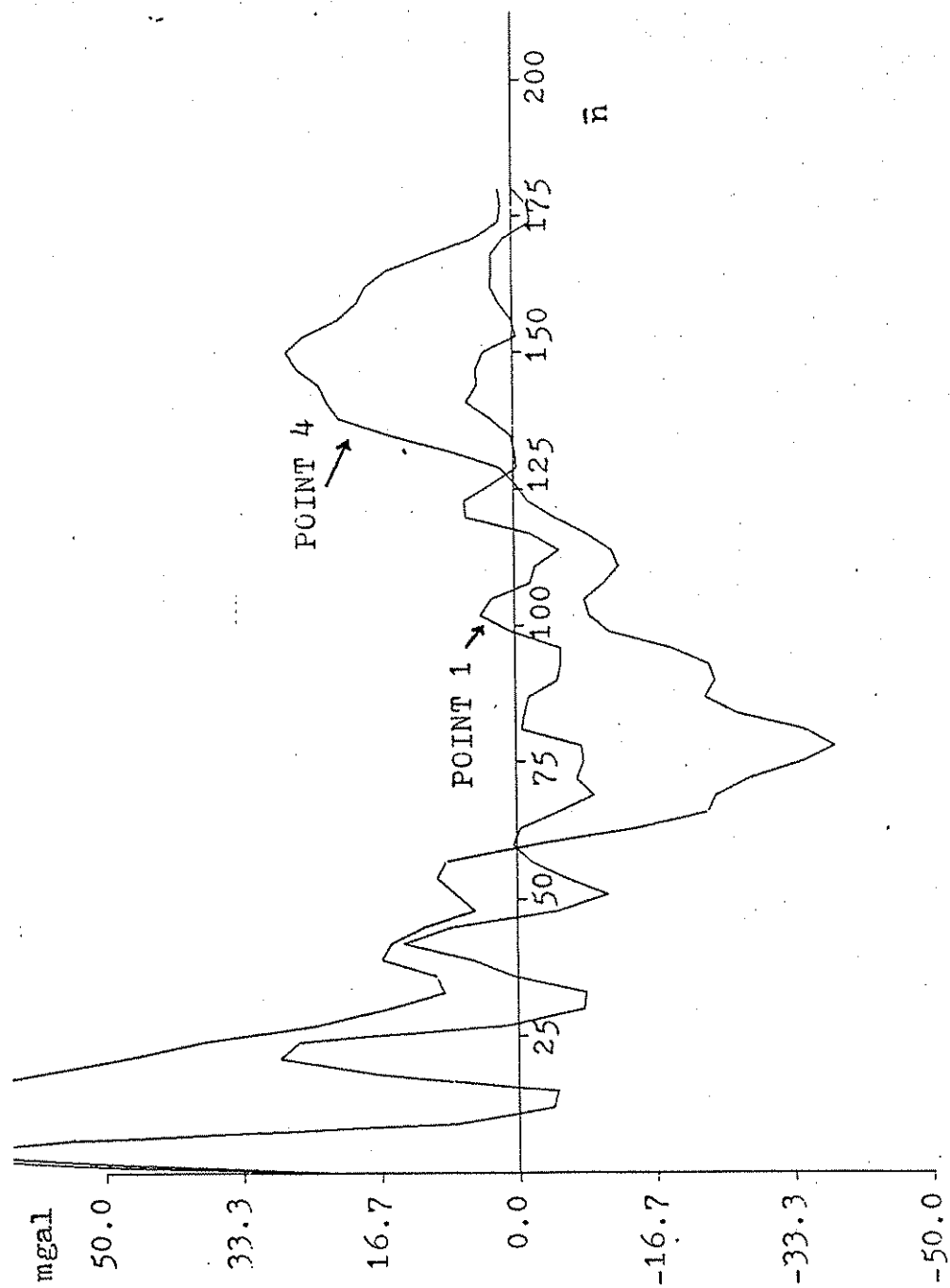


Figure 12: Partial sums of downward continuation error in Δg (volumetric density model) for points 1 and 4 of Figure 11 and $0 \leq \bar{n} \leq 180$.

called a "free air" spectrum of the gravity anomaly, while the "true" partial sum represents the spectrum of a field on a sphere that is partially embedded inside the earth. These arguments and the supporting numerical analysis reinforce the statement made in section 2.2.2 that the individual terms of equation (2.53), or in the strictest sense, any finite aggregate of terms, do not yield corrections to corresponding downward continued terms. This is reemphasized here because just such a procedure is occasionally implied in the literature (Cook, 1967; Morrison, 1970).

It may be noted that the kernel of the error integral (2.54) can be expanded as a series in $\hat{h}=1-r/r_p$. Then the infinite series of the constant and linear terms in \hat{h} of the downward continuation error sum to zero (see section 2.3.3). Without these terms the numerical values of Figure 11 would decrease by 1, 2, or more orders of magnitude. However, this does not alter the essential conclusion drawn above.

If $\bar{n} \rightarrow \infty$, then the "true" partial sum converges to the actual surface value of the gravity anomaly, approaching the downward continued series before it diverges. Some indication of this is given by Fig. 12 which shows an overall decrease in magnitude of the error with increasing \bar{n} . Thus, the next step in the analysis would be a densification of the grid on which the elevations and densities are assigned, thereby allowing expansions of the error to higher degrees. However, the modeling of the disturbing potential to a high degree by volumetric density distributions, or (what is almost equivalent) point masses, on a global scale is generally associated with a considerable computational effort (Needham, 1970), as a distribution of masses is sought which fits, in a least squares sense, our knowledge of the exterior gravity field (see also Balmino, 1972). In our case, no information on the earth's gravity field, except postulated mean densities, was used to define the distribution. One should therefore not expect this type of model to produce a close resemblance of the earth's potential. Even the use of the isostatic model of Airy and Heiskanen (equation (2.82)), instead of the model depicted in Figure 10, does not produce significant changes in the numerical results. This model is therefore not further used in the analysis of the downward continuation error. In the following section the earth model is also determined by a density distribution, which although not optimal, is entirely adequate to produce a realistic potential.

2.3 The Density Layer Model

2.3.1 The Derivation of the Error Series

Other than volumetric masses, Newtonian potentials are generated as well by simple layer and double layer density distributions. The formulation of the potential of a simple layer is completely analogous to (2.26), except that the integration is over a surface instead of a volume, and, of course, the mass is distributed as an infinitesimally thin layer on a surface. This leads directly to the Molodenskii boundary-value problem where the density of the layer, as an unknown quantity, is related to the boundary values of the resulting gravity field through an integral equation. This integral equation can be solved readily if the surface is a sphere and by successive approximations for more complicated surfaces such as the earth's surface. For the present purposes, the choice of formulation of the disturbing potential is dictated by our objective not only to find a reasonable solution to the density, but also to expand the potential in spherical harmonic series above and below the bounding sphere. The solution for the density will be determined approximately by our knowledge of the gravity field, that is, the bounding values; hence the disturbing potential generated by this density layer should more faithfully represent the actual exterior potential of the earth. Note that in the following, no attempt is made to find the optimal density that fits our knowledge of the gravity field.

This method of formulating the downward continuation error originates with Petrovskaya (1979). It is here derived in more detail and from a slightly different angle of approach.

Let us then consider the following formulation of the disturbing potential (with respect to a suitable reference potential), according to Brovar (1964),

$$T_p = \frac{R^2}{4\pi} \iint_{\sigma} v(\theta, \lambda) E d\sigma \quad (2.84)$$

where, as before, R is the radius of the bounding sphere; v is a generalized density which contains also the inclination term that transforms the integration over the earth's surface to an integration over the unit sphere; and the kernel E is a function of θ , λ , r_p , θ_p , λ_p , and is defined

by

$$E = -\frac{\ell}{r_p^2} - \frac{r_s \cos \psi}{r_p^2} \ln \frac{r_p + \ell - r_s \cos \psi}{2r_p} \quad (2.85)$$

where $r_s = r_s(\theta, \lambda)$ describes the radial distance to the earth's surface. In general, the definition of the kernel is contingent only on the requirement that the function T be a potential, i.e. harmonic in free space and regular at infinity, otherwise it is arbitrary. In order for T to be harmonic, E as a function of the point P must satisfy Laplace's equation and be regular at infinity. This was shown by Brovar (1964) to be the case for the above definition; in fact, the difference between E and the generalized Stokes function S is easily recognized to be (Heiskanen and Moritz, 1967, p.93)

$$3E - S = \frac{5r_s \cos \psi}{r_p^2} - \frac{1}{r_p} - \frac{2}{\ell} \quad (2.86)$$

Stokes' function and the terms on the right side of (2.86) all are harmonic functions. Unlike the usual density integral in which $1/\ell$ is the kernel, the expression (2.84) has continuous derivatives when crossing the surface and is therefore characteristic of the potential of a volumetric density distribution (see Brovar, 1964, and Moritz, 1966b, p.55).

The radial derivative of T is

$$\frac{\partial T}{\partial r_p} = \frac{R^2}{4\pi} \iint_{\sigma} v(\theta, \lambda) \frac{\partial E}{\partial r_p} d\sigma \quad (2.87)$$

where

$$\frac{\partial E}{\partial r_p} = \frac{2\ell - r_s \cos \psi}{r_p^3} - \frac{1}{\ell r_p} + \frac{2r_s \cos \psi}{r_p^3} \ln \frac{r_p + \ell - r_s \cos \psi}{2r_p} \quad (2.88)$$

This combined with $2E/r_p$ results in the simple expression

$$-\frac{\partial E}{\partial r_p} - \frac{2}{r_p} E = \frac{1}{r_p} \left(\frac{1}{\ell} - \frac{r_s \cos \psi}{r_p^2} \right) \quad (2.89)$$

For points P on the earth's surface, we have the boundary condition (with the spherical approximation as described for (2.42))

$$\Delta g_p = -\frac{\partial T_p}{\partial r_p} - \frac{2}{r_p} T_p \quad (2.90)$$

so that, because the derivatives of the right side of (2.84) are continuous at the surface,

$$\Delta g_p = \frac{R^2}{4\pi r_p} \iint_{\sigma} v(\theta, \lambda) \left(\frac{1}{\ell} - \frac{r_s \cos \psi}{r_p^2} \right) d\sigma \quad (2.91)$$

and the reason for the choice of E is now apparent. The expression (2.91) is a Fredholm integral equation of the first kind and if the earth's surface is approximated by a sphere with radius \bar{R} ($r_s = \text{const} = \bar{R}$, $r_p = \bar{R}$) on which Δg is a known function, the solution for the density is found by expanding $1/\ell$ and Δg in series of spherical harmonics (Petrovskaya, 1979; see also equation (2.7)):

$$\begin{aligned} \sum_{n=0}^{\infty} \sum_{m=-n}^n \tilde{g}_{nm} \bar{Y}_{nm}(\theta_p, \lambda_p) &= \Delta g_p = \\ &= \frac{R}{4\pi \bar{R}^2} \sum_{\substack{n=0 \\ n \neq 1}}^{\infty} \sum_{m=-n}^n \frac{1}{2n+1} \iint_{\sigma} v(\theta, \lambda) \bar{Y}_{nm}(\theta, \lambda) d\sigma \bar{Y}_{nm}(\theta_p, \lambda_p) \end{aligned} \quad (2.92)$$

This holds for arbitrary points P on the sphere, hence

$$\tilde{g}_{nm} = \frac{1}{2n+1} \frac{R^2}{4\pi \bar{R}^2} \iint_{\sigma} v(\theta, \lambda) \bar{Y}_{nm}(\theta, \lambda) d\sigma \quad (2.93)$$

Therefore, the spectrum of the density in spherical approximation is $(2n+1)\tilde{g}_{nm}$:

$$v(\theta, \lambda) = \left(\frac{R}{r}\right)^2 \sum_{n=0}^{\infty} \sum_{m=-n}^n (2n+1) \tilde{g}_{nm} \bar{Y}_{nm}(\theta, \lambda) \quad (2.94)$$

Because the gravity anomaly has no first degree term in its series representation (equation (2.51)), this term for the density, hence for the potential T , must be obtained from other data.

The series expansion of Δg follows directly from (2.91) if the boundary condition (2.90) is used as the definition of the gravity anomaly in all of space. Using (2.7) and (2.8), we obtain for $r_p > R$

$$\Delta g_p = \sum_{n=0}^{\infty} \sum_{m=-n}^n \left(\frac{R}{r_p}\right)^{n+2} g_{nm} \bar{Y}_{nm}(\theta_p, \lambda_p) \quad (2.95)$$

where

$$g_{nm} = \begin{cases} 0 & , \quad n = 1 \\ \frac{1}{2n+1} \frac{1}{4\pi} \iint_{\sigma} v(\theta, \lambda) \left(\frac{r_s}{R}\right)^n \bar{Y}_{nm}(\theta, \lambda) d\sigma & , \quad n \neq 1 \end{cases} \quad (2.96)$$

and for $r_p < R$

$$\Delta g_p = \sum_{n=0}^{\infty} \sum_{m=-n}^n c_{nm}(r_p) \bar{Y}_{nm}(\theta_p, \lambda_p) \quad (2.97)$$

where

$$c_{nm}(r_p) = \begin{cases} \frac{1}{3} \frac{R^2}{4\pi r_p^2} \iint_{\sigma_2} v(\theta, \lambda) \left[\left(\frac{r_p}{r_s}\right)^2 - \frac{r_s}{r_p} \right] \bar{Y}_{1m}(\theta, \lambda) d\sigma & , \quad n = 1 \\ \frac{1}{2n+1} \frac{R^2}{4\pi r_p^2} \left[\iint_{\sigma_1} v(\theta, \lambda) \left(\frac{r_s}{r_p}\right)^n \bar{Y}_{nm}(\theta, \lambda) d\sigma + \right. & (2.98) \\ \left. + \iint_{\sigma_2} v(\theta, \lambda) \left(\frac{r_p}{r_s}\right)^{n+1} \bar{Y}_{nm}(\theta, \lambda) d\sigma \right] & , \quad n \neq 1 \end{cases}$$

where $\sigma_1 = \{(\theta, \lambda)/r_s, (\theta, \lambda) \leq r_p\}$ and $\sigma_2 = \{(\theta, \lambda)/r_s, (\theta, \lambda) > r_p\}$. The downward continuation error is the difference between the truncated series (2.95) evaluated at the earth's surface and the true series expansion (2.97):

$$\begin{aligned} \varepsilon(\Delta \hat{g}) = & \sum_{n=0}^{\bar{n}} \sum_{m=-n}^n d_{nm}(r_p) \bar{Y}_{nm}(\theta_p, \lambda_p) + \\ & + \sum_{n=\bar{n}+1}^{\infty} \sum_{m=-n}^n d'_{nm}(r_p) \bar{Y}_{nm}(\theta_p, \lambda_p) \end{aligned} \quad (2.99)$$

where

$$\begin{aligned} d_{nm}(r_p) &= \left(\frac{R}{r_p}\right)^{n+2} g_{nm} - c_{nm}(r_p) \\ &= \frac{R^2}{4\pi^2 p} \frac{1}{2n+1} \iint_{\sigma_2} v(\theta, \lambda) \left[\left(\frac{r_s}{r_p}\right)^n - \left(\frac{r_p}{r_s}\right)^{n+1} \right] \cdot \bar{Y}_{nm}(\theta, \lambda) d\sigma, \quad n \geq 0 \end{aligned} \quad (2.100)$$

and

$$d'_{nm}(r_p) = -c_{nm}(r_p) = d_{nm}(r_p) - \left(\frac{R}{r_p}\right)^{n+2} g_{nm} \quad (2.101)$$

The expansion into series of the disturbing potential is more involved and requires the expansion of the kernel E into series which are valid below, as well as above, the bounding sphere. Anticipating the result, let us consider the integral (Gradshteyn and Ryzshik, 1980, p.83)

$$\int \frac{r_p}{l} dr_p = l + r_s \cos \psi \ln 2(r_p + l - r_s \cos \psi) + a(r_s) \quad (2.102)$$

where $a(r_s)$ is the constant of integration. Substituting

the uniformly convergent series (2.7) into the integral yields

$$\begin{aligned} \int \frac{r_p}{l} dr_p &= \sum_{n=0}^{\infty} \int \left(\frac{r_s}{r_p} \right) dr_p P_n(\cos \psi) \\ &= - \sum_{\substack{n=0 \\ n \neq 1}}^{\infty} \frac{1}{n-1} \frac{r_s^n}{r_p^{n-1}} P_n(\cos \psi) + r_s \cos \psi \ln \frac{r_p}{r_s} + b(r_s) \end{aligned} \quad (2.103)$$

where $r_p > r_s$. Hence

$$\begin{aligned} \sum_{\substack{n=0 \\ n \neq 1}}^{\infty} \frac{1}{n-1} \frac{r_s^n}{r_p^{n-1}} P_n(\cos \psi) &= -l - r_s \cos \psi \ln \frac{2(r_p + l - r_s \cos \psi)}{r_p} \\ &\quad + b(r_s) - a(r_s) \end{aligned} \quad (2.104)$$

This holds for any $r_p > r_s$, in particular as $r_p \rightarrow \infty$, so that

$$\lim_{r_p \rightarrow \infty} (l - r_p) + 0 = -r_s \cos \psi \ln 4 + b(r_s) - a(r_s) \quad (2.105)$$

Rewriting $l - r_p$ as

$$l - r_p = \frac{\sqrt{1 + \frac{r_s^2}{r_p^2} - \frac{2r_s \cos \psi}{r_p}} - 1}{\frac{1}{r_p}} \quad (2.106)$$

L'Hopital's rule gives

$$\lim_{r_p \rightarrow \infty} (l - r_p) = -r_s \cos \psi \quad (2.107)$$

Therefore the total constant of integration is given by

$$b(r_s) - a(r_s) = r_s \cos \psi (\ln 4 - 1) \quad (2.108)$$

Putting (2.108) into (2.104) finally yields

$$\sum_{\substack{n=0 \\ n \neq 1}}^{\infty} \frac{1}{n-1} \frac{r_s^n}{r_p^{n-1}} P_n(\cos \psi) = \quad (2.109)$$

$$- \ell - r_s \cos \psi \ln \frac{r_p + \ell - r_s \cos \psi}{2r_p} - r_s \cos \psi$$

Similarly, the uniformly convergent series (2.8) substituted into the integral of equation (2.102) results in

$$\begin{aligned} \int \frac{r_p}{\ell} dr_p &= \sum_{n=0}^{\infty} \int \left(\frac{r_p}{r_s}\right)^{n+1} dr_p P_n(\cos \psi) \\ &= \sum_{n=0}^{\infty} \frac{1}{n+2} \frac{r_p^{n+2}}{r_s^{n+1}} P_n(\cos \psi) + c(r_s) \end{aligned} \quad (2.110)$$

where $c(r_s)$ is the integration constant, and $r_p < r_s$. With (2.102) this becomes

$$\begin{aligned} \sum_{n=0}^{\infty} \frac{1}{n+2} \frac{r_p^{n+2}}{r_s^{n+1}} P_n(\cos \psi) &= \ell + r_s \cos \psi \ln 2(r_p + \ell - r_s \cos \psi) \\ &\quad + a(r_s) - c(r_s) \end{aligned} \quad (2.111)$$

This also holds for $r_p = r_s$ if $\psi \neq 0$, since then $P_n(\cos \psi)/(n+2) = O(n^{-1/2})$ and the series converges. Hence

$$\begin{aligned} r_s \sum_{n=0}^{\infty} \frac{1}{n+2} P_n(\cos \psi) &= \ell_s + r_s \cos \psi \ln 2(r_s + \ell_s - r_s \cos \psi) \\ &\quad + a(r_s) - c(r_s) \end{aligned} \quad (2.112)$$

where $\ell_s = r_s \sqrt{2-2\cos\psi}$. But the first two terms on the right side of (2.112) can be expressed as a series according to (2.109) with $r_p = r_s$ ($\psi \neq 0$). Thus

$$a(r_s) - c(r_s) = r_s \sum_{n=0}^{\infty} \frac{1}{n+2} P_n(\cos\psi) + r_s \sum_{\substack{n=0 \\ n \neq 1}}^{\infty} \frac{1}{n-1} P_n(\cos\psi) + r_s \cos\psi - r_s \cos\psi \ln 4r_s \quad (2.113)$$

Putting this into (2.111) and combining the series, we obtain

$$\begin{aligned} \sum_{\substack{n=0 \\ n \neq 1}}^{\infty} \left[r_s \left(\frac{1}{n+2} + \frac{1}{n-1} \right) - \frac{1}{n+2} \frac{r_p^{n+2}}{r_s^{n+1}} \right] P_n(\cos\psi) = \\ = -\ell - r_s \cos\psi \ln \frac{r_p + \ell - r_s \cos\psi}{2r_p} - \left(\frac{4}{3} r_s - \frac{1}{3} \frac{r_p^3}{r_s^2} \right) \cos\psi \quad (2.114) \\ + r_s \cos\psi \ln \frac{r_p}{r_s} \end{aligned}$$

Recalling the definition (2.85) of the kernel E and using (2.109) and (2.114), we finally arrive at the desired series representation:

$$E = \begin{cases} \sum_{\substack{n=0 \\ n \neq 1}}^{\infty} \frac{1}{n-1} \frac{r_s^n}{r_p^{n+1}} P_n(\cos\psi) + \frac{r_s \cos\psi}{r_p^2}, & r_p > r_s \\ \sum_{\substack{n=0 \\ n \neq 1}}^{\infty} \left[\frac{r_s}{r_p} \left(\frac{1}{n+2} + \frac{1}{n-1} \right) - \frac{1}{n+2} \frac{r_p^n}{r_s^{n+1}} \right] P_n(\cos\psi) + \\ + \frac{r_s \cos\psi}{r_p^2} \left[\frac{4}{3} - \frac{1}{3} \left(\frac{r_p}{r_s} \right)^3 + \ln \frac{r_p}{r_s} \right], & r_p < r_s, \\ & \psi \neq 0 \end{cases} \quad (2.115)$$

The kernel E , as a function of the point P , is harmonic everywhere except on the line segment $r_p \leq r_s$, $\psi = 0$ where it is not defined and where in any case we will have no need to evaluate it.

Substituting the series (2.115) into the formula for the disturbing potential (2.84),

$$T_p = \sum_{n=0}^{\infty} \sum_{m=-n}^n \left(\frac{R}{r_p}\right)^{n+1} t_{nm} \bar{Y}_{nm}(\theta_p, \lambda_p), \quad r_p > R \quad (2.116)$$

where

$$t_{nm} = \begin{cases} \frac{R}{4\pi} \frac{1}{2n+1} \iint_{\sigma} \frac{v(\theta, \lambda)}{n-1} \left(\frac{r_s}{R}\right)^n \bar{Y}_{nm}(\theta, \lambda) d\sigma, & n \neq 1 \\ \frac{R}{4\pi} \frac{1}{3} \iint_{\sigma} v(\theta, \lambda) \frac{r_s}{R} \bar{Y}_{1m}(\theta, \lambda) d\sigma, & n = 1 \end{cases} \quad (2.117)$$

and for points below the bounding sphere:

$$T_p = \sum_{n=0}^{\infty} \sum_{m=-n}^n b_{nm}(r_p) \bar{Y}_{nm}(\theta_p, \lambda_p), \quad r_p < R \quad (2.118)$$

where

$$b_{nm}(r_p) = \frac{R^2}{4\pi} \frac{1}{2n+1} \left[\frac{1}{n-1} \iint_{\sigma_1} v \frac{r_s^n}{r_p^{n+1}} \bar{Y}_{nm}(\theta, \lambda) d\sigma + \iint_{\sigma_2} v \left[\frac{r_s^2}{r_p^2} \left(\frac{1}{n+2} + \frac{1}{n-1} \right) - \frac{1}{n+2} \frac{r_p^n}{r_s^{n+1}} \right] \bar{Y}_{nm}(\theta, \lambda) d\sigma \right], \quad n \neq 1 \quad (2.119)$$

$$b_{1m}(r_p) = \frac{R^2}{4\pi} \frac{1}{3} \left[\iint_{\sigma_1} v \frac{r_s}{r_p^2} \bar{Y}_{1m}(\theta, \lambda) d\sigma + \iint_{\sigma_2} v \frac{r_s}{r_p^2} \left[\frac{4}{3} - \frac{1}{3} \left(\frac{r_p}{r_s} \right)^3 + 2n \frac{r_p}{r_s} \right] \bar{Y}_{1m}(\theta, \lambda) d\sigma \right], \quad n = 1$$

With the spherical approximations as defined for (2.56) the expansions of the height anomaly follow immediately from (2.116) and (2.118): for $r_p > R$,

$$\zeta_p = \sum_{n=0}^{\infty} \sum_{m=-n}^n \left(\frac{R}{r_p}\right)^{n-1} z_{nm} \bar{Y}_{nm}(\theta_p, \lambda_p), \quad z_{nm} = \frac{R^2}{\kappa M} t_{nm} \quad (2.120)$$

and for $r_p < R$,

$$\zeta_p = \sum_{n=0}^{\infty} \sum_{m=-n}^n y_{nm}(r_p) \bar{Y}_{nm}(\theta_p, \lambda_p), \quad y_{nm}(r_p) = \frac{r_p^2}{\kappa M} b_{nm}(r_p) \quad (2.121)$$

The above series and the corresponding series (2.97) for the gravity anomaly, although formulated specifically for points below the bounded sphere, may be regarded as convergent series for the height, or gravity, anomaly anywhere in the exterior space, since they revert to (2.120) and (2.95) for $r_p > R$; that is,

$$y_{nm}(r_p) = \left(\frac{R}{r_p}\right)^{n-1} z_{nm}; \quad c_{nm}(r_p) = \left(\frac{R}{r_p}\right)^{n+2} g_{nm}; \quad (2.122)$$

$r_p > R$

Finally, the downward continuation error of the height anomaly is obtained by subtracting (2.121) from the series (2.120) truncated at \bar{n} :

$$\begin{aligned} \varepsilon(\hat{\zeta}_p) = & \sum_{n=0}^{\bar{n}} \sum_{m=-n}^n e_{nm}(r_p) \bar{Y}_{nm}(\theta_p, \lambda_p) + \\ & + \sum_{n=\bar{n}+1}^{\infty} \sum_{m=-n}^n e'_{nm}(r_p) \bar{Y}_{nm}(\theta_p, \lambda_p) \end{aligned} \quad (2.123)$$

where

$$e_{nm}(r_p) = \left(\frac{R}{r_p}\right)^{n-1} \frac{R^2}{\kappa M} t_{nm} - \frac{r_p^2}{\kappa M} b_{nm}(r_p) = \quad (2.124)$$

$$= \frac{r_p R^2}{4\pi\kappa M} \frac{1}{2n+1} \left\{ \begin{aligned} & \iint_{\sigma_2} v \left[\frac{1}{n+2} \left(\frac{r_p}{r_s} \right)^{n+1} + \frac{1}{n-1} \left(\frac{r_s}{r_p} \right)^n - \frac{r_s}{r_p} \left(\frac{1}{n+2} + \frac{1}{n-1} \right) \right] \bar{Y}_{nm}(\theta, \lambda) d\sigma, \quad n \neq 1 \\ & \iint_{\sigma} v \left[\frac{1}{3} \left(\frac{r_p}{r_s} \right)^2 - \frac{1}{3} \frac{r_s}{r_p} + \frac{r_s}{r_p} \ln \frac{r_s}{r_p} \right] \bar{Y}_{1m}(\theta, \lambda) d\sigma, \quad n = 1 \end{aligned} \right.$$

and

$$e'_{nm}(r_p) = \frac{r_p^2}{\kappa M} b_{nm}(r_p) = e_{nm}(r_p) - \frac{R^2}{\kappa M} \left(\frac{R}{r_p} \right)^{n-1} t_{nm} \quad (2.125)$$

2.3.2 The Description of the Model

As with the volumetric density model certain simplifications of the earth's surface are required in order to evaluate the integrations; however, this model places almost no limits on the complexity of the density function $v(\theta, \lambda)$, given by (2.94). The necessity of a highly complex model, when aiming for expansions of the potential and gravity anomaly to degree and order, say 300, is prescribed essentially by the Nyquist law. Although this law holds only for expansions of functions in Cartesian space, for the present purposes it serves as a sufficient guide. The Nyquist law (applied to a great circle) states that the Fourier spectral components of a function whose values are known at a uniform interval of $180^\circ/\bar{n}$ can be resolved to a degree no higher than \bar{n} (Bath, 1974, p.146). Hence, for $\bar{n}=300$, we should specify values of the model on a 0.6° grid. Instead of equal area blocks, as for the volumetric density model, equiangular blocks delimited by coordinate lines will be used here so as to take advantage of the Fast Fourier Transform of data along bands of constant latitude (see below) and thereby to make the computations manageable. However, the convergence of the meridians toward the poles is accompanied by an increase in the concentration of the data. This nonuniformity of the data implies a somewhat larger frequency content.

Unfortunately, data sets at a resolution of $0.6^\circ \approx 67$ km do not exist, especially for the gravity field. With the (180,180) solution of harmonic coefficients (derived by Rapp from $1^\circ \times 1^\circ$ mean gravity anomalies obtained in (Rapp, 1978)) as a base, the coefficients from degree 181 to 300 could be generated from random numbers which decay according to a specified degree variance model for the gravity anomaly. Such a model was obtained by Tscherning and Rapp (1974) and, in fact, it has not been significantly vitiated in light of

the more recent (180,180) solution (Rapp, 1979). However, it was decided to use the more complex "two-component" model (ibid.), since its parameters were determined, in essence, by this high degree solution. On the other hand, to obtain a smooth transition from the actual degree variances to the model, the (180,180) solution was used only up to degree 100:

$$\tilde{g}_{nm} = \begin{cases} \frac{1}{\beta_n} (\text{coefficients of the (180, 180) solution}), & n = 2, \dots, 100 \\ u_{nm} \sqrt{\frac{c_n}{b_n}}, & n = 101, \dots, 300 \end{cases} \quad (2.126)$$

where β_n is the (approximate) frequency response for the operator which averages a function over $1^\circ \times 1^\circ$ blocks (Pellinen, 1966; $\psi_0 = 0.564$ in equation (2.63)), the u_{nm} are uniformly distributed random values in the interval $[-0.5, 0.5]$, b_n is their degree variance,

$$b_n = \sum_{m=-n}^n u_{nm}^2 \quad (2.127)$$

and the gravity anomaly degree variance c_n is modeled in mgal^2 according to (see Rapp, 1979)

$$c_n = \frac{3.405(n-1)}{n+1} (0.998006)^{n+2} + \frac{140.03(n-1)}{(n-2)(n+2)} (0.914232)^{n+2}, \quad n \geq 3 \quad (2.128)$$

The division of the (180,180) coefficients, being spectral components of the 1° mean anomaly, by β_n transforms them to spectral components of the point anomaly (see equation (2.64)).

We note that the coefficients (2.126) define only the density distribution, as given by (2.94), and not the gravity field of the model. The expansion (2.94) for the density, being the solution to the integral equation (2.91) if the earth is a sphere, obviously does not correspond to reality. But since the earth is, in fact, nearly spherical and a lack of knowledge necessitates a certain amount of simulation of the data, a density model based on (2.94), though not optimal, is with these arguments also not

indeterminable. (Petrovskaya (1979) gives a formula by which the integral equation could be solved iteratively, given the shape of the earth's surface; however, it is not necessary to implement this procedure for the present purposes.) The zero and first degree terms in the expansion of the density have been omitted on the usual assumption associated with the spherical approximation that the average and first moments of the density with respect to the origin of the coordinate system are zero. However, when the density is weighted by the surface radius as in (2.117), the first moments do not vanish and the potential of the earth model does contain a first degree term. (Also, a zero degree term is present because the discrete grid values of the density do not average exactly to zero.)

The earth's surface can be modeled in the first place on the basis of $1^\circ \times 1^\circ$ mean elevations, available as a global data set (provided by DMAAC, 1979) and describing the surface with respect to sea level with a resolution of approximately 110 km (higher towards the poles). The additional finer detail from degree 181 to 300 again must be fabricated by a random number generator. This is facilitated and improves the verity of the model if, instead of ascertaining an independent degree variance model for elevations, we invoke the probable correlation between high degree potential coefficients and short wavelength topography (Lambeck, 1979, p.590). This correlation can be derived by assuming that the high degree components of the disturbing potential are generated by the masses of the topographic features, including isostatic compensations, condensed onto a mean earth sphere. In order to account for the lower density, $\mu_w = 1.03 \text{ g/cm}^3$, of the oceans relative to the crust, "equivalent rock topography" has been introduced (Balmino et al., 1973) whereby the oceans have been replaced, on the ocean floor, by an equivalent rock layer of crustal density μ_c and thickness $\mu_w d / \mu_c$, where d is the depth of the ocean ($d > 0$). The equivalent rock topography, H_r , is measured with respect to the geoid and is therefore negative in ocean areas:

$$H_r(\theta, \lambda) = \begin{cases} H(\theta, \lambda) & , \text{ for land areas} \\ -(1 - \frac{\mu_w}{\mu_c})d & , \text{ for ocean areas} \end{cases} \quad (2.129)$$

Lambeck (ibid., p.592) gives the following relationship between the (disturbing) potential harmonic coefficients t_{nm} and the corresponding coefficients of the equivalent rock topography h_{nm} :

$$t_{nm} = 4\pi\bar{R}\kappa \mu_c \left[1 - \left(\frac{\bar{R}-D}{\bar{R}}\right)^n\right] \frac{h_{nm}}{2n+1} \quad (2.130)$$

where μ_c is assumed constant (2.67 g/cm³), \bar{R} is the mean earth radius (6371 km), and D is the depth of compensation in the Airy-Heiskanen isostasy model (a value of $D=50$ km was found to give better agreement between the (180,180) solution and the 1°x1° elevations than $D=30$ km (Rapp, private communication)).

The coefficients h_{nm} were determined to degree 180 from the 1°x1° mean elevation data set (which includes negative depths $-d$ in ocean areas) and the definition of H_r (2.129) and hence constitute its spectrum for $0 \leq n \leq 180$. The spectrum from degree 181 to 300, assumed to be related to the potential spectrum according to (2.130), is directly obtained from the random coefficients (2.126):

$$h_{nm} = \begin{cases} \frac{1}{4\pi} \iint_{\sigma} H_r(\theta, \lambda) \bar{Y}_{nm}(\theta, \lambda) d\sigma, & 0 \leq n \leq 180 \\ \frac{2n+1}{n-1} \frac{u_{nm}}{4\pi\kappa \mu_c \left[1 - \left(\frac{\bar{R}-D}{\bar{R}}\right)^n\right]} \sqrt{\frac{c_n}{b_n}}, & 181 \leq n \leq 300 \end{cases} \quad (2.131)$$

Having thus obtained its spectrum to degree 300, the equivalent rock topography is evaluated on a 0.6 by 0.6 global grid using the expansion

$$H_r(\theta, \lambda) = \sum_{n=0}^{300} \sum_{m=-n}^n h_{nm} \bar{Y}_{nm}(\theta, \lambda) \quad (2.132)$$

and the actual topographic surface of the model (with respect to the geoid) is then

$$H(\theta, \lambda) = \begin{cases} H_r(\theta, \lambda), & \text{if } H_r(\theta, \lambda) \geq 0 \\ 0, & \text{if } H_r(\theta, \lambda) < 0 \end{cases} \quad (2.133)$$

The degree variances of h_{nm} are shown in Fig. 13. Although the coefficients h_{nm} , $0 \leq n \leq 180$ refer to mean topography, no unsmoothing of this portion of the spectrum was performed,

as with the potential spectrum (see (2.126)), since it would have destroyed the essentially continuous transition to the modeled high degree part of the spectrum. These types of manipulations, while perhaps not strictly acceptable from the theoretical viewpoint, are designed to produce a model which renders as faithfully a representation of the earth as possible including the requirement that the spectra of gravity and topography decay with no major jump discontinuities.

The coefficients \tilde{g}_{nm} (equation (2.126)) find further utility in the definition of the geoid height $N(\theta, \lambda)$

$$N(\theta, \lambda) = \frac{\bar{R}^3}{\kappa M} \sum_{n=2}^{300} \sum_{m=-n}^n \frac{\tilde{g}_{nm}}{n-1} \bar{Y}_{nm}(\theta, \lambda) \quad (2.134)$$

This, of course, is not the true undulation of the earth model, since the set of coefficients \tilde{g}_{nm} is not the gravity anomaly spectrum of the model; but (2.134) serves well enough for the present purposes. Finally, the geocentric distance to the model surface is given by

$$r_s(\theta, \lambda) = \rho(\theta) + N(\theta, \lambda) + H(\theta, \lambda) \quad (2.135)$$

where ρ is the geocentric distance to the reference ellipsoid (equation (2.81)).

A typical profile of the resulting model surface is depicted in Fig. 14, and contrasted with the 5° and 1° mean values of r_s . The farthest distance of the modeled surface from the origin of coordinates is $r_s(\max) = 6381989.115$ m, at a latitude of -9.3° . The radius of the bounding sphere was rounded to $R = 6382000$ m. The RMS deviations of the surface from this bounding sphere range from 3760 m at the equator to 25100 m near the north pole.

2.3.3 The Equations for the Numerical Analysis

The integration of the density integrals is tractable only if r_s and γ are assumed constant within each $0.6^\circ \times 0.6^\circ$ equiangular compartment. The resulting salient surface does not satisfy Liapunov's condition of continuous curvature (Günter, 1967) and the convergence of the potential and its first derivatives to their respective values on the surface is not guaranteed. However, the need for evaluations

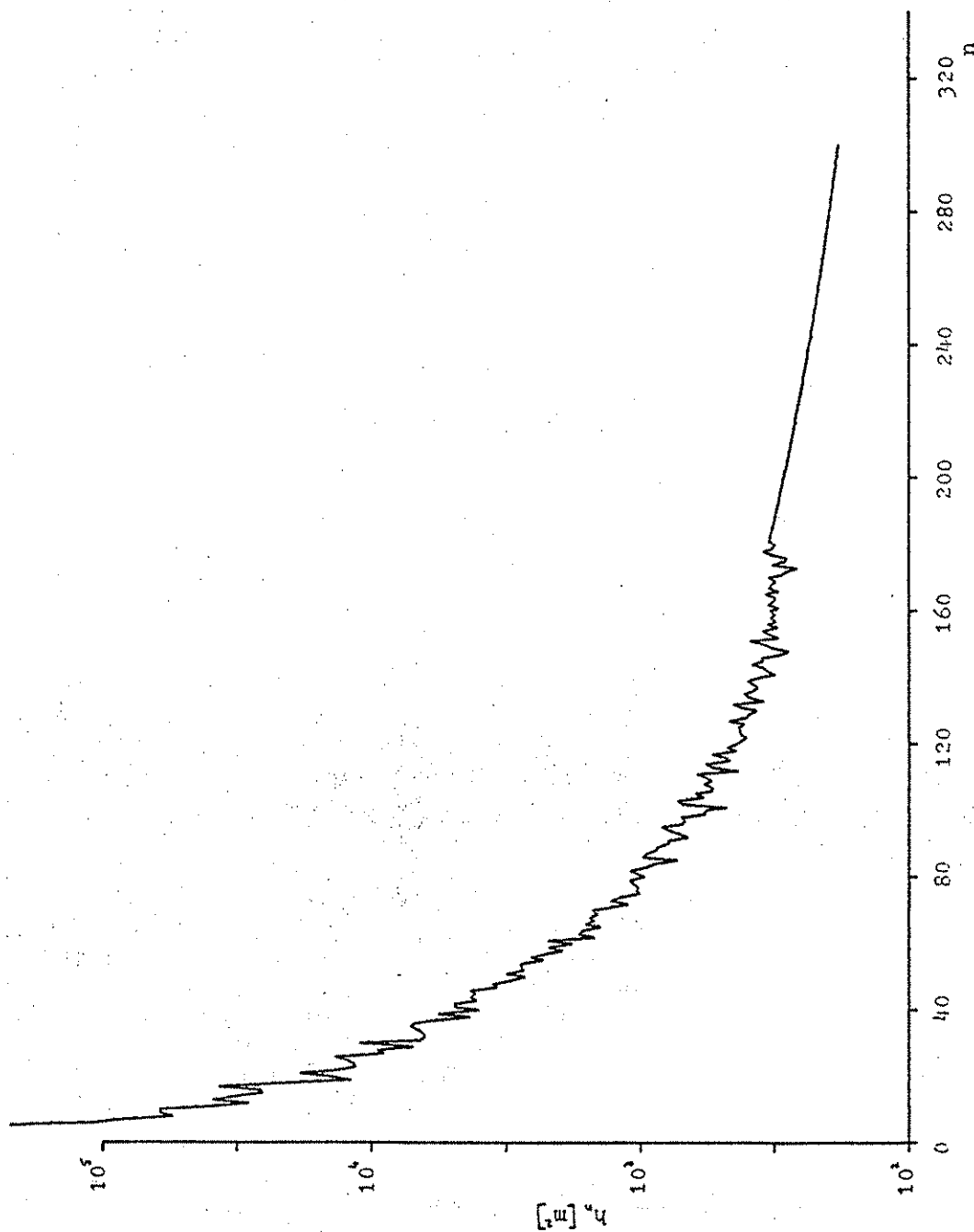


Figure 13: Degree variances of equivalent rock topography used to define model of earth's surface.

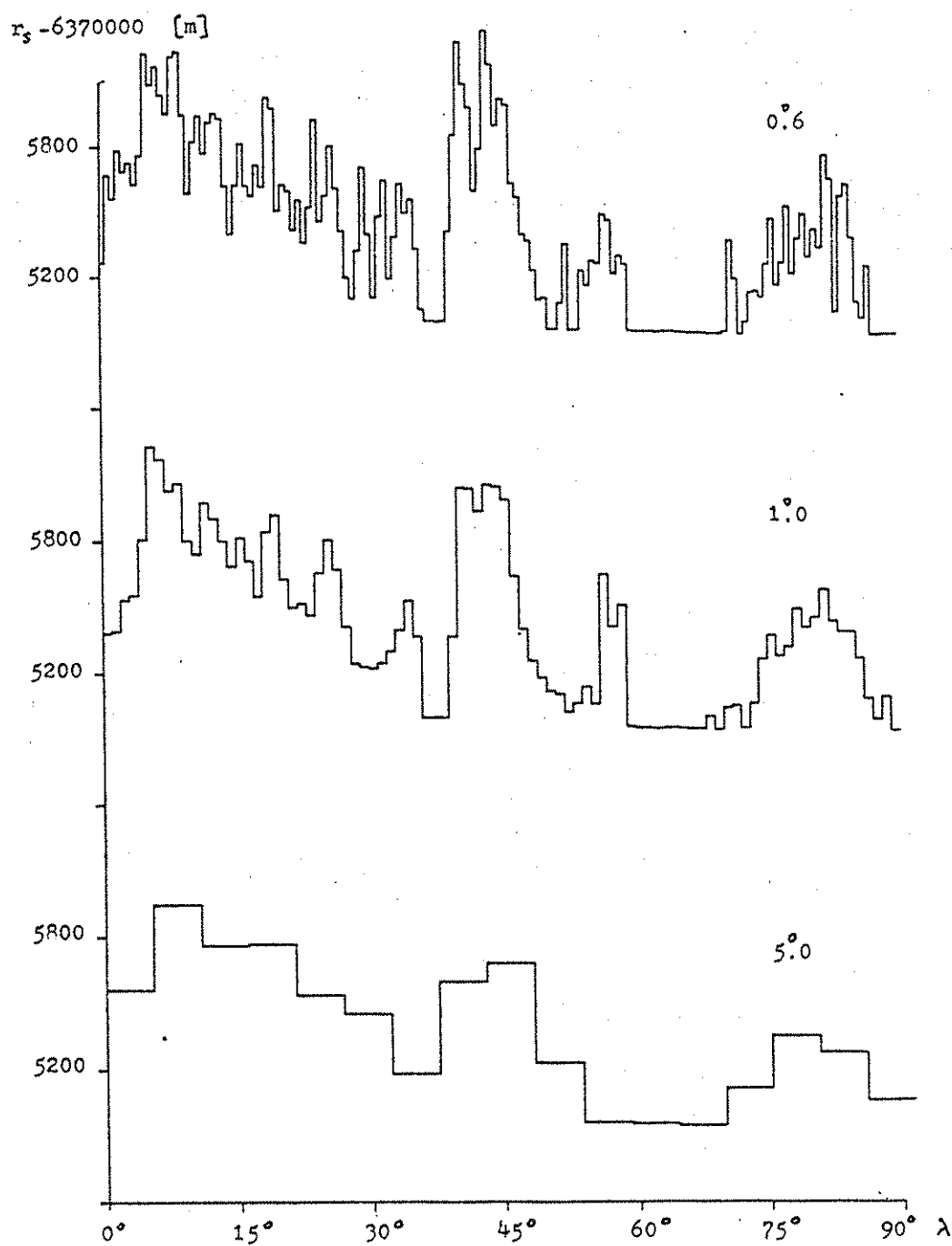


Figure 14: Comparison of Topographical profiles $\varphi = 22.5^\circ$, $0^\circ \leq \lambda \leq 90^\circ$, based on 5° , 1° , and 0.6° mean elevations and geoid undulations (0.6° mean elevations/undulations include random harmonics for $101 \leq n \leq 300$).

exactly on the surface will generally not arise in these numerical studies. We then have, for example, from equation (2.117)

$$t_{nm} = \frac{R}{4\pi} \frac{\eta_n}{2n+1} \sum_{i=0}^{N-1} \sum_{j=0}^{2N-1} v(\theta_{i+\frac{1}{2}}, \lambda_{j+\frac{1}{2}}) \left[\frac{r_s(\theta_{i+\frac{1}{2}}, \lambda_{j+\frac{1}{2}})}{R} \right]^n \int_{\theta_i}^{\theta_{i+1}} \bar{P}_{n|m}(\cos \theta) \sin \theta d\theta \int_{\lambda_j}^{\lambda_{j+1}} \left(\frac{\cos^m \lambda}{\sin^{|m|} \lambda} \right) d\lambda \quad (2.136)$$

where $\eta_n = 1/(n-1)$, $n \geq 0$, $n \neq 1$, and $\eta_1 = 1$; and where

$$\begin{aligned} \theta_i &= i\Delta\theta, \quad i = 0, 1, \dots, N-1 \\ \lambda_j &= j\Delta\lambda, \quad j = 0, 1, \dots, 2N-1 \end{aligned}, \quad N = \frac{180^\circ}{\Delta\theta} \quad (2.137)$$

where $\Delta\theta = 0.6^\circ = \Delta\lambda$, $N=300$. Note that r_s and v are evaluated at $(\theta_{i+\frac{1}{2}}, \lambda_{j+\frac{1}{2}})$, i.e. at the center of each compartment.

The computation of all $(N+1)^2$ coefficients t_{nm} is virtually impossible for large N , such as $N=300$, without the aid of the Fast Fourier Transform (FFT). This is an extremely efficient routine for computing the Fourier spectrum of a function. In our case, the FFT is applied N times, once for each of the latitudinal bands $\theta_i = \text{constant}$ in which r_s and v are functions of longitude only. Most of the following derivations are found also in a more generalized form in (Colombo, 1981), but are included here for the sake of completeness. Denote by χ_{nmi} the integrals of the Legendre functions:

$$\chi_{nmi} = \int_{\theta_i}^{\theta_{i+1}} \bar{P}_{nm}(\cos \theta) \sin \theta d\theta \quad (2.138)$$

These can be computed using the recursive algorithm of Paul (1978) and by noting that

$$\chi_{n,m,N-i-1} = (-1)^{n-m} \chi_{nmi}, \quad i = 0, 1, \dots, \frac{1}{2}N-1 \quad (2.139)$$

It has been found that Paul's recursives are sufficiently

accurate (for the tests conducted here) up to degree 300 for all latitude intervals (Colombo, personal communication).
Now let

$$F_{nij} = v(\theta_{i+\frac{1}{2}}, \lambda_{j+\frac{1}{2}}) \left[\frac{r_{s(\theta_{i+\frac{1}{2}}, \lambda_{j+\frac{1}{2}})}}{R} \right]^n \quad (2.140)$$

then we have

$$t_{nm} = \frac{R\eta_n}{4\pi(2n+1)} \sum_{i=0}^{N-1} x_n |m| i \sum_{j=0}^{2N-1} F_{nij} \int_{\lambda_j}^{\lambda_{j+1}} (\cos m \lambda \over \sin |m| \lambda) d\lambda \quad (2.141)$$

And if we let

$$\begin{aligned} a_{mj} &= \cos m \lambda_j, & \alpha_{mj} &= \int_{\lambda_j}^{\lambda_{j+1}} \cos m \lambda d\lambda \\ b_{mj} &= \sin m \lambda_j, & \beta_{mj} &= \int_{\lambda_j}^{\lambda_{j+1}} \sin m \lambda d\lambda \end{aligned} \quad (2.142)$$

then using (2.137) and the angle sum formula for sinusoids, we find

$$\begin{aligned} \alpha_{mj} &= B_m a_{mj} - A_m b_{mj} \\ \beta_{mj} &= A_m a_{mj} + B_m b_{mj} \end{aligned} \quad (2.143)$$

where

$$A_m = \begin{cases} \frac{1}{m}(1 - a_{m1}) & , m > 0 \\ 0 & , m = 0 \end{cases}; \quad B_m = \begin{cases} \frac{1}{m}b_{m1} & , m > 0 \\ \Delta\lambda & , m = 0 \end{cases} \quad (2.144)$$

Now let

$$\begin{Bmatrix} p_{nmi} \\ q_{nmi} \end{Bmatrix} = \sum_{j=0}^{2N-1} F_{nij} \begin{Bmatrix} \cos m \lambda_j \\ \sin m \lambda_j \end{Bmatrix} \quad (2.145)$$

then with (2.142) and (2.143), (2.141) becomes

$$t_{nm} = \frac{R\eta_n}{4\pi(2n+1)} \sum_{i=0}^{N-1} \chi_{nmi} [B_m p_{nmi} - A_m q_{nmi}], \quad m \geq 0$$

$$t_{n,-m} = \frac{R\eta_n}{4\pi(2n+1)} \sum_{i=0}^{N-1} \chi_{nmi} [A_m p_{nmi} + B_m q_{nmi}], \quad m > 0 \quad (2.146)$$

The Fourier spectra (2.145) are computed simultaneously by the FFT; but only relatively minor savings in time are achieved with respect to the standard midpoint numerical integrations, because, as equations (2.145) stand, the FFT must be applied once for each i and n , i.e. a total of N^2 times. A substantial reduction in the computational time results by introducing the binomial expansion of the functions F_{nij} . Letting

$$\hat{h}(\theta, \lambda) = 1 - \frac{r_s(\theta, \lambda)}{R} \quad (2.147)$$

we have the usual binomial series

$$\left(\frac{r_s}{R}\right)^n = (1 - \hat{h})^n = \sum_{k=0}^n \binom{n}{k} (-1)^k \hat{h}^k \quad (2.148)$$

Since $0 < \hat{h} < 1$, it is not necessary to take more than a few terms, say $K+1$, in order to achieve sufficient accuracy. The Fourier transforms p_{nmi} , q_{nmi} then become

$$\begin{Bmatrix} p_{nmi} \\ q_{nmi} \end{Bmatrix} = \sum_{k=0}^K (-1)^k \binom{n}{k} \sum_{j=0}^{2N-1} \hat{F}_{kij} \begin{Bmatrix} \cos m \lambda_j \\ \sin m \lambda_j \end{Bmatrix} \quad (2.149)$$

where

$$\hat{F}_{kij} = v(\theta_{i+\frac{1}{2}}, \lambda_{j+\frac{1}{2}}) [\hat{h}(\theta_{i+\frac{1}{2}}, \lambda_{j+\frac{1}{2}})]^k \quad (2.150)$$

requiring a total of $(K+1)N$ applications of the FFT.

The density integrals corresponding to the downward continuation error in the gravity anomaly and height anomaly are treated similarly. The factor depending on the powers of the surface radius in the case of gravity anomalies (equation (2.100)) is expanded as follows, where

$$\bar{h}(\theta, \lambda) = 1 - \frac{r_p}{r_s(\theta, \lambda)} \quad (2.151)$$

Then

$$\begin{aligned} \left(\frac{r_s}{r_p}\right)^n - \left(\frac{r_p}{r_s}\right)^{n+1} &= (1 - \bar{h})^{-n} - (1 - \bar{h})^{n+1} = \\ &= (2n+1) \left[\bar{h} + \frac{n(n+1)}{6} (\bar{h}^3 + \bar{h}^4) + \frac{n(n+1)(n^2+n+18)}{120} \bar{h}^5 + \dots \right] \end{aligned} \quad (2.152)$$

For the height anomaly, we have (see equation (2.124)) for $n \neq 1$

$$\begin{aligned} \frac{1}{n+2} \left[\left(\frac{r_p}{r_s}\right)^{n+1} - \frac{r_s}{r_p} \right] + \frac{1}{n-1} \left[\left(\frac{r_s}{r_p}\right)^n - \frac{r_s}{r_p} \right] &= \\ &= \frac{2n+1}{2} \frac{r_s}{r_p} \left[\bar{h}^2 + \frac{n(n+1)}{60} (5\bar{h}^4 + 4\bar{h}^5) + \frac{n(n+1)(n^2+n+18)}{360} \bar{h}^6 + \dots \right] \end{aligned} \quad (2.153)$$

Since

$$\ln \frac{r_s}{r_p} = \bar{h} + \frac{1}{2}\bar{h}^2 + \frac{1}{3}\bar{h}^3 + \dots \quad (2.154)$$

we note that the series (2.153) represents also the first degree term in (2.124).

If we substitute the series in \bar{h} (2.152) into the error coefficients $d_{nm}(r_p)$ (equation (2.100)), then

$$d_{nm}(r_p) = \frac{R^2}{4\pi r_p^2} \iint_{\sigma_2} v(\theta, \lambda) \bar{h} \bar{Y}_{nm}(\theta, \lambda) d\sigma + \bar{d}_{nm}(r_p) \quad (2.155)$$

where $\bar{d}_{nm}(r_p)$ represents the part of the error coefficient containing \bar{h} to the third and higher powers:

$$\bar{d}_{nm} = \frac{R^2}{4\pi r_p^2} \iint_{\sigma_2} v(\theta, \lambda) \left[\frac{n(n+1)}{6} (\bar{h}^3 + \bar{h}^4) + \dots \right] \cdot \bar{Y}_{nm}(\theta, \lambda) d\sigma \quad (2.156)$$

The total downward continuation error (2.99) becomes

$$\begin{aligned} \varepsilon(\hat{\Delta}g) = & \frac{R^2}{r_p^2} \sum_{n=0}^{\infty} \sum_{m=-n}^n \frac{1}{4\pi} \iint_{\sigma_2} v(\theta, \lambda) \bar{h} \bar{Y}_{nm}(\theta, \lambda) d\sigma \bar{Y}_{nm}(\theta_p, \lambda_p) \\ & + \sum_{n=0}^{\infty} \sum_{m=-n}^n \bar{d}_{nm}(r_p) \bar{Y}_{nm}(\theta_p, \lambda_p) + \\ & + \sum_{n=\bar{n}+1}^{\infty} \sum_{m=-n}^n \bar{d}'_{nm}(r_p) \bar{Y}_{nm}(\theta_p, \lambda_p) \end{aligned} \quad (2.157)$$

where $\bar{d}'_{nm}(r_p) = \bar{d}_{nm}(r_p) - (R/r_p)^{n+2} g_{nm}$. The value of the first term above is zero if the point P lies on or above the earth's surface. To show this, let r_p be fixed (thus fixing the set σ_2) and consider the function

$$D(\theta, \lambda) = \begin{cases} v(\theta, \lambda) \bar{h} & , (\theta, \lambda) \in \sigma_2 \\ 0 & , (\theta, \lambda) \in \sigma_1 \end{cases} \quad (2.158)$$

(recall that $\bar{h} = 1 - r_p/r_1(\theta, \lambda)$). The function D is continuous and is therefore expandable as a series of spherical harmonics. With a change of notation, we can write

$$D(\theta_p, \lambda_p) = \sum_{n=0}^{\infty} \sum_{m=-n}^n \frac{1}{4\pi} \iint_{\sigma_2} v(\theta, \lambda) \bar{h} \bar{Y}_{nm}(\theta, \lambda) d\sigma \cdot \bar{Y}_{nm}(\theta_p, \lambda_p) \quad (2.159)$$

where (θ_p, λ_p) is any point on the sphere of radius r_p , and where the coefficients of this series are determined by substituting (2.158) into (1.6). But since the error series is to be evaluated only for points in σ , the series (2.159), hence the first term in (2.157), vanishes. When formulating the downward continuation error for the mean anomaly, the same arguments apply. In this case, we consider the average of the function D over a spherical cap on the sphere of radius r_p (the set σ , thereby decreases in measure).

A similar reasoning clearly leads to a downward continuation error in the height anomaly, where the quadratic term \bar{h}^2 is absent:

$$\begin{aligned} \epsilon(\zeta_p) = & \sum_{n=0}^{\infty} \sum_{m=-n}^n \bar{e}_{nm}(r_p) \bar{Y}_{nm}(\theta_p, \lambda_p) \\ & + \sum_{n=\bar{n}+1}^{\infty} \sum_{m=-n}^n \bar{e}'_{nm}(r_p) \bar{Y}_{nm}(\theta_p, \lambda_p) \end{aligned} \quad (2.160)$$

where

$$\begin{aligned} \bar{e}_{nm}(r_p) = & \frac{r_p R^2}{8\pi \kappa M} \iint_{\sigma_2} v(\theta, \lambda) \frac{r_s}{r_p} \left[\frac{n(n+1)}{60} (5\bar{h}^4 + 4\bar{h}^5) + \dots \right] \cdot \\ & \cdot \bar{Y}_{nm}(\theta, \lambda) d\sigma \end{aligned} \quad (2.161)$$

and

$$\bar{e}'_{nm}(r_p) = \bar{e}_{nm}(r_p) - \frac{R^2}{\kappa M} \left(\frac{R}{r_p} \right)^{n-1} t_{nm} \quad (2.162)$$

Equations (2.156) and (2.161) are essentially equivalent to those of Petrovskaya (1979) - if we assume $r_p \approx r_s \approx R$, then

$$\bar{e}_{nm}(r_p) \Big|_{\text{equation (2.161)}} = \frac{n(n+1)}{(n+\frac{1}{2})^2} \bar{e}_{nm}(r_p) \Big|_{\text{Petrovskaya}} \quad (2.163)$$

Since the function D , defined by (2.158), has discontinuous derivatives at the curve separating the surfaces σ_1 and σ_2 , the series (2.159) converges very slowly to zero for points near the earth's surface (a case of the well known Gibbs' phenomenon). This seems to be the reason for the increase by one, two, or more orders of magnitude in the sum of the first \bar{n} error coefficients (2.100) (or (2.124)) when the linear (or quadratic) term in the \bar{h} -series is retained.

With the assumed constancy of r_s and ν over the 0.6 by 0.6 compartments, equations (2.156) turn into

$$\begin{aligned}\bar{d}_{nm}(r_p) &= \frac{R^2}{4\pi r_p^2} \sum_{i=0}^{N-1} x_{nmi} [B_m \bar{p}_{nmi} - A_m \bar{q}_{nmi}] , \quad m \geq 0 \\ \bar{d}_{n,-m}(r_p) &= \frac{R^2}{4\pi r_p^2} \sum_{i=0}^{N-1} x_{nmi} [A_m \bar{p}_{nmi} + B_m \bar{q}_{nmi}] , \quad m > 0\end{aligned}\quad (2.164)$$

where the Fourier transforms are given by

$$\begin{Bmatrix} \bar{p}_{nmi} \\ \bar{q}_{nmi} \end{Bmatrix} = \sum_{k=3}^K x_{nk} \sum_{j=0}^{2N-1} \Delta_{ij} \bar{F}_{kij} \begin{Bmatrix} \cos m \lambda_j \\ \sin m \lambda_j \end{Bmatrix} \quad (2.165)$$

and where

$$\bar{F}_{kij} = \nu(\theta_{i+\frac{1}{2}}, \lambda_{i+\frac{1}{2}})] \bar{h}(\theta_{i+\frac{1}{2}}, \lambda_{j+\frac{1}{2}})]^k , \quad (2.166)$$

$$x_{n3} = x_{n4} = \frac{n(n+1)}{6} , \quad x_{n5} = \frac{n(n+1)(n^2+n+18)}{120} , \quad \dots$$

and finally, where

$$\Delta_{ij} = \begin{cases} 1 & , \quad \text{if } r_p < r_s (\theta_{i+\frac{1}{2}}, \lambda_{j+\frac{1}{2}}) \\ 0 & , \quad \text{if } r_p \geq r_s (\theta_{i+\frac{1}{2}}, \lambda_{j+\frac{1}{2}}) \end{cases} \quad (2.167)$$

The factor Δ_{ij} in (2.165) ensures that only points on the surface above the sphere of computation (radius r_p) contribute to the error, and only those latitudinal bands in which at least one such point exists are included in the sums (2.164). The coefficients of the downward continuation error in height anomalies, equation (2.161), then also become

$$\begin{aligned}\bar{e}_{n,m} &= \frac{R^2 r_p}{8\pi K M} \sum_{i=0}^{N-1} \chi_{nmi} [B_n \tilde{p}_{nmi} - A_m \tilde{q}_{nmi}], \quad m \geq 0 \\ \bar{e}_{n,-m} &= \frac{R^2 r_p}{8\pi K M} \sum_{i=0}^{N-1} \chi_{nmi} [A_m \tilde{p}_{nmi} + B_m \tilde{q}_{nmi}], \quad m > 0\end{aligned}\quad (2.168)$$

where

$$\begin{Bmatrix} \tilde{p}_{nmi} \\ \tilde{q}_{nmi} \end{Bmatrix} = \sum_{k=4}^K y_{nk} \sum_{j=0}^{2N-1} \Delta_{ij} F_{kij} \begin{Bmatrix} \cos m \lambda_j \\ \sin m \lambda_j \end{Bmatrix} \quad (2.169)$$

and where

$$\begin{aligned}\tilde{F}_{kij} &= \frac{1}{r_p} r_s(\theta_{i+\frac{1}{2}}, \lambda_{j+\frac{1}{2}}) \bar{F}_{kij} \\ y_{n4} &= \frac{n(n+1)}{12}, \quad y_{n5} = \frac{n(n+1)}{15}, \quad y_{n6} = \frac{n(n+1)(n^2+n+18)}{360}, \dots\end{aligned}\quad (2.170)$$

2.3.4 The Numerical Results of the Error Analysis

As in the case of the volumetric density model, the radial dependence of the error "coefficients" (2.100) and (2.124) precludes the mapping of the error on a global scale. On the other hand, because the earth's surface is more or less rotationally symmetric, a reasonably thorough analysis lies within feasibility if we limit the latitudinal extent of our investigation to a few representative degrees. Table 1 lists the regions to be considered, as well as several representative radii for each range of latitudes,

Table 1: The Region of the surface model in which the downward continuation errors are computed.

Region, defined by latitudinal range of φ_i	Representative radii, R_i [m]	Longitudinal ranges of λ_i	No. of points on <u>all</u> spheres of radius R_i such that $0 \leq r_p - r_s \leq t$	
			$t = \begin{cases} 300 \text{ m} \\ 100 \text{ m} \\ 50 \text{ m} \\ 10 \text{ m} \end{cases}$	
I $12^\circ.3 \leq \varphi_i \leq 24^\circ.3$	6374550 6374850 6375150 6375450 6375750 6376050 6376350 6376650 6376950 6377250	[0°3, 359°7]	North Lat.	South Lat.
			11938	11781
			4112	4326
		[69°9, 89°7]	2275	2505
			394	667
			683	714
		[290°1, 309°9]	234	273
			87	161
			17	0
		[290°1, 309°9]	714	461
			273	176
			144	92
II $47^\circ.1 \leq \varphi_i \leq 57^\circ.3$	6363350 6363750 6364150 6364550 6364950 6365350 6365750 6366150 6366550	[0°3, 359°7]	North Lat.	South Lat.
			6800	6783
			2111	1827
		[60°3, 80°1]	1003	811
			196	189
			361	411
		[260°1, 285°3]	116	123
			62	70
			10	29
		[260°1, 285°3]	483	486
			147	114
			78	71
III $75^\circ.3 \leq \varphi_i \leq 84^\circ.3$	6357250 6357550 6357850 6358150 6358450	[0°3, 359°7]	North Lat.	South Lat.
			8914	6329
			2924	2092
		[170°1, 260°1]	1609	959
			720	168
			2415	2090
		[170°1, 260°1]	861	572
			537	171
			258	19

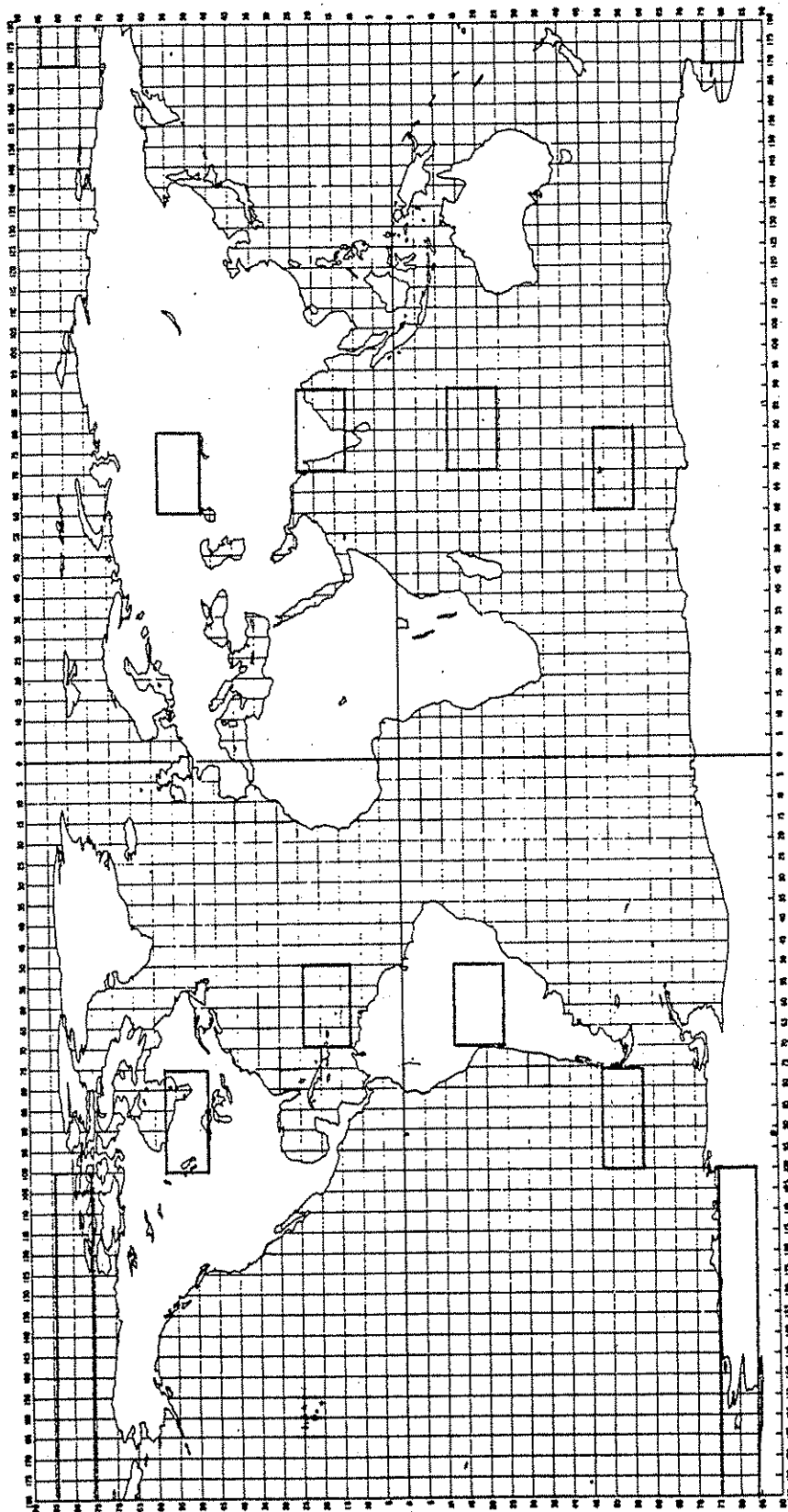


Figure 15: Subregions over which RMS downward continuation errors are computed.

see also Fig. 15. We note that for each constant $r_p = R_p$, the coefficients (2.100), or (2.124), correspond to the error at any point which lies on the sphere of radius R_p and above the earth's surface. Therefore, instead of evaluating the error series at a few isolated points on the surface, a more characteristic, although less realistic, assessment is obtained if the series is evaluated on the given spheres at all those points which are removed from the surface by no more than, say, 100 m (see Fig. 17). Table 1 also shows the number of points on a 0.6×0.6 grid that lie on the spheres having radii R_p and within a tolerance of 300 m, 100 m, 50 m, or 10 m above the modeled surface.

The amount of calculations can be further reduced by requiring no more than two- or three-digit accuracy in the error estimates; any attempt at greater computational accuracy is unavailing and therefore unjustified. Hence, we may accordingly restrict the number of terms of the series in \bar{h} , (2.152) and (2.153). Table 2 correlates the accuracy of the series with the number of included terms for the worst cases in each of the regions of Table 1. The worst case occurs when $n=300$ and $\bar{h}=\max(\bar{h}_i)$. Similarly, the series in \hat{h} (2.148) may be limited to several terms (see Table 2). Numerical tests confirmed that the relative accuracy guaranteed for the truncated series in \bar{h} was not degraded in the process of determining the error coefficients.

Equation (2.146), with the approximate transforms (2.149) substituted, was used to determine the spectrum of the gravity field model on the bounding sphere (radius $R=6382000$ m). The series in \hat{h} was developed to $K=10$ thus ensuring six-digit accuracy. The corresponding degree variances are shown in Fig. 16. The series (2.95) and (2.120) for the gravity and height anomalies above the bounding sphere then provide, in conjunction with the error series, the corresponding inner series, which converge below the bounding sphere, namely (2.97) and (2.121). All series were truncated at degree 300.

Once again, it must be remembered that individual terms of the error series do not indicate errors in the harmonic constituents of the potential (or gravity anomaly), since the inner series is not a spectral representation of the field on the surface. In the strictest sense, the difference between truncated inner and outer series is just as meaningless, since it implies a comparison of "bands" of frequencies. The comparison is valid only if the inner series has converged with sufficient accuracy to the true value being estimated. Otherwise, when limiting the evaluation of the downward continuation error series to terms of degree no greater than \bar{n} , we must be aware of the

Table 2: Accuracy of series (2.152) (without the linear term), series (2.153) (without the quadratic term), and series (2.148) versus the number of included terms.

Region	(meters) $\bar{h} = \max(\bar{h}_i)$ if	K , the highest power of \bar{h}	Series (2.152) No. of accurate digits	Series (2.153) No. of accurate digits
I	$r_p = 6374550$ $r_s = R$	3 4 5 6	1 2 4-5 5	- 2 2-3 4
II	$r_p = 6363350$ $r_s = R$	3 4 5 6 7	1 1 2-3 3 4	- 1 1 3 4-5
III	$r_p = 6357250$ $r_s = R$	3 4 5 6 7	1 1 2 2 3	- 1 1-2 3 3
			Series (2.148)	
	$\hat{h} = \max(\hat{h}_i)$ if	K , the highest power of \hat{h}	No. of accurate digits	
	$r_p = R$ $r_s = 6356000$	2 4 6 8 10	0 1 2 4 6	

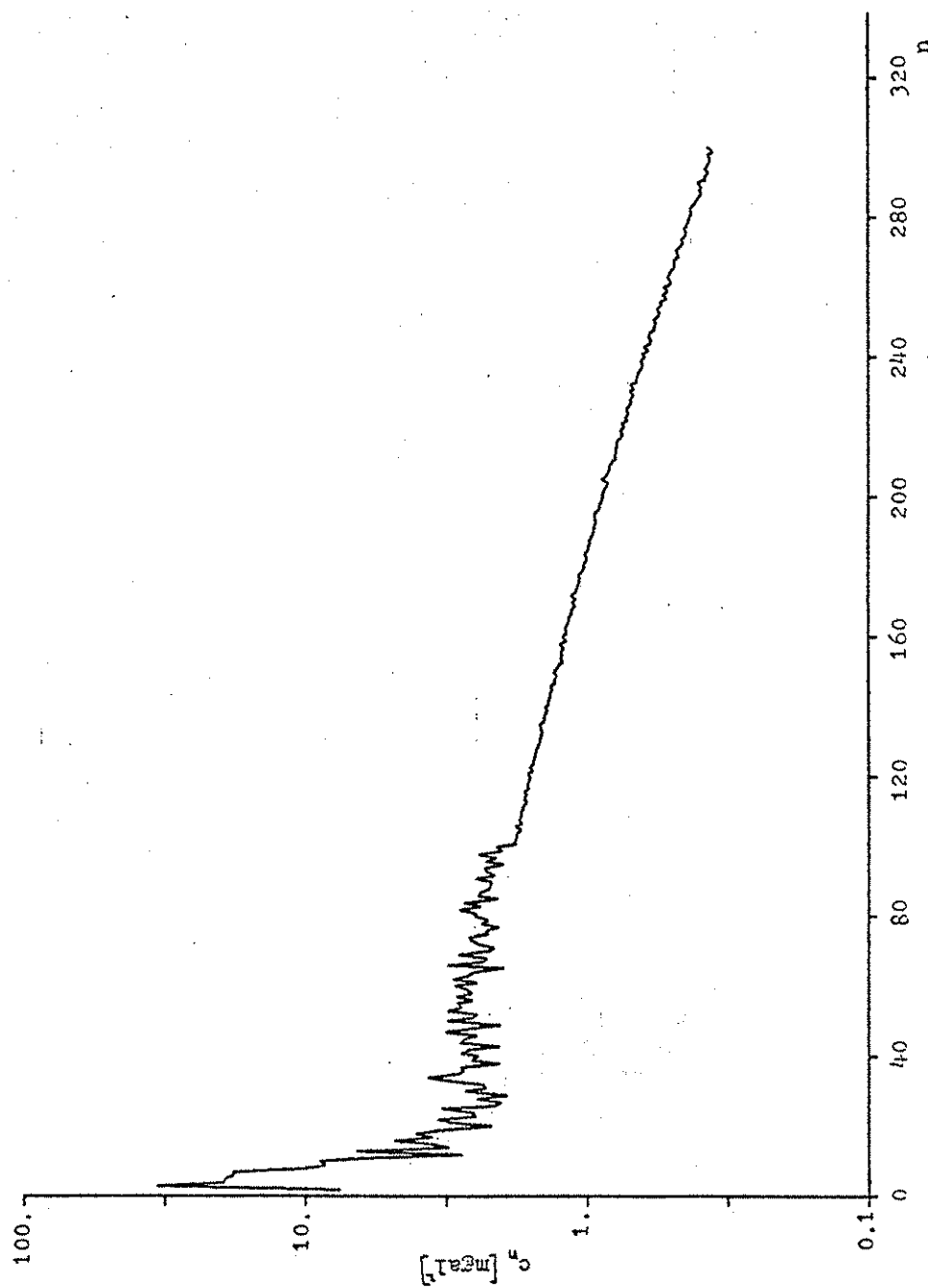


Figure 16: Degree variances of gravity anomaly on bounding sphere.

effect of truncation, which is, of course, not known. With the present density model, it appears likely that the usual degree variance models of the earth's gravity field will provide estimates of the neglect of higher degree terms, although this is not evident from equation (2.101) or (2.125). If $\bar{n}=300$, then the RMS (root mean square) values of the truncation error, based on the model (2.128) and a spherical earth, are about 36 cm for the height anomaly and a considerably more significant 30 mgal for the gravity anomaly. The root mean squares of the evaluations of the error series truncated at $\bar{n}=300$ over each of the regions of Table 1 are shown in Table 3 for the gravity anomaly and in Table 4 for the height anomaly. Also shown for comparison are the RMS values of the truncated series of the respective anomalies themselves. Some maximum absolute values of the error are also shown parenthetically. Note that the units in the error columns are $\mu\text{gal}=10^{-8} \text{ m/s}^2$ (Table 3) and $\mu\text{m}=10^{-6} \text{ m}$ (Table 4).

A perusal of these tables indicates that the errors are generally insensitive to the distance t of the evaluation point from the model surface, if it is 300 m or less. The RMS values of the anomalies, on the other hand, show a (disconcertingly strong and unexplained) decrease as the point of evaluation approaches the surface. There is, of course, the expected increase in error with increasing latitude; and within each latitudinal range, the RMS errors show a significant increase (not shown) with each decrease in radial distance R_p . Some correlation between the error and large-scale topographic features can be detected. For example, the error over central South America is generally twice as large as in the topographically lower Caribbean Sea. Here, in turn, the errors are almost double those over both the Indian Ocean and subcontinent (just south of the Himalayan massif), showing that the correlation is somewhat inscrutable. No definite correlations with topography are discernible (by visual inspection) from the values listed for the subregions in the midlatitudes and polar areas.

Table 5 shows how the errors accumulate in steps of 30 degrees. The accumulation is generally monotonic for $\bar{n} \leq 270$, but a noticeable downward trend occurs at $\bar{n}=300$. In view of Figures 6 and 7 this is not an unexpected feature.

To eliminate the difficulty of interpreting these results, we could consider a smoothed gravity field, where the resolution, by definition, is limited to the first 300 harmonic constituents. In order to make the meaning of limited resolution for the inner and outer series comparable, we identify the cutting off, or filtering, of higher frequencies with a weighted averaging process as

Table 3: RMS downward continuation error of spherical harmonic series of gravity anomaly and RMS gravity anomaly evaluated (first 300 terms) at the points of Table 1 and at the indicated subregions. Maximum absolute values for each region and sub-region are given parenthetically.

Region	RMS $\varepsilon(\Delta g)$ (max $\varepsilon(\Delta g)$) $0 \leq n \leq 300$ [μgal]			RMS Δg $0 \leq n \leq 300$ [mgal]		
	$t = \begin{cases} 300 \text{ m} \\ 100 \text{ m} \\ 50 \text{ m} \\ 10 \text{ m} \end{cases}$			$t = \begin{cases} 300 \text{ m} \\ 100 \text{ m} \\ 50 \text{ m} \\ 10 \text{ m} \end{cases}$		
I	λ 0°3-359°7	69°9-89°7	290°1-309°9	0°3-359°7	69°9-89°7	290°1-309°9
N	.28	.26	.41	26.80	31.23	43.38
	.33 (2.0)	.26 (1.0)	.50 (1.8)	26.90	29.85	44.38
	.35	.29	.43	25.84	27.99	32.14
	.33 (2.0)	.33 (.73)	.30 (.30)	24.25	26.11	102.98
S	.46	.27	1.1	25.23	23.30	27.27
	.48 (6.1)	.33 (1.1)	1.1 (4.4)	24.89	22.35	28.59
	.51	.31	1.2	25.00	22.27	26.73
	.47 (4.1)	-	1.1 (4.1)	24.36	-	28.18
II	λ 0°3-359°7	60°3-80°1	260°1-285°3	0°3-359°7	60°3-80°1	260°1-285°3
N	22.	21.	18.	28.4	20.4	33.4
	22. (74.)	22. (57.)	16. (41.)	28.6	18.3	31.6
	21.	22.	16.	29.2	18.9	35.6
	20. (62.)	29. (57.)	16. (33.)	27.8	9.7	37.2
S	23.	18.	19.	23.4	31.3	19.4
	22. (97.)	17. (48.)	21. (46.)	23.3	33.9	19.7
	21.	16.	21.	23.5	34.6	21.5
	22. (97.)	16. (34.)	23. (46.)	26.2	37.0	19.4
III	λ 0°3 - 359°7	170°1 - 260°1		0°3-359°7	170°1-260°1	
N	86.	85.		22.08	25.17	
	82. (290)	81. (240)		22.24	24.36	
	81.	77.		22.16	25.67	
	82. (290)	82. (240)		20.78	23.60	
S	88.	88.		25.03	28.39	
	86. (260)	86. (260)		24.10	28.86	
	84.	87.		22.48	27.81	
	85. (210)	88. (190)		21.05	16.85	

Table 4: RMS downward continuation error of spherical harmonic series of height anomaly and RMS height anomaly evaluated (first 300 terms) at the points of Table 1 and at the indicated subregions. Maximum absolute values for each region and sub-region are given parenthetically.

Region	RMS $\varepsilon(\xi)$ (max $\varepsilon(\xi)$) $0 \leq n \leq 300$ [μm]			RMS ξ $0 \leq n \leq 300$ [m]		
	$t = \begin{cases} 300 \text{ m} \\ 100 \text{ m} \\ 50 \text{ m} \\ 10 \text{ m} \end{cases}$			$t = \begin{cases} 300 \text{ m} \\ 100 \text{ m} \\ 50 \text{ m} \\ 10 \text{ m} \end{cases}$		
I	λ 0°3-359°7	69°9-89°7	290°1-309°9	0°3-359°7	69°9-89°7	290°1-309°9
N	.26	.23	.43	33.52	68.12	44.36
	.32 (2.1)	.24 (.93)	.53 (1.8)	33.64	67.44	45.01
	.33	.28	.45	31.73	65.73	42.35
	.30 (1.5)	.36 (.88)	.28 (.28)	25.19	62.39	57.12
S	.51	.24	1.1	28.98	44.89	18.23
	.53 (7.7)	.30 (1.3)	1.2 (5.0)	27.38	40.77	18.25
	.58	.27	1.3	26.57	40.12	16.18
	.52 (5.0)	-	1.4 (4.6)	20.96	-	11.63
II	λ 0°3-359°7	60°3-80°1	260°1-285°3	0°3-359°7	60°3-80°1	260°1-285°3
N	70.	67.	57.	30.27	27.27	37.81
	69. (250)	69. (180)	49. (140)	32.17	26.34	36.81
	66.	68.	49.	30.27	27.23	37.65
	64. (190)	89. (170)	52. (120)	26.94	25.83	39.13
S	73.	57.	62.	23.41	34.87	5.12
	68. (360)	52. (150)	64. (140)	24.43	35.94	4.41
	63.	47.	62.	24.27	35.79	4.12
	71. (360)	46. (95.)	66. (140)	29.32	36.86	3.42
III	λ 0°3 - 359°7	170°1 - 260°1		0°3-359°7	170°1-260°1	
N	410	410		14.82	5.75	
	400 (1400)	390 (1300)		14.06	4.38	
	390	370		10.64	4.20	
	390 (1400)	400 (1300)		8.17	3.65	
S	420	420		30.43	41.85	
	410 (1300)	410 (1300)		29.92	43.08	
	400	420		25.39	37.62	
	400 (1000)	430 (1000)		25.17	39.30	

Table 5: RMS downward continuation error of gravity anomaly and height anomaly spherical harmonic series in steps of 30 degrees: $\bar{n}=30,60,\dots,300$, based on those points of Table 1 for which $t=100$ m.

Region	\bar{n}	RMS $\varepsilon(\Delta g)$ μgal $\lambda: 0^\circ.3 - 359^\circ.7$		RMS $\varepsilon(\zeta)$ μm $\lambda: 0^\circ.3 - 359^\circ.7$	
		N	S	N	S
I	30	.0028	.0079	.0036	.011
	60	.015	.034	.018	.046
	90	.041	.092	.046	.12
	120	.061	.14	.068	.17
	150	.091	.15	.090	.18
	180	.14	.19	.14	.22
	210	.22	.28	.21	.32
	240	.28	.40	.26	.43
	270	.40	.50	.39	.55
	300	.33	.48	.32	.53
II	30	.077	.066	.26	.20
	60	.57	.58	1.8	1.9
	90	2.1	1.6	6.6	5.5
	120	3.4	3.0	11.	9.5
	150	5.6	6.0	18.	19.
	180	9.2	8.5	29.	26.
	210	15.	13.	47.	41.
	240	18.	18.	57.	55.
	270	23.	24.	74.	75.
	300	22.	22.	69.	68.
III	30	.22	.23	1.0	1.1
	60	1.9	1.6	8.9	8.2
	90	6.3	4.7	30.	24.
	120	12.	12.	57.	57.
	150	21.	20.	100	93.
	180	31.	32.	140	150
	210	46.	46.	220	220
	240	59.	69.	280	320
	270	81.	91.	390	420
	300	82.	86.	400	410

mathematically detailed in section 2.2.2. However, the filter then cannot perfectly eliminate the effect of truncation. Because the Gaussian filter is relatively efficient in this respect, it is chosen here, with parameters $a=15021$, $\psi_0=1^\circ 4$. The average is thus taken over a spherical cap of radius ψ_0 , with values at the edge of the cap weighted by 0.01. The frequency response (2.74) admits only 5% of the harmonic coefficients of degree 300 and thereafter decreases rapidly to zero. The difference between the smoothed downward continued series and the smoothed inner series is then the downward continuation error with relatively little truncation effect. The RMS truncation error, based on model (2.128) and a spherical earth, is .3 mgal for the smoothed gravity anomaly and .7 cm for the smoothed height anomaly. The downward continuation errors are shown in Tables 6 and 7 and follow the same basic pattern as in Tables 3 and 4, but are about one order of magnitude smaller (an obvious consequence of smoothing, since the higher degree harmonics, which are most affected by the series divergence, are decreased in magnitude). Also included are the RMS values of the smoothed anomalies.

Finally, we note that the relative downward continuation error of the gravity anomaly is approximately three orders of magnitude greater than the relative error of the height anomaly.

Table 6: RMS downward continuation error of spherical harmonic series of mean gravity anomaly and RMS mean gravity anomaly evaluated (first 300 terms) at the points of Table 1 and at the indicated subregions. Maximum absolute values for each region and subregion are given parenthetically.

Region	RMS $\varepsilon(\Delta\bar{g})$ (max $\varepsilon(\Delta\bar{g})$) $0 \leq n \leq 300$ [μgal]			RMS $\Delta\bar{g}$ $0 \leq n \leq 300$ [μgal]		
	$t = \begin{Bmatrix} 300 \text{ m} \\ 100 \text{ m} \\ 50 \text{ m} \\ 10 \text{ m} \end{Bmatrix}$			$t = \begin{Bmatrix} 300 \text{ m} \\ 100 \text{ m} \\ 50 \text{ m} \\ 10 \text{ m} \end{Bmatrix}$		
I	λ 0°3-359°7	69°9-89°7	290°1-309°9	0°3-359°7	69°9-89°7	290°1-309°9
N	.014	.012	.019	20.17	25.11	37.98
	.017 (.35)	.012 (.048)	.024 (.084)	20.36	24.01	39.04
	.018	.014	.021	18.92	22.24	27.51
	.018 (.17)	.016 (.034)	.014 (.014)	17.28	17.17	95.83
S	.039	.013	.061	18.16	15.61	20.98
	.042 (1.3)	.016 (.052)	.070 (.43)	17.81	14.23	22.93
	.039	.015	.030	17.28	14.11	20.26
	.026 (.34)	-	.051 (.17)	16.75	-	20.62
II	λ 0°3-359°7	60°3-80°1	260°1-285°3	0°3-359°7	60°3-80°1	260°1-285°3
N	1.1	1.0	.88	21.41	12.54	27.66
	1.0 (3.5)	1.0 (2.8)	.75 (1.9)	21.58	11.90	25.42
	1.0	1.0	.74	22.00	12.77	28.56
	.97 (3.0)	1.4 (2.7)	.78 (1.7)	20.25	8.11	28.82
S	1.1	.85	.92	15.42	25.93	9.41
	1.0 (4.6)	.82 (2.3)	1.0 (2.2)	15.79	28.29	9.33
	1.0	.76	.98	15.99	28.17	10.34
	1.0 (4.6)	.79 (1.6)	1.1 (2.2)	19.01	27.65	7.68
III	λ 0°3 - 359°7	170°1 - 260°1		0°3-359°7	170°1-260°1	
N	4.1	4.1		12.25	14.84	
	3.9 (14.)	3.8 (11.)		12.15	13.31	
	3.9	3.7		11.71	14.58	
	3.9 (14.)	3.9 (12.)		10.27	12.44	
S	4.2	4.2		17.56	22.09	
	4.1 (12.)	4.1 (12.)		17.02	22.19	
	4.0	4.2		15.40	20.90	
	4.1 (10.)	4.2 (9.4)		14.17	17.61	

Table 7: RMS downward continuation error of spherical harmonic series of mean height anomaly and RMS mean height anomaly evaluated (first 300 terms) at the points of Table 1 and at the indicated subregions. Maximum absolute values for each region and subregion are given parenthetically.

Region	RMS $\xi(\bar{\lambda})$ (max $\xi(\bar{\lambda})$) $0 \leq n \leq 300$ [μ m]			RMS ξ $0 \leq n \leq 300$ [m]		
	$t = \begin{cases} 300 \text{ m} \\ 100 \text{ m} \\ 50 \text{ m} \\ 10 \text{ m} \end{cases}$			$t = \begin{cases} 300 \text{ m} \\ 100 \text{ m} \\ 50 \text{ m} \\ 10 \text{ m} \end{cases}$		
I	λ 0°3-359°7	69°9-89°7	290°1-309°9	0°3-359°7	69°9-89°7	290°1-309°9
N	.013	.011	.020	33.49	68.10	44.28
	.016 (.24)	.011 (.047)	.025 (.085)	33.60	67.47	44.90
	.016	.014	.022	31.72	65.83	42.45
	.015 (.12)	.018 (.047)	.012 (.012)	25.20	62.51	56.27
S	.039	.012	.057	28.96	44.87	18.26
	.044 (1.4)	.015 (.059)	.064 (.29)	27.37	40.12	16.22
	.040	.013	.057	26.56	40.12	16.22
	.028 (.30)	-	.063 (.20)	20.93	-	11.53
II	λ 0°3-359°7	60°3-80°1	260°1-285°3	0°3-359°7	60°3-80°1	260°1-285°3
N	3.3	3.2	2.7	30.23	27.28	37.74
	3.3 (12.)	3.3 (8.5)	2.3 (6.5)	32.13	26.38	36.78
	3.1	3.3	2.3	30.20	27.24	37.53
	3.0 (9.2)	4.2 (8.1)	2.5 (5.7)	26.82	25.84	38.99
S	3.5	2.7	3.0	23.39	34.81	5.09
	3.2 (17.)	2.5 (7.0)	3.1 (6.8)	24.40	35.90	4.42
	3.0	2.2	2.9	24.24	35.75	4.12
	3.4 (17.)	2.2 (4.5)	3.1 (6.8)	29.33	36.87	3.50
III	λ 0°3 - 359°7	170°1 - 260°1		0°3-359°7	170°1-260°1	
N	20.	20.		14.81	5.64	
	19. (66.)	19. (60.)		14.05	4.28	
	18.	18.		10.64	4.07	
	19. (66.)	19. (60.)		8.19	3.61	
S	20.	20.		30.38	41.81	
	19. (66.)	20. (62.)		29.88	43.04	
	19.	20.		25.36	37.58	
	20. (50.)	21. (48.)		25.16	39.42	

3. The Ellipsoidal Harmonic Series

There exist two systems of so-called ellipsoidal coordinates in geodesy; they differ in the definition of the latitude. The system with the geodetic latitude (defining the direction of the normal to the reference ellipsoid) is most commonly used. However, its three dimensional generalization, obtained by including the height above the ellipsoid as coordinate, while forming a triply orthogonal system (Golodenskii et al., 1962, p.9), does not yield a form of Laplace's equation that is solvable by separation of variables. In order to have any hope of solving Laplace's equation with this standard method, the coordinate system must be orthogonal - choices of the third coordinate, such as the semiminor axis, render the system nonorthogonal.

The spheroidal coordinates u, δ, λ form a triply orthogonal system (Hobson, 1965, p.421) in which the second coordinate, in geodetic terminology, is the complement of the reduced latitude; we may call it the reduced colatitude (in fact, $\delta \leq \theta$). Although, strictly stated, u, δ, λ are oblate spheroidal coordinates, we may use the less precise nomenclature "ellipsoidal coordinates" as no other system will come under consideration. Their definition in terms of Cartesian coordinates is (see Figure 18)

$$\begin{aligned}x &= \sqrt{u^2 + E^2} \sin\delta \cos\lambda \\y &= \sqrt{u^2 + E^2} \sin\delta \sin\lambda \\z &= u \cos\delta\end{aligned}\tag{3.1}$$

where E is a parameter of the system. From the consequent relationship

$$\frac{x^2 + y^2}{u^2 + E^2} + \frac{z^2}{u^2} = 1\tag{3.2}$$

it noted that the coordinate surface $u=\text{constant}$ is an ellipsoid of revolution with linear eccentricity E (the distance from the origin to either of the focal points), and

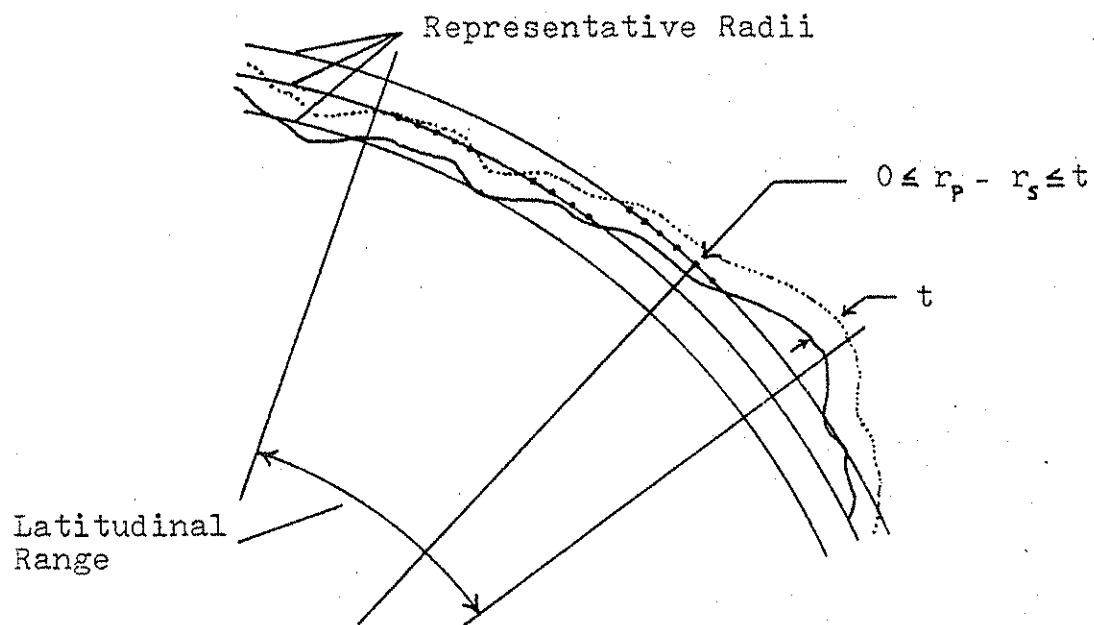


Figure 17: Schematic illustration of the points contributing to the computed RMS downward continuation error.

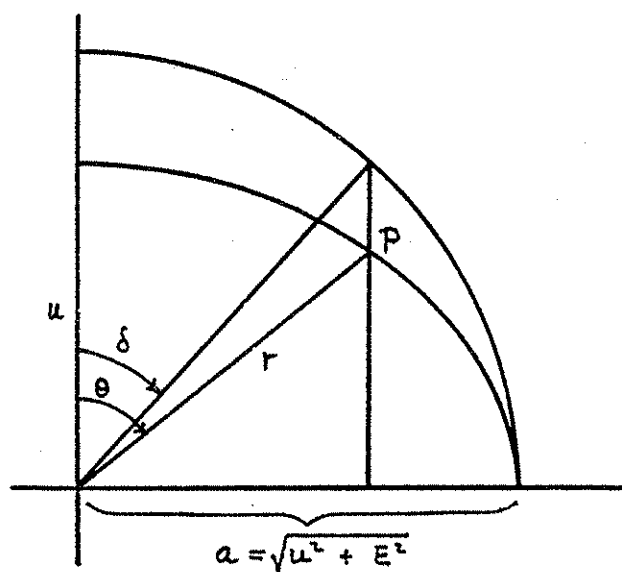


Figure 18: Ellipsoidal coordinates (u, δ, λ) versus spherical coordinates (r, θ, λ) of the point P.

semiminor axis u . Hence the set of coordinate surfaces $u=\text{constant}$ is a set of confocal ellipsoids. The squares of the first and second eccentricities are given by

$$e^2 = \frac{E^2}{E^2 + u^2}, \quad e'^2 = \frac{E^2}{u^2} \quad (3.3)$$

showing that as $u \rightarrow \infty$ the ellipsoid approaches a sphere. Substituting (3.3) into (2.81) and noting that $a^2 = u^2 + E^2$ (see Fig. 18), we find

$$r = \frac{u \sqrt{u^2 + E^2}}{\sqrt{u^2 + E^2 \cos^2 \theta}} \quad (3.4)$$

or conversely,

$$u^2 = \frac{1}{2}(r^2 - E^2) + \frac{1}{2}[r^4 + E^4 - 2r^2 E^2 (1 - 2 \cos^2 \theta)]^{\frac{1}{2}} \quad (3.5)$$

Since the ratio $\sqrt{x^2 + y^2}/z$ is the tangent of the spherical colatitude θ , equations (3.1) yield

$$\tan \delta = \frac{u}{\sqrt{u^2 + E^2}} \tan \theta \quad (3.6)$$

Equations (3.5) and (3.6) provide the transformation from spherical to ellipsoidal coordinates. The reverse transformation is, from (3.1) and (3.6),

$$r = \sqrt{u^2 + E^2 \sin^2 \delta}$$

$$\tan \theta = \frac{\sqrt{u^2 + E^2}}{u} \tan \delta \quad (3.7)$$

The choice of the linear eccentricity was based on its relation to the semimajor axis " a " and flattening f of any of the confocal ellipsoids:

$$E = a\sqrt{2f - f^2} \quad (3.8)$$

For example, we may choose

$$\begin{aligned} a &= 6378140 \text{ m} \\ f &= 1/298.257 \end{aligned} \quad (3.9)$$

giving $E=521854.4492 \text{ m}$.

A detailed solution of Laplace's equation in ellipsoidal coordinates may be found in (Heiskanen and Moritz, 1967, pp41-43). The solutions for regions containing the origin are $\bar{P}_{nm}(iu/E)\bar{Y}_{nm}(\delta, \lambda)$, and for regions containing infinity, they are $\bar{Q}_{nm}(iu/E)\bar{Y}_{nm}(\delta, \lambda)$. Being interested primarily in the latter region, we find the general solution to Laplace's equation in the form

$$F(u, \delta, \lambda) = \sum_{n=0}^{\infty} \sum_{m=-n}^n \phi_{nm} \bar{Q}_{nm}\left(i \frac{u}{E}\right) \bar{Y}_{nm}(\delta, \lambda) \quad (3.10)$$

where the constant ellipsoidal harmonic coefficients ϕ_{nm} are necessarily complex numbers if F is to be a real function. They are determined uniquely if the boundary values of F are known on an ellipsoid, say $u=b$. Multiplying both sides of (3.10) by $\bar{Y}_{nm}(\delta, \lambda)$ and integrating over the domain $\sigma = \{(\delta, \lambda) / 0 \leq \lambda \leq 2\pi, 0 \leq \delta \leq \pi\}$, we obtain by the orthogonality of \bar{Y}_{nm}

$$\phi_{nm} = \frac{1}{\bar{Q}_{nm}\left(i \frac{b}{E}\right)} \frac{1}{4\pi} \iint_{\sigma} F(b, \delta, \lambda) \bar{Y}_{nm}(\delta, \lambda) d\sigma \quad (3.11)$$

where $d\sigma = \sin\delta d\delta d\lambda$. In this way, we can define the ellipsoidal spectrum of F with respect to the Legendre transform. However, the integral in (3.11) is not a surface integral over the ellipsoid $u=b$, instead it is an integral over the unit sphere onto which the points of the ellipsoid with coordinates (δ, λ) are mapped according to the one-to-one correspondence

$$\theta = \delta$$

(3.12)

$$\lambda = \lambda$$

3.1 The Transformation from Spherical to Ellipsoidal Harmonic Coefficients

A brief account of the transformation between ellipsoidal and spherical harmonic coefficients has been given by Hotine (1969, pp194-5). However, the formulas are not directly amenable to practical computations because of a lack of stabilizing normalizations in the formulas and the inconvenience (from the geodetic point of view) of working with complex coefficients. A complete derivation of the transformation will be presented below, which by introducing a different "normalization" of \bar{Q}_{nm} becomes feasible, as well as accurate, for high degree expansions.

The relationship between spherical and ellipsoidal solid harmonic functions is established by using a more general form of the addition theorem for Legendre polynomials (Hobson, 1965, p.364)

$$P_n(vv' - \sqrt{v^2-1} \sqrt{v'^2-1} \cos \omega) =$$

(3.13)

$$\frac{1}{2n+1} \sum_{m=0}^n (-1)^m \bar{P}_{nm}(v) \bar{P}_{nm}(v') \cos m \omega$$

where $v, v' \in \mathbb{C} - [-1, 1]$. If one or both of the variables v, v' belongs to the real interval $[-1, 1]$, then it must be approached in the limit through the complex plane, as in (1.11). The formulas (1.13) for Legendre functions with real arguments are then applicable. With $v = iu/E$, $v' = \cos \delta + i0$, equation (3.13) becomes with (1.11)

$$P_n\left(i \frac{u}{E} \cos \delta + \sqrt{1 + \frac{u^2}{E^2}} \sin \delta \cos \omega\right) =$$

(3.14)

$$\frac{1}{2n+1} \sum_{m=0}^n i^m \bar{P}_{nm}\left(i \frac{u}{E}\right) \bar{P}_{nm}(\cos \delta) \cos m \omega$$

Substituting $\omega = \lambda - t$, this becomes with (3.1)

$$P_n\left(\frac{1}{E}(iz + x \cos t + y \sin t)\right) = \quad (3.15)$$

$$\frac{1}{2n+1} \sum_{m=0}^n i^m \bar{P}_{nm}\left(i \frac{u}{E}\right) \bar{P}_{nm}(\cos \delta) \cos m(\lambda-t)$$

If we multiply both sides by $\cos m't$ or $\sin m't$ and integrate with respect to t over the interval $[-\pi, \pi]$, then, since

$$\int_{-\pi}^{\pi} \cos m(\lambda-t) \begin{pmatrix} \cos m't \\ \sin m't \end{pmatrix} dt = 2\pi \epsilon_m \begin{pmatrix} \cos m'\lambda \\ \sin m'\lambda \end{pmatrix} \quad (3.16)$$

we obtain with $q=(iz+x\cos t+ys\sin t)/E$

$$\frac{1}{2\pi} \int_{-\pi}^{\pi} P_n(q) \begin{pmatrix} \cos m't \\ \sin m't \end{pmatrix} dt = \frac{i^m \epsilon_m}{2n+1} \bar{P}_{nm}\left(i \frac{u}{E}\right) \bar{P}_{nm}(\cos \delta) \cdot \begin{pmatrix} \cos m\lambda \\ \sin m\lambda \end{pmatrix} \quad (3.17)$$

Next, consider the relationship (Hobson, 1965, p.98)

$$\frac{1}{\pi} \int_0^{\pi} (i \cos \theta + \sin \theta \cos t)^n \cos m t dt = \frac{n! i^{n-m} \sqrt{\epsilon_m}}{[(2n+1)(n+m)!(n-m)!]^{\frac{1}{2}}} \bar{P}_{nm}(\cos \theta) \quad (3.18)$$

We note that the integrand above is an even function and periodic with period 2π . Hence

$$\frac{1}{2\pi} \int_{-\pi+\lambda}^{\pi+\lambda} (i \cos \theta + \sin \theta \cos t)^n \cos m t dt = \frac{n! i^{n-m} \sqrt{\epsilon_m}}{[(2n+1)(n+m)!(n-m)!]^{\frac{1}{2}}} \bar{P}_{nm}(\cos \theta) \quad (3.19)$$

for arbitrary λ . Now

$$\frac{1}{2\pi} \int_{-\pi+\lambda}^{\pi+\lambda} (i \cos \theta + \sin \theta \cos t)^n \cos m t \left(\frac{\cos m \lambda}{\sin m \lambda} \right) dt = \quad (3.20)$$

$$= \frac{1}{2\pi} \int_{-\pi+\lambda}^{\pi+\lambda} (i \cos \theta + \sin \theta \cos t)^n \left(\frac{\cos m (\lambda-t)}{\sin m (\lambda-t)} \right) dt \\ + \frac{1}{2\pi} \int_{-\pi+\lambda}^{\pi+\lambda} (i \cos \theta + \sin \theta \cos t)^n \sin m t dt \left(\frac{\sin m \lambda}{\cos m \lambda} \right)$$

The second integral on the right side is again periodic, but an odd function; the integral is therefore zero. Consider the same point (x, y, z) as above, but now in spherical coordinates:

$$\begin{aligned} x &= r \sin \theta \cos \lambda \\ y &= r \sin \theta \sin \lambda \\ z &= r \cos \theta \end{aligned} \quad (3.21)$$

Then $i \cos \theta + \sin \theta \cos (\lambda - t) = Eq/r$. Now multiply (3.19) by $\cos m \lambda$ or $\sin m \lambda$ and substitute (3.20), thus arriving at

$$\frac{1}{2\pi} \int_{-\pi}^{\pi} q^n \left(\frac{\cos m t}{\sin m t} \right) dt = \left(\frac{r}{E} \right)^n \frac{i^{n-m} \sqrt{\epsilon_m} n!}{[(2n+1)(n-m)!(n+m)!]^{\frac{1}{2}}} \quad (3.22) \\ \bar{P}_{nm}(\cos \theta) \left(\frac{\cos m \lambda}{\sin m \lambda} \right)$$

Note that by the orthogonality of the sinusoidal functions, the integral in (3.22) is zero for $m > n$. $P_n(q)$ is simply a polynomial in q :

$$P_n(q) = \frac{1}{2^n} \sum_{k=0}^v \frac{(-1)^k (2n-2k)!}{k!(n-k)!(n-2k)!} q^{n-2k}, \quad v = \left[\frac{n}{2} \right] \quad (3.23)$$

while q^n can likewise be expressed as a finite sum of Legendre polynomials (Hobson, 1965, p.44):

$$q^n = n! \sum_{k=0}^v \frac{2^{n-2k} (n-k)!(2n-4k+1)}{k!(2n-2k+1)!} P_{n-2k}(q), \quad v = \left[\frac{n}{2} \right] \quad (3.24)$$

where $[x]$ denotes the largest integer less than or equal to x .

Substituting (3.23) into (3.17) and using (3.22), we find the transformation from spherical harmonics to ellipsoidal harmonics:

$$\frac{\sqrt{\epsilon_m}}{2n+1} \bar{P}_{n|m|} \left(i \frac{u}{E} \right) \bar{Y}_{nm}(\delta, \lambda) = \frac{(-1)^m i^n}{2^n} \sum_{k=0}^s \frac{(2n-2k)!}{k!(n-k)!} \left(\frac{r}{E} \right)^{n-2k} \frac{\bar{Y}_{n-2k,m}(\theta, \lambda)}{[(2n-4k+1)(n-2k-m)!(n-2k+m)!]^{\frac{1}{2}}} \quad (3.25)$$

$$-n \leq m \leq n, \quad s = \left[\frac{n-|m|}{2} \right]$$

And substituting (3.24) into (3.22), making use of (3.17), we obtain the reverse transformation, from ellipsoidal to spherical harmonics:

$$\left(\frac{r}{E} \right)^n \bar{Y}_{nm}(\theta, \lambda) = \frac{(-1)^m}{i^n} [(2n+1) \epsilon_m (n+m)!(n-m)!]^{\frac{1}{2}} \sum_{k=0}^s \frac{2^{n-2k} (n-k)!}{(2n-2k+1)! k!} \bar{P}_{n-2k,|m|} \left(i \frac{u}{E} \right) \bar{Y}_{n-2k,m}(\delta, \lambda) \quad (3.26)$$

$$-n \leq m \leq n, \quad s = \left[\frac{n-|m|}{2} \right]$$

It is important to realize that equations (3.25) and (3.26) represent transformations between (inner) solid harmonic functions, i.e. they hold for points in three-dimensional space. Therefore it would be fallacious to deduce the relationship between spherical and ellipsoidal harmonic coefficients simply by inserting (3.25) or (3.26) into the respective harmonic series. We recall that, according to one interpretation, the harmonic coefficients constitute the spectrum of a function restricted to a coordinate surface, either a sphere or an ellipsoid. But since neither r nor u is constant, respectively, on the ellipsoid or sphere, (3.25), (3.26) do not provide the relationship between surface harmonic functions on corresponding coordinate surfaces.

To derive the transformation between the harmonic coefficients of the two series, we resort to their alternative interpretation, namely as density integrals. The realization of ellipsoidal harmonic coefficients as density integrals is immediate once a series expansion is found for the reciprocal distance. We have for $u_p > u$

$$\frac{1}{\ell} = \frac{i}{E} \sum_{n=0}^{\infty} \sum_{m=-n}^n \frac{(-1)^m \epsilon_m}{2n+1} \bar{Q}_{n|m|} \left(i \frac{u_p}{E} \right) \bar{P}_{n|m|} \left(i \frac{u}{E} \right) \cdot \bar{Y}_{nm}(\delta_p, \lambda_p) \bar{Y}_{nm}(\delta, \lambda) \quad (3.27)$$

For $u_p < u$, the roles of u_p and u are obviously interchanged. Equation (3.27) was derived by Neumann (1848) and a much more thorough derivation, though unfortunately replete with typographical errors, can be found in (Hobson, 1965, pp424-430). The series (3.27) converges uniformly for $u_p > u$ and can therefore be integrated term by term when inserted into the integral for the potential:

$$V_p = V(u_p, \delta_p, \lambda_p) = \kappa \iiint_{\Omega} \frac{\mu}{\ell} d\Omega = \sum_{n=0}^{\infty} \sum_{m=-n}^n \bar{Q}_{n|m|} \left(i \frac{u_p}{E} \right) u_{nm} \bar{Y}_{nm}(\delta_p, \lambda_p) \quad (3.28)$$

where

$$u_{nm} = \frac{i \kappa (-1)^m \epsilon_m}{E(2n+1)} \iiint_{\Omega} \mu(u, \delta, \lambda) \bar{P}_{n|m|} \left(i \frac{u}{E} \right) \bar{Y}_{nm}(\delta, \lambda) d\Omega \quad (3.29)$$

Changing to spherical coordinates under the integral sign and using (3.25) yields

$$u_{nm} = \frac{i^{n+1} \sqrt{\epsilon_m}}{2^n E} \sum_{k=0}^S \frac{(2n-2k)!}{k!(n-k)!} \left(\frac{R}{E} \right)^{n-2k} \cdot [(2n-4k+1)(n-2k-m)!(n-2k+m)!]^{-\frac{1}{2}} \kappa \iiint_{\Omega} \mu \left(\frac{r}{R} \right)^{n-2k} \cdot \bar{Y}_{n-2k,m}(\theta, \lambda) d\Omega \quad (3.30)$$

Recalling the density integral interpretation for the spherical harmonic coefficients (2.31), this results in

$$u_{nm} = \frac{i^{n+1} \sqrt{\epsilon_m}}{2^n} \sum_{k=0}^s \frac{(2n-2k)!}{k!(n-k)!} \sqrt{\frac{2n-4k+1}{(n-2k-m)!(n-2k+m)!}} \cdot \left(\frac{R}{E}\right)^{n-2k+1} v_{n-2k,m} \quad (3.31)$$

Both the Legendre functions \bar{Q}_{nm} and the coefficients of the above sum are difficult to calculate for large n with computers using finite digit arithmetic. With the goal of more tractable computations in mind, consider the definition

$$\bar{S}_{nm}(\sigma_p) = \frac{\sigma_0^{n+1} i^{n+1} (2n+1)!}{2^n n!} \sqrt{\frac{\epsilon_m}{(2n+1)(n-m)!(n+m)!}} \cdot \bar{Q}_{nm}(i\sigma_p) \quad (3.32)$$

where $\sigma_p = u_p/E$, $\sigma_0 = R/E$. Then the ellipsoidal series expansion of V (equation (3.28)) changes to

$$V_p = \sum_{n=0}^{\infty} \sum_{m=-n}^n \bar{S}_{n|m|}(\sigma_p) \bar{u}_{nm} \bar{Y}_{nm}(\delta_p, \lambda_p) \quad (3.33)$$

where now, by combining (3.31) and (3.32), we have

$$\bar{u}_{nm} = \sum_{k=0}^s \lambda_{nmk} v_{n-2k,m}, \quad s = \left[\frac{n-|m|}{2} \right] \quad (3.34)$$

with

$$\lambda_{nmk} = \frac{(2n-2k)! n!}{(2n)! k! (n-k)!} \left[\frac{(2n-4k+1)(n-m)!(n+m)!}{(2n+1)(n-2k-m)!(n-2k+m)!} \right]^{\frac{1}{2}} \frac{1}{\sigma_0^{2k}} \quad (3.35)$$

$$n \geq 0, \quad -n \leq m \leq n, \quad 0 \leq k \leq s$$

The calculation of λ_{nmk} using the above expression is yet unmanageable on account of the factorials, but now a stable recursive formula is available:

$$\lambda_{nmk} = \frac{[(2n-4k+1)(n-2k-m+1)(n-2k-m+2)(n-2k+m+1)(n-2k+m+2)]^{\frac{1}{2}}}{2k(2n-2k+1)[2n-4k+5]^{\frac{1}{2}}} \cdot \frac{1}{\sigma_0^2} \lambda_{nm, k-1}$$

$$1 \leq k \leq s, \quad -n \leq m \leq n, \quad n \geq 0$$
(3.36)

with

$$\lambda_{nmo} = 1, \quad \text{for all } n, m$$
(3.37)

The above recursion is easily obtained from (3.35) by expanding the factorials.

Formulas (3.34), (3.35), and (3.37) show that the ellipsoidal harmonic coefficient \bar{v}_{nm} equals the spherical coefficient of the same degree and order plus a linear combination of spherical coefficients of lower degree (and same order). The ratio R/E for the earth is approximately $\sigma_0 \approx 12$, hence from equation (3.35), the coefficients λ_{nmk} , $k > 0$ in this combination are generally much less than 1 for low values of n . However, increasing values of n compensate the rapid decrease of $1/\sigma_0^{2k}$ thus also slowing the rate of decrease of λ_{nmk} with k ; and in fact, they are generally not monotonic, since for $n > 4\sigma_0^2 + 2$, $\lambda_{no1} > 1$. Therefore, the larger degree ellipsoidal harmonics may have considerably more, or less, power than their spherical counterparts, depending on how the spherical coefficients combine to form the ellipsoidal coefficients. Equation (3.34) also shows that a finite number of spherical coefficients generates an infinity of ellipsoidal coefficients; thus, if the function is band limited in spherical coordinates, its ellipsoidal spectrum is infinite. However, in this case all ellipsoidal harmonics of degree higher than the highest spherical degree are linearly dependent on the lower degree harmonics. Because the equatorial and rotational symmetries are retained when transforming to ellipsoidal coordinates, a spherical series of even and/or odd zonal harmonics transforms into an ellipsoidal series of even and/or odd zonals, respectively; this is also obvious from equation

(3.34).

The transformation from ellipsoidal to spherical harmonic coefficients is derived similarly. Substituting (3.26) into the density integral (2.31);

$$\begin{aligned}
 v_{nm} = & \frac{\kappa}{R(2n+1)} \left(\frac{E}{R}\right)^n \frac{(-1)^m}{i^n} [(2n+1) \varepsilon_m (n+m)! (n-m)!]^{\frac{1}{2}} \cdot \\
 & \cdot \sum_{k=0}^s \frac{2^{n-2k} (n-k)!}{(2n-2k+1)! k!} \iiint_{\Omega} \mu(u, \delta, \lambda) \bar{P}_{n-2k, |m|} \left(i \frac{u}{E}\right) \cdot \\
 & \cdot \bar{Y}_{n-2k, m}(\delta, \lambda) d\Omega
 \end{aligned} \quad (3.38)$$

which, with (3.29), becomes

$$\begin{aligned}
 v_{nm} = & \frac{(n+m)! (n-m)!}{2n+1} \left(\frac{E}{R}\right)^{n+1} \sum_{k=0}^s \frac{(-1)^k (n-k)! (2n-4k+1)!}{k! (n-2k)! (2n-2k+1)!} \cdot \\
 & \cdot \frac{2n-4k+1}{(n-2k-m)! (n-2k+m)!} \frac{1}{\sigma_0^{2k}} \bar{u}_{n-2k, m} \\
 = & \sum_{k=0}^s L_{nmk} \bar{u}_{n-2k, m}, \quad s = \left[\frac{n-|m|}{2}\right]
 \end{aligned} \quad (3.39)$$

where

$$\begin{aligned}
 L_{nmk} = & \frac{(-1)^k (n-k)! (2n-4k+1)!}{k! (n-2k)! (2n-2k+1)!} \left[\frac{(2n-4k+1) (n-m)! (n+m)!}{(2n+1) (n-2k-m)! (n-2k+m)!} \right]^{\frac{1}{2}} \cdot \\
 & \cdot \frac{1}{\sigma_0^{2k}}
 \end{aligned} \quad (3.40)$$

or, recursively,

$$L_{nmo} = 1, \quad \text{for all } n, m$$

$$L_{nmk} = \frac{(2n-2k+3)}{2k(2n-4k+3)(2n-4k+5)} \quad (3.41)$$

$$\cdot \left[\frac{(2n-4k+1)(n-2k-m+1)(n-2k-m+2)(n-2k+m+1)(n-2k+m+2)^{\frac{1}{2}}}{2n-4k+5} \right]$$

$$\cdot \frac{1}{\sigma_0^2} L_{nm,k-1}$$

$$1 \leq k \leq s, \quad -n \leq m \leq n, \quad n \geq 0$$

Comparing this with the transformation from spherical to ellipsoidal coefficients, the general comments made for the latter obviously apply here as well. It is equally obvious that each transformation is the inverse of the other since the set of harmonic coefficients is unique for a given function.

With the renormalization of \bar{Q}_{nm} as in (3.32), these functions become computational tractable. From (Hobson, 1965, p.108) and with the usual normalization (1.14),

$$\bar{Q}_{nm}(\mu) = \left[\frac{(2n+1)(n-m)!}{\epsilon_m(n+m)!} \right]^{\frac{1}{2}} \frac{2^n n! (n+m)!}{(2n+1)!} (\mu^2 - 1)^{\frac{1}{2}m} \frac{1}{\mu^{n+m+1}} \quad (3.42)$$

$$\cdot F\left(\frac{n+m+2}{2}, \frac{n+m+1}{2}; n+\frac{3}{2}; \frac{1}{\mu^2}\right)$$

where μ is any complex number with $|\mu| > 1$; and F denotes the hypergeometric series. Using the explicit expansion of F (Abramowitz and Stegun, 1970, p.556), $\mu = i\sigma_r$, and equation (3.32), we find for the function \bar{S}_{nm}

$$\bar{S}_{nm}(\sigma_p) = \left(1 + \frac{1}{\sigma_p^2}\right)^{\frac{1}{2}m} \left(\frac{\sigma_0}{\sigma_p}\right)^{n+1} \left[1 - \frac{(m+n+1)(m+n+2)}{2 \cdot 1! (2n+3)} \cdot \frac{1}{\sigma_p^2} + \frac{(m+n+1)(m+n+2)(m+n+3)(m+n+4)}{2^2 \cdot 2! (2n+3)(2n+5)} \frac{1}{\sigma_p^4} - \dots \right] \quad (3.43)$$

We note that as $E \rightarrow 0$ (ellipsoidal coordinate system degenerates into the spherical coordinate system), $u_p \rightarrow r_p$, $\sigma_p \rightarrow \infty$, $F \rightarrow 1$, $\sigma_0/\sigma_p = R/u_p \rightarrow R/r_p$ and hence

$\bar{S}_{nm}(\sigma_p) \rightarrow (R/r_p)^{n+1}$. Also $\lambda_{nmk} \rightarrow 0$ for $k > 0$, so that $\bar{v}_{nm} \rightarrow v_{nm}$ and the ellipsoidal series (3.33) reverts to the spherical series (2.30), as it must for $E=0$.

For later use, the functions \bar{P}_{nm} are similarly renormalized. Let

$$\bar{R}_{nm}(\sigma) = (-1)^m \sqrt{\epsilon_m (2n+1)(n-m)!(n+m)!} \frac{2^n n!}{\sigma_0^n i^n (2n+1)!} \bar{P}_{nm}(i\sigma) \quad (3.44)$$

then the reciprocal distance, in terms of \bar{S}_{nm} and \bar{R}_{nm} , is

$$\frac{1}{\ell} = \frac{1}{R} \sum_{n=0}^{\infty} \sum_{m=-n}^n \frac{1}{2n+1} \bar{S}_{n|m|}(\sigma_p) \bar{R}_{n|m|}(\sigma) \bar{Y}_{nm}(\delta_p, \lambda_p) \cdot \bar{Y}_{nm}(\delta, \lambda) \quad (3.45)$$

With (Hobson, 1965, p.95), we find

$$\bar{R}_{nm}(\sigma) = \left(1 + \frac{1}{\sigma^2}\right)^{\frac{1}{2}m} \left(\frac{\sigma}{\sigma_0}\right)^n \left[1 + \frac{(n-m)(n-m-1)}{2(2n-1)} \frac{1}{\sigma^2} + \dots\right] \quad (3.46)$$

which is a finite sum, the last term being $O(\sigma^{-(n-m)})$. Using the recursion formula for the Legendre functions:

$$\bar{P}_{nm}(i\sigma) = i\sigma \alpha_{n-1,m} \bar{P}_{n-1,m}(i\sigma) - \beta_{n-2,m} \bar{P}_{n-2,m}(i\sigma),$$

$$n \geq 2, \quad 0 \leq m \leq n-2$$

$$\bar{P}_{n,n-1}(i\sigma) = i\sigma\sqrt{2n+1} \bar{P}_{n-1,n-1}(i\sigma), \quad n \geq 1 \quad (3.47)$$

$$\bar{P}_{nn}(i\sigma) = -i\sqrt{1+\sigma^2} \sqrt{\frac{2n+1}{2n}} \bar{P}_{n-1,n-1}(i\sigma), \quad n \geq 2$$

where

$$\alpha_{n-1,m} = \sqrt{\frac{(2n-1)(2n+1)}{(n-m)(n+m)}}, \beta_{n-2,m} = \sqrt{\frac{(2n+1)(n+m-1)(n-m-1)}{(2n-3)(n+m)(n-m)}} \quad (3.48)$$

we obtain a stable and accurate recursion for the \bar{R}_{nm} :

$$\bar{R}_{nm}(\sigma) = \frac{\sigma}{\sigma_0} \bar{R}_{n-1,m}(\sigma) + \frac{(n+m-1)(n-m-1)}{(2n-1)(2n-3)} \frac{1}{\sigma_0^2} \bar{R}_{n-2,m}(\sigma)$$

$$n \geq 2, \quad 0 \leq m \leq n-2$$

$$\bar{R}_{n,n-1}(\sigma) = \frac{\sigma}{\sigma_0} \bar{R}_{n-1,n-1}(\sigma), \quad n \geq 1 \quad (3.49)$$

$$\bar{R}_{n,n}(\sigma) = \sqrt{\frac{1+\sigma^2}{\sigma_0^2}} \bar{R}_{n-1,n-1}(\sigma), \quad n \geq 1$$

$$\bar{R}_{0,0}(\sigma) = 1$$

3.2 The Ellipsoidal Series of the Gravity and Height Anomalies

The above formulas establish the transformation from spherical to ellipsoidal harmonic series (and vice versa) for an arbitrary (Newtonian) potential in the regions where the series converge uniformly. Utilizing the powerful theorem that harmonic functions and Newtonian potentials are equivalent (Kellogg, 1953, p.218), the transformation of series coefficients of the gravity anomaly and height anomaly follow immediately if we retain their definitions based on the spherical approximation (equations (2.42) and (2.57)). Because

$$r_p \Delta g_p = -r_p \frac{\partial T_p}{\partial r_p} - 2T_p, \quad \frac{1}{r_p^2} \zeta_p = \frac{1}{\kappa M} T_p \quad (3.50)$$

are both harmonic functions in the exterior space, application of equations (3.33) and (3.34) to equations (2.50) and (2.58) yields

$$\Delta g(u_p, \delta_p, \lambda_p) = \frac{R}{r_p} \sum_{n=0}^{\infty} \sum_{m=-n}^n \bar{S}_{n|m|}(\sigma_p) \bar{Y}_{nm} \bar{Y}_{nm}(\delta_p, \lambda_p) \quad (3.51)$$

with

$$\bar{\gamma}_{nm} = \sum_{k=0}^s \lambda_{nmk} g_{n-2k,m}, \quad s = \left[\frac{n-m}{2} \right] \quad (3.52)$$

and

$$\zeta_p = \frac{r_p^2}{R^2} \sum_{n=0}^{\infty} \sum_{m=-n}^n \bar{S}_{n|m|}(\sigma_p) \xi_{nm} \bar{\gamma}_{nm}(\delta_p, \lambda_p) \quad (3.53)$$

where

$$\bar{\xi}_{nm} = \sum_{k=0}^s \lambda_{nmk} z_{n-2k,m}, \quad s = \left[\frac{n-m}{2} \right] \quad (3.54)$$

and where $\bar{S}_{nm}(\sigma_p)$ and λ_{nmk} are given by (3.43) and (3.35).

The coefficients $\bar{\gamma}_{nm}$, or $\bar{\xi}_{nm}$, do not represent the ellipsoidal spectrum (as defined by (3.11)) of the gravity anomaly or height anomaly since the above sums are premultiplied by r_p , which is a function of u_p, δ_p and hence not constant on any ellipsoid. Finally we note that $\bar{\gamma}_{lm} = 0$ for $l = -1, 0, 1$, since $g_{lm} = 0$; also if $g_{00} = 0$ and $z_{00} = 0$, then the corresponding zero degree ellipsoidal coefficients vanish as well.

3.3 The Derivation of the Error Series

Using the formulation of the disturbing potential as an integral of a generalized density layer, the downward continuation error of the ellipsoidal harmonic series is similarly derived for the gravity anomaly. Attempting a corresponding development for the potential requires the expansion of the kernel E , above and below the bounding ellipsoid, into ellipsoidal harmonics. A starting point for such a derivation might be the spherical series (2.115), but this may prove to be a formidable task. It is not pursued here because the series divergence has the greater relative effect on the series for the gravity anomaly.

Thus consider the equation

$$T_p = \frac{R^2}{4\pi} \iint_{\omega} v(\delta, \lambda) K d\omega \quad (3.55)$$

where $d\omega = \sin\delta d\delta d\lambda$ (ellipsoidal coordinates) and K (the notation is modified to avoid the conflict with the linear eccentricity) is the same kernel as before (equation (2.85)), but in ellipsoidal coordinates; that is, only v has changed to include the Jacobian of the spherical to ellipsoidal coordinate transformation. Using the same definition of the gravity anomaly (equation (2.42)), we get, as before (see (2.91)),

$$\Delta g_p = \frac{R^2}{4\pi r_p} \iint_{\omega} v(\delta, \lambda) \left(\frac{1}{\ell} - \frac{r_s \cos\psi}{r_p^2} \right) d\omega \quad (3.56)$$

By the addition theorem (1.9)

$$\frac{r_s \cos\psi}{r_p^2} = \frac{1}{3} \frac{r_s}{r_p^2} \sum_{m=-1}^1 \bar{Y}_{1m}(\theta, \lambda) \bar{Y}_{1m}(\theta_p, \lambda_p) \quad (3.57)$$

Since $\bar{Y}_{1m}(\theta_p, \lambda_p)/r_p^2$ satisfies Laplace's equation and is regular at infinity, it is a potential; therefore, the transformation equations (3.33), (3.34) from spherical to ellipsoidal harmonic series apply:

$$\frac{1}{r_p^2} \bar{Y}_{1m}(\theta_p, \lambda_p) = \sum_{n=0}^{\infty} \sum_{t=-n}^n \bar{S}_{n|t|}(\sigma_p) \bar{n}_{nt} \bar{Y}_{nt}(\delta_p, \lambda_p) \quad (3.58)$$

where

$$\bar{n}_{nt} = \sum_{k=0}^S \lambda_{ntk} q_{n-2k,t} \quad (3.59)$$

and the q_{nt} are the corresponding spherical harmonic

coefficients:

$$q_{nt} = \begin{cases} 0 & \text{if } n \neq 1 \\ \frac{1}{R^2} & \text{if } n = 1 \text{ and } t = -1, 0, 1 \end{cases} \quad (3.60)$$

Inserting (3.60) and (3.59) into (3.58), we find

$$\frac{1}{r_p^2} \bar{Y}_{1m}(\theta_p, \lambda_p) = \sum_{\substack{n=1 \\ n \text{ odd}}}^{\infty} \bar{S}_{n|m|}(\sigma) \bar{n}_{nm} \bar{Y}_{nm}(\delta_p, \lambda_p) \quad (3.61)$$

Finally, by substituting (3.61) into (3.57) and considering the transformation between inner harmonic functions, equation (3.26), we obtain the formula

$$\frac{r_s \cos \psi}{r_p^2} = \frac{1}{3R} \sum_{n=0}^{\infty} \sum_{m=-n}^n u_{nm} \bar{R}_{1,|m|}(\sigma) \bar{S}_{n|m|} \bar{Y}_{1,|m|}(\delta, \lambda) \cdot \bar{Y}_{nm}(\delta_p, \lambda_p) \quad (3.62)$$

where the explicit expression for u_{nm} is not difficult to find, but of no consequence in the present derivation; it is noted, however, that $u_{1m}=1$, for all m . Combining (3.62) with the ellipsoidal series expansion for the reciprocal distance, equation (3.46), and inserting this into (3.56) results in

$$\Delta g_p = \frac{R^2}{4\pi r_p} \sum_{n=0}^{\infty} \sum_{m=-n}^n \bar{S}_{n|m|}(\sigma_p) \iint_{\omega} v(\delta, \lambda) \alpha_{nm}(u, \delta, \lambda) d\omega \cdot \bar{Y}_{nm}(\delta_p, \lambda_p) \quad (3.63)$$

where the point P is located above the bounding ellipsoid ($u_p > b$) and

$$\alpha_{nm} = \frac{1}{R} \left[\frac{1}{2n+1} \bar{R}_{n|m|}(\bar{\sigma}) \bar{Y}_{nm}(\delta, \lambda) - \frac{1}{3} u_{nm} \bar{R}_{1,|m|}(\bar{\sigma}) \cdot \bar{Y}_{1m}(\delta, \lambda) \right] \quad (3.64)$$

(Note that $\alpha_{1,0} = 0$.) If the earth's surface is an ellipsoid (with semiminor axis b , e.g. $\bar{b} = 6356755.288$ m for the mean earth ellipsoid) on which the gravity anomaly is a known function,

$$\Delta g_p = \frac{1}{r_p} \sum_{\substack{n=0 \\ n \neq 1}}^{\infty} \sum_{m=-n}^n \bar{S}_{n|m|}(\bar{b}/E) \tilde{Y}_{nm} \bar{Y}_{nm}(\delta_p, \lambda_p) \quad (3.65)$$

then in this case the integral equation (3.63) can be solved, since a comparison with (3.65) shows that

$$\begin{aligned} \tilde{Y}_{nm} &= \frac{R^2}{4\pi} \iint_{\omega} v(\delta, \lambda) \alpha_{nm}(u, \delta, \lambda) d\omega \\ &= \frac{R}{4\pi} \iint_{\omega} v(\delta, \lambda) \left[\frac{1}{2n+1} \bar{R}_{n|m|}(\bar{\sigma}) \bar{Y}_{nm}(\delta, \lambda) - \frac{1}{3} u_{nm} \bar{R}_{1,|m|}(\bar{\sigma}) \bar{Y}_{1m}(\delta, \lambda) \right] d\omega \\ &= \frac{R}{2n+1} \bar{R}_{n|m|}(\bar{\sigma}) \bar{S}_{n|m|}(\bar{\sigma}) D_{nm} - \frac{R}{3} u_{nm} \bar{R}_{1,|m|}(\bar{\sigma}) D_{1m} \end{aligned} \quad (3.66)$$

where $\bar{\sigma} = \bar{b}/E$ and

$$v(\bar{b}, \delta, \lambda) = \sum_{n=0}^{\infty} \sum_{m=-n}^n \bar{S}_{n|m|}(\bar{\sigma}) D_{nm} \bar{Y}_{nm}(\delta, \lambda) \quad (3.67)$$

Since $u_{1,0} = 1$ and $\tilde{Y}_{1,0} = 0$, $D_{1,0}$ cannot be determined from equation (3.66); we may assume $D_{0,0} = D_{1,0} = 0$. Then

$$D_{nm} = \frac{2n+1}{R} \frac{1}{\bar{R}_{n|m|}(\bar{\sigma}) \bar{S}_{n|m|}(\bar{\sigma})} \tilde{Y}_{nm} \quad (3.68)$$

For points below the bounding ellipsoid, consider the regions

$$\omega_1 = \{(\delta, \lambda) / u_p > b\}, \quad \omega_2 = \{(\delta, \lambda) / u_p < b\} \quad (3.69)$$

If $(\delta_p, \lambda_p) \in \omega_2$, the reciprocal distance is expanded as

$$\begin{aligned} \ell^{-1} = \frac{1}{R} \sum_{n=0}^{\infty} \sum_{m=-n}^n \frac{1}{2n+1} \bar{S}_{n|m|}(\sigma) \bar{R}_{n|m|}(\sigma_p) \bar{Y}_{nm}(\delta, \lambda) \cdot \\ \cdot \bar{Y}_{nm}(\delta_p, \lambda_p) \end{aligned} \quad (3.70)$$

Substituting this and the series for $r, \cos \psi / r_p^2$ (3.62) into (3.56) yields

$$\begin{aligned} \Delta g_p = \frac{R^2}{4\pi r_p} \sum_{n=0}^{\infty} \sum_{m=-n}^n \bar{S}_{n|m|}(\sigma_p) \iint_{\omega_1} v(\delta, \lambda) \alpha_{nm} d\omega \bar{Y}_{nm}(\delta, \lambda) + \\ + \frac{R}{4\pi r_p} \sum_{n=0}^{\infty} \sum_{m=-n}^n \iint_{\omega_2} v(\delta, \lambda) \left[\frac{1}{2n+1} \bar{R}_{n|m|}(\sigma_p) \bar{S}_{n|m|}(\sigma) \cdot \bar{Y}_{nm}(\delta, \lambda) + \right. \\ \left. - \frac{u_{nm}}{3} \bar{S}_{n|m|}(\sigma_p) \bar{R}_{1,|m|}(\sigma) \bar{Y}_{1m}(\delta, \lambda) \right] d\omega \bar{Y}_{nm}(\delta_p, \lambda_p) \end{aligned} \quad (3.71)$$

Note that $\sigma = u/E$ is a function of (δ, λ) , since u is the coordinate of a point on the earth's surface.

The downward continuation error of the ellipsoidal harmonic series for Δg is then the difference between (3.63), truncated at $n=\bar{n}$, and the true series (3.71). After several simplifications, in which (3.64) is duly considered, this error can be expressed as

$$\begin{aligned} \varepsilon(\hat{\Delta g}_p) = \sum_{n=0}^{\bar{n}} \sum_{m=-n}^n d_{nm}(\sigma_p) \bar{Y}_{nm}(\delta_p, \lambda_p) + \\ + \sum_{n=\bar{n}+1}^{\infty} \sum_{m=-n}^n d'_{nm}(\sigma_p) \bar{Y}_{nm}(\delta_p, \lambda_p) \end{aligned} \quad (3.72)$$

where

$$d_{nm}(r_p) = \frac{R}{4\pi r_p} \frac{1}{2n+1} \iint_{\omega_2} v(\delta, \lambda) [\bar{S}_{n|m|}(\sigma_p) \bar{R}_{n|m|}(\sigma) - \bar{R}_{n|m|}(\sigma_p) \bar{S}_{n|m|}(\sigma)] \bar{Y}_{nm}(\delta, \lambda) d\omega \quad (3.73)$$

and

$$d'_{nm}(r_p) = d_{nm}(r_p) - \frac{1}{r_p} \bar{S}_{n|m|}(\sigma_p) \gamma_{nm} \quad (3.74)$$

γ_{nm} being the ellipsoidal coefficients of the outer series of $r_p \Delta g_p$. In view of (3.43) and (3.46) the kernel of (3.73) can be expanded as a series in

$$\bar{w} = 1 - \frac{\sigma_p}{\sigma} \quad (3.75)$$

By using the series expressions for $\bar{S}_{nm}(\sigma)$ and $\bar{R}_{nm}(\sigma)$, namely equations (3.43) and (3.46), and collecting like powers of \bar{w} and σ_p^{-1} , it is found (through a lengthy and tedious derivation) that

$$\begin{aligned} & \bar{S}_{nm}(\sigma_p) \bar{R}_{nm}(\sigma) - \bar{S}_{nm}(\sigma) \bar{R}_{nm}(\sigma_p) = \\ & = (2n+1) \frac{\sigma_0}{\sigma_p} [\bar{w} (1 + \tau_{11} \frac{1}{\sigma_p^2} + \tau_{12} \frac{1}{\sigma_p^4} + O(\frac{1}{\sigma_p^6})) + \\ & \quad + \bar{w}^2 (\tau_{21} \frac{1}{\sigma_p^2} + \tau_{22} \frac{1}{\sigma_p^4} + O(\frac{1}{\sigma_p^6})) + \\ & \quad + \bar{w}^3 (\tau_{30} + \tau_{31} \frac{1}{\sigma_p^2} + \tau_{32} \frac{1}{\sigma_p^4} + O(\frac{1}{\sigma_p^6})) + \\ & \quad + \bar{w}^4 (\tau_{40} + \tau_{42} \frac{1}{\sigma_p^4} + O(\frac{1}{\sigma_p^6})) + \\ & \quad + O(\bar{w}^5)] \end{aligned} \quad (3.76)$$

where

$$\tau_{11} = -1, \quad \tau_{12} = 1, \quad \tau_{21} = 1, \quad \tau_{22} = -2$$

$$\tau_{30} = \tau_{40} = \frac{n(n+1)}{6}, \quad \tau_{31} = -\frac{m^2(2n+1)(n+1)}{6} \quad (3.77)$$

$$\tau_{32} = 2 + \frac{1}{2}(n^2 + n + m^2), \quad \tau_{42} = 1 - \tau_{32}$$

As with the total downward continuation error in spherical harmonic series, the linear, as well as quadratic, terms in \bar{w} sum to zero for points on or above the earth's surface. The expression (3.76) provides two- to three-digit accuracy for $n=300$, $m=0, 150, 300$ and $\sigma_p=12.180886$, $\sigma=12.193239$ which represent the worst situations; that is, when the point of computation, P , and the point of integration are farthest apart in terms of the coordinate u (then the ratio σ_p/σ is least and \bar{w} is largest).

3.4 The Results of the Numerical Analysis

Since the infinite ellipsoidal harmonic series of the gravity (or potential) converges with certainty only outside the bounding ellipsoid, the evaluation of the truncated series at the earth's surface is associated with a downward continuation error. However, we should expect the error to be smaller than for the spherical series since the penetration into the region of (probable) divergence is generally not as deep, especially in the polar areas. Although this is almost obvious, it can be verified by examining the divergence of the zonal series corresponding to the simple density distributions of section 2.1. For example, Figure 19 shows the differences between the partial sums of the ellipsoidal series and the true value of the gravity anomaly evaluated at the point ($r_p=6357200$ m, $\theta_p=72.5^\circ$). The eccentricity of the coordinate system was taken as $E=450000$ m so that the evaluation point lies below the bounding ellipsoid: -5300 m for the equatorial disk and -3500 m for the serrated ellipsoid. The ellipsoidal harmonic coefficients were determined by applying the transformation (3.52). Clearly, in contrast to Fig. 5, the effect of divergence is more subdued, becoming noticeable only when $\bar{n} > 1800$.

The above expectations are not realized when comparing the truncated ellipsoidal series of the gravity field generated by the density layer of section 2.3 against the corresponding truncated inner spherical series. The differences between the partial sums for $\bar{n}=300$ can be orders of magnitude larger than the values listed in Tables 3 and 4. The only admissible conclusion, that this is a comparison of incompatible spectra and is therefore meaningless, reemphasizes the inherent danger in the comparison of partial sums of different series representing the same function.

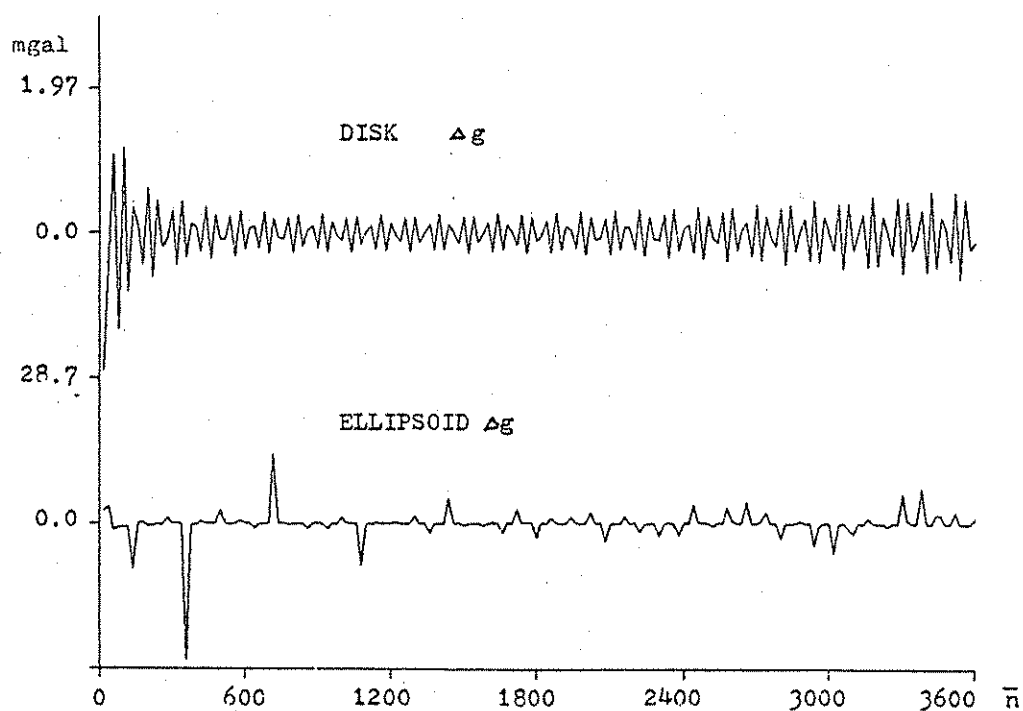


Figure 19: Partial sums of ellipsoidal harmonic series of Δg for equatorial disk and serrated ellipsoid density distributions (Figures 2 and 3) minus corresponding true values evaluated at $r_p = 6357200$ m, $\theta_p = 7.5^\circ$.

For the numerical study of the downward continuation error, we can specify the density model by (3.68) in conjunction with the coefficients (2.126). The quantities $\bar{S}_{nlm}(\bar{r}) \tilde{Y}_{nm}/R$ were set equal to \tilde{g}_{nm} , recognizing that a different gravity model ensues and that the correlation to the topography is no longer given by (2.131). This choice of \tilde{Y}_{nm} is equivalent to the assumption that the function $r_p \Delta g_p$ (approximately on an ellipsoid) was analyzed in the ellipsoidal coordinate system (δ, λ) to yield $R\tilde{g}_{nm}$. (The degree variances of D_{nm} (3.68) and of $(2n+1)\tilde{g}_{nm}$, equation (2.94), differed only in the third digit.) Moreover, to avoid unnecessary complications, the same surface model was adopted, but the grid coordinates were identified as ellipsoidal coordinates: $\delta_i = i\Delta\delta$, where $\Delta\delta = 0.6^\circ$. Hence

$$u_{si} = \sqrt{r_{si}^2 - E^2 \sin^2 \delta_{i+\frac{1}{2}}} \quad (3.78)$$

The semiminor axis of the bounding ellipsoid (with $E=521854.4492$ m, see (3.9)) was found to be $u_p=6363096.071$ m. The surface deviates from this ellipsoid by an RMS value of 6114 m; the deviation is around 6000 m whether at the pole or equator. Other choices of the linear eccentricity E may produce a closer overall fit to the surface; for example, with $E=523836.8873$ m ($a=6378140$ m, $f=1/296$), the bounding ellipsoid is closer to the surface at the poles, but more distant at the equator, with a total RMS deviation of 6085 m.

The evaluation of the coefficients d_{nm} of the downward continuation error of ellipsoidal series is almost identically performed as for the spherical series. The expansion (3.76) minus the linear and quadratic terms in \bar{w} is substituted into (3.73), which, in turn, is discretized according to the assumption that the surface model consists of ellipsoidal compartments delineated by the coordinate lines $\delta=\text{constant}$, $\lambda=\text{constant}$, and that v is a step function constant within each compartment.

In contrast to the determination of the error in the spherical harmonic series, one value of u_p ($u_p=6356800$ m) sufficed to yield an ellipsoid with an adequate supply of points within 100 m above the surface model, in all regions. The RMS values of the downward continuation error series, truncated at $\bar{n}=300$, at these points are shown in Table 8 for the regions of Table 1 (where the latitudinal ranges now refer to the reduced latitude). Also shown are the numbers of total points on which the RMS values are based, as well as the maximum absolute value in each group.

Table 8: RMS downward continuation error of ellipsoidal harmonic series of gravity anomaly in regions of Table 1 (latitude ranges refer to reduced latitude) at points on the ellipsoid $u_p=6356800$ m ($E=521854.4492$ m) and above the surface model no more than 100 m. Maximum absolute values for each region are given parenthetically.

Region	RMS $\varepsilon(\Delta g)$ (max $\varepsilon(\Delta g)$) , μgal , $0 \leq n \leq 300$ $\lambda: 0^\circ.3 - 359^\circ.7$			
	No. of points	N	No. of points	S
I	7410	1.9×10^{-4} (3.2×10^{-3})	8355	2.7×10^{-4} (4.1×10^{-3})
II	5003	1.7×10^{-4} (1.1×10^{-3})	9328	$.94 \times 10^{-4}$ ($.45 \times 10^{-3}$)
III	7282	1.1×10^{-4} ($.96 \times 10^{-3}$)	2071	1.3×10^{-4} ($.63 \times 10^{-3}$)

The numerical results are limited to the demonstration that the effect of divergence ($\bar{n}=300$) of ellipsoidal harmonic series near the earth's surface is considerably less pronounced than in the case of series of spherical harmonics. Note also the essential uniformity of the errors over all the latitudinal ranges.

4. Corrections to the Spherical Approximations

The ellipsoidal correction expounded by Lelgemann (1970) and Moritz (1980) amend the spherical approximation by accounting for the general ellipticity of the earth's shape. The spherical approximation of the relevant geodetic quantities, Δg , ζ , defined by (2.42) and (2.57), however, do not conform precisely to Moritz's definitions. To achieve the spatial spherical harmonic expansion of the height anomaly (equation (2.56)), as well as the corresponding ellipsoidal expansion, the normal gravity was equated with the gravity produced by a homogeneous ball of mass M , instead of the conventional average value of γ over the spheropotential surface (the latter being assumed by Moritz). Furthermore, the spherical approximation of the gravity anomaly, according to Moritz (ibid., p.425), is defined by

$$T_p = \frac{\bar{R}}{4\pi} \iint_{\sigma} \Delta g^{\circ} S(\psi) d\sigma \quad (4.1)$$

which represents the solution to the (third) boundary value problem if the bounding surface is a sphere; $S(\psi)$ is Stokes' function. In equation (4.1) T is the actual disturbing potential with no spherical approximation, and both T and Δg° are functions on the ellipsoid that approximates the earth's surface, with semiminor axis, say b . Using coordinates for which the ellipsoid is a coordinate surface, for example, ellipsoidal coordinates (u, δ, λ) (Moritz uses geodetic coordinates), the angle ψ loses its usual geometric meaning since it is defined by

$$\cos \psi = \cos \delta \cos \delta_p + \sin \delta \sin \delta_p \cos(\lambda - \lambda_p) \quad (4.2)$$

where (δ, λ) and (δ_p, λ_p) are points on the ellipsoid. ψ may be interpreted as the central angle between the projections of ellipsoidal points onto the unit sphere according to the correspondence (3.12). Expressing T and S in terms of harmonic functions,

$$T(b, \delta_p, \lambda_p) = \sum_{n=0}^{\infty} \sum_{m=-n}^n A_{nm} \bar{Y}_{nm}(\delta_p, \lambda_p) \quad (4.3)$$

$$S(\delta, \lambda, \delta_p, \lambda_p) = \sum_{n=2}^{\infty} \sum_{m=-n}^n \frac{1}{n-1} \bar{Y}_{nm}(\delta, \lambda) \bar{Y}_{nm}(\delta_p, \lambda_p) \quad (4.4)$$

directly yields

$$\Delta g^o(b, \delta, \lambda) = \sum_{n=2}^{\infty} \sum_{m=-n}^n \frac{n-1}{R} A_{nm} \bar{Y}_{nm}(\delta, \lambda) \quad (4.5)$$

Equation (4.5) obviously differs from (3.51) because of the latter's dependence on r . Hence the ellipsoidal corrections of Moritz (1980, pp.318,327) to ζ and Δg are not applicable here.

When abandoning the spherical approximations (2.42) and (2.57), the simple spectral relationship between the potential and gravity, or height, anomaly is lost. Nevertheless, to the approximation developed below and knowing their relationship in the space domain, the latter are still representable as series involving the spherical harmonic functions.

In the following, we will build on the premise that the disturbing potential is known to any desired accuracy, for example, as a series of spherical or ellipsoidal harmonics. The corrections to the spherical approximation of the height anomaly and gravity anomaly will be derived to an accuracy determined by the neglect of terms involving the fourth power of the first eccentricity. Furthermore, derivatives along spheropotential surface normals and along ellipsoidal normals are not distinguished (they are identical on the reference ellipsoid, if it is an equipotential surface in the normal gravity field). Thus the height anomaly is

$$\zeta_p = \frac{1}{\gamma_Q} [T_p + \zeta_p^2 \frac{\partial^2 U}{\partial h^2} |_Q + \dots] \quad (4.6)$$

where $\partial/\partial h$ is the directional derivative along the

ellipsoid normal. The vertical gradient of the normal gravity, $\partial\gamma/\partial h = \partial^2 U/\partial h^2$, is on the order of $2\gamma/r \approx 3 \times 10^{-6} \text{ s}^{-2}$, so that, with $\zeta_p < 100 \text{ m}$, its omission causes at most an error of 3 mm. In order to achieve 0.5 cm accuracy in the height anomaly, the normal gravity must be accurate to about 50 mgal, so that in view of the above gradient of about 0.3 mgal/m, γ_p may be substituted for γ_q in (4.6). Similarly, the gravity anomaly in its most rigorous form is

$$\Delta g_p = - \frac{\partial W_p}{\partial H_p} + \frac{\partial U_p}{\partial h_p} + \frac{\partial \gamma}{\partial h} \Big|_Q \zeta_p + \frac{\partial^2 \gamma}{\partial h^2} \zeta_p^2 + \dots \quad (4.7)$$

where W is the earth's gravity potential, U is the normal potential, and $\partial/\partial H$ is the derivative along the plumb line, i.e. the gradient. Terms of second and higher order can be neglected, causing an error of at most $1.5 \times 10^{-3} \text{ mgal}$, since $\partial^2 \gamma/\partial h^2 \approx 6 \kappa M/R^3 \approx 1.5 \times 10^{-12} \text{ m}^{-1} \text{ s}^{-2}$. Furthermore, as this also gives the change in the vertical gradient of γ with height, the value of Δg changes by no more than $1.5 \times 10^{-3} \text{ mgal}$ if $\partial\gamma/\partial h$ is evaluated at P instead of Q .

Fig. 20 shows the direction of the plumb line with respect to the orthogonal directions of dh , $Zd\phi$, $N\cos\phi d\lambda$ at a point P ; Z is the meridional radius of curvature of the ellipsoid, N is the radius of curvature in the prime vertical, and ϕ is the geodetic latitude. If Θ is the total deflection of the vertical (angle between dh and dH) with components ξ and η , then, since these are small angles, the direction cosines of dH with respect to the normal directions are $\cos\Theta$, ξ , and η . Hence

$$\frac{\partial}{\partial H} = \cos\Theta \frac{\partial}{\partial h} + \xi \frac{\partial}{Z \partial \phi} + \eta \frac{\partial}{N \cos \phi \partial \lambda} \quad (4.8)$$

Considering Fig. 21, the directional derivative along the ellipsoid normal is

$$\frac{\partial}{\partial h} = \cos\psi \frac{\partial}{\partial r} - \sin\psi \frac{\partial}{r \partial \theta} \quad (4.9)$$

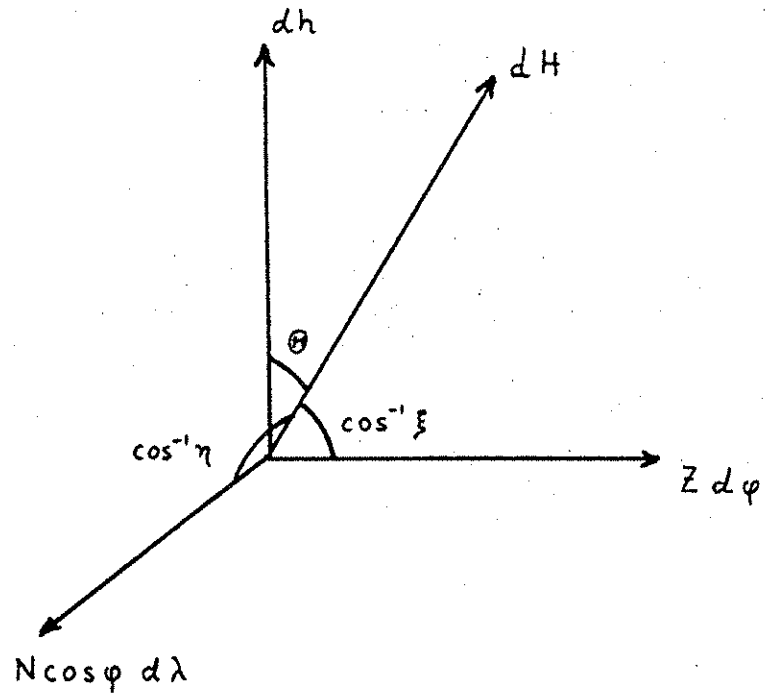


Figure 20: The deflection of the vertical.

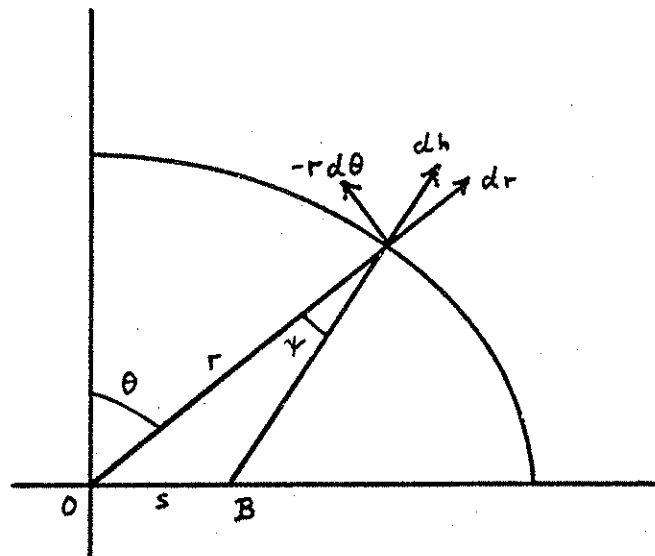


Figure 21: The normal directional derivative.

where ψ is the angle between dh and dr . The ellipsoid normal intersects the equator at a distance s from the center; we have

$$s = \frac{ae^2\sqrt{1-e^2} \sin\theta}{\sqrt{1-e^2} \sin^2\theta} ; r = \frac{a\sqrt{1-e^2}}{\sqrt{1-e^2} \sin^2\theta} \quad (4.10)$$

Using the law of sines on the triangle OBQ , we obtain

$$\frac{r}{s} = \cot\psi \cos\theta + \sin\theta \quad (4.11)$$

Hence with (4.10)

$$\tan \psi = \frac{e^2 \sin\theta \cos\theta}{1 - e^2 \sin^2\theta} \quad (4.12)$$

Pythagoras' theorem then easily furnishes the expressions

$$\sin\psi = e^2 \sin\theta \cos\theta - \frac{1}{2}e^4(e^2 - 2) \sin^3\theta \cos\theta + O(e^6) \quad (4.13)$$

$$\cos\psi = 1 - \frac{1}{2}e^4 \sin^2\theta + \frac{29}{3} e^4 \sin^4\theta + O(e^6) \quad (4.14)$$

Hence, neglecting terms of $O(e^4)$,

$$\frac{\partial}{\partial h} = \frac{\partial}{\partial r} - e^2 \sin\theta \cos\theta \frac{\partial}{r\partial\theta} \quad (4.15)$$

Note that e^2 depends on the coordinate surface $u=b$ under consideration, but to the accuracies involved here, it can be treated as a constant for points near the earth's surface.

The normal potential, U , is given as a series of spherical harmonics by Heiskanen and Moritz (1967, p.73):

$$U = \frac{\kappa M}{r} \left[1 - \sum_{n=1}^{\infty} J_{2n} \left(\frac{a}{r} \right)^{2n} P_{2n}(\cos \theta) \right] + \frac{1}{2} \omega^2 r^2 \sin^2 \theta \quad (4.16)$$

where $J_{2n} = O(e^{2n})$ and ω is the rotational speed of the earth: $\omega^2 \approx 5 \times 10^{-1} \text{ s}^{-2}$. The normal gravity, being the gradient of U , is therefore

$$\begin{aligned} \gamma &= - \frac{\partial U}{\partial h} = - \frac{\partial U}{\partial r} + e^2 \sin \theta \cos \theta \frac{\partial U}{r \partial \theta} \\ &= \frac{\kappa M}{r^2} - 3 \frac{\kappa M}{r^2} J_2 \left(\frac{a}{r} \right)^2 P_2(\cos \theta) - \omega^2 r \sin^2 \theta (1 - e^2 \cos^2 \theta) \\ &\quad + O(e^4) \end{aligned} \quad (4.17)$$

We note that $\omega^2 r \approx 0.03 \text{ m/s}^2 \approx 0.003 \gamma \approx O(e^1)$, so that the terms with $\omega^2 r e^2$ can also be neglected. From (4.17), the normal derivative of γ is found to be

$$\begin{aligned} \frac{\partial \gamma}{\partial h} &= \frac{\partial \gamma}{\partial r} - e^2 \sin \theta \cos \theta \frac{\partial r}{r \partial \theta} \\ &= - \frac{2}{r} \left[\gamma - 3 \frac{\kappa M}{r^2} J_2 \left(\frac{a}{r} \right)^2 P_2(\cos \theta) + \frac{3}{2} \omega^2 r \sin^2 \theta \right] + O(e^4) \end{aligned} \quad (4.18)$$

Hence

$$\begin{aligned} \frac{1}{\gamma} \frac{\partial \gamma}{\partial h} &= - \frac{2}{r} + \left(\frac{6 \kappa M}{r^3} J_2 \left(\frac{a}{r} \right)^2 P_2 - 3 \omega^2 \sin^2 \theta + O(e^4) \right) \frac{r^2}{\kappa M} \\ &\quad \left(1 - 3 J_2 \left(\frac{a}{r} \right)^2 P_2 - \omega^2 r \sin^2 \theta + O(e^4) \right)^{-1} \end{aligned} \quad (4.19)$$

$$= - \frac{2}{r} \left[1 - 3 J_2 \left(\frac{a}{r} \right)^2 P_2(\cos \theta) + \frac{3 \omega^2 r^3}{2 \kappa M} \sin^2 \theta \right] + O(e^4)$$

Substituting (4.17) into (4.6), the height anomaly becomes

$$\zeta_p = \frac{r_p^2 T_p}{\kappa M} \left[1 + 3J_2 \left(\frac{a}{r_p} \right)^2 P_2(\cos \theta_p) + \frac{\omega^2 r_p^3}{\kappa M} \sin^2 \theta_p \right] + O(e^4) \quad (4.20)$$

The correction above reaches a maximum value (0.33%) at the poles, $\theta_p = 0^\circ, 180^\circ$.

Taking note of (4.15) and (4.8), the gravity anomaly (4.7), upon substituting (4.19), becomes

$$\begin{aligned} \Delta g_p &= -\frac{\partial T_p}{\partial r_p} - e^2 \sin \theta_p \cos \theta_p \frac{\partial T_p}{r_p \partial \theta_p} + \frac{1}{\gamma_p} \frac{\partial \gamma}{\partial h} \Big|_p T_p + \varepsilon_p + O(e^4) \\ &= -\frac{\partial T_p}{\partial r_p} - \frac{2}{r_p} T_p - e^2 \sin \theta_p \cos \theta_p \frac{\partial T_p}{r_p \partial \theta_p} + \\ &\quad + (6J_2 \frac{a^2}{r_p^3} P_2(\cos \theta_p) - \frac{3\omega^2 r_p^2}{\kappa M} \sin^2 \theta_p) T_p + \varepsilon_p + O(e^4) \end{aligned} \quad (4.21)$$

where $T_p = W_p - U_p$ is the disturbing potential and

$$\begin{aligned} \varepsilon_p &= (1 - \cos \theta_p) \frac{\partial W_p}{\partial h_p} - \xi_p \frac{\partial W_p}{Z_p \partial \phi_p} - \eta_p \frac{\partial W_p}{N_p \cos \phi_p \partial \lambda_p} \\ &= (1 - \cos \theta_p) \frac{\partial W_p}{\partial h_p} - \xi_p \frac{\partial T_p}{Z_p \partial \phi_p} - \eta_p \frac{\partial T_p}{N_p \cos \phi_p \partial \lambda_p} + \xi_p \frac{\partial U_p}{Z_p \partial \phi_p} \end{aligned} \quad (4.22)$$

in which we used the fact that the normal potential does not vary in longitude. The derivatives of T in (4.22) are the components of the deflection of the vertical multiplied by the normal gravity, and the derivative of U is

$$\frac{\partial U}{Z \partial \phi} \approx -\frac{\partial U}{R \partial \theta} = -\left(\frac{3\kappa M}{R^2} J_2 + \omega^2 \bar{R} \right) \sin \theta \cos \theta \quad (4.23)$$

Finally,

$$-\frac{\partial W}{\partial h} \approx g \quad (4.24)$$

so that an approximate upper bound for the magnitude of ε_p is

$$|\varepsilon_p| \leq |\theta_p^2 g_p| + |\xi_p^2 \gamma_p| + |\eta_p^2 \gamma_p| + \\ + |\xi_p (\frac{3\kappa M}{R^2} J_2 + \omega^2 \bar{R}) \sin\theta \cos\theta| \quad (4.25)$$

Using $g \approx \gamma \approx 9.8 \text{ m/s}^2$ and $\xi \approx \eta \approx 10''$, we find $|\varepsilon_p| < 0.34 \text{ mgal}$; the dominant term is the last one, hence this bound varies linearly with the magnitude of ξ_p . In view of its relation to the deflection of the vertical, the horizontal derivative of T has typical values of $\gamma \xi = 50 \text{ mgal}$, with an upper bound ($\xi < 1'$) of 300 mgal . Therefore the third term in (4.21) has a value of about 0.2 mgal (at most 1 mgal), while the last two terms in (4.21) rarely amount to more than 0.1 mgal . The formulas (4.20) and (4.21) are valid anywhere on the earth's surface or above with an accuracy of about $e^* \xi < 5 \text{ mm}$ and $e^* \Delta g < 1 \times 10^{-2} \text{ mgal}$, respectively. Equation (4.21) generalizes the correction derived by Molodenskii et al. (1962, p.212) for anomalies on the reference ellipsoid and is quite unlike the correction of Moritz because of the different definition of spherical approximation.

The equations (4.20) and (4.21) were developed in order to provide the means for the precise evaluation of the gravity and height anomalies using the spherical (or ellipsoidal) harmonic series, whose formulation depends on the adopted spherical approximation, namely (2.42) and (2.57).

5. Summary, Conclusion, Recommendation

The expansion of the earth's gravitational potential into a series of spherical harmonic functions has long been used to describe it on a global basis. The question of the validity of such an expansion at the earth's surface, though propounded from the outset, has been addressed firmly only recently and then primarily from a purely theoretical standpoint (e.g. the Runge-Krarup theorem). While these represent important advances, a definitive answer has yet to be, or may never be, found. In the practical situation, the infinite series is necessarily truncated at some degree \bar{n} . What effect the (possible, or even probable) divergence of the infinite series at the earth's surface has on its partial sums has received only a "first-generation" analysis. With the present study, we have taken a second look at this effect, but the subsequent conclusions must be carefully phrased and are necessarily lacking in numerical specificity.

The downward continuation error, being defined here in connection with the effect of series divergence, is a deterministic, or systematic, error; it has no stochastic properties (one could argue this point if the convergence surface is itself a stochastic process). Therefore, its assessment is forthcoming if the true value of the field which the series represents is known, such as in the case of the simple density distributions of section 2.1. These distributions were not designed to simulate the earth's density, but their dimensions and the numerical investigations were selected with the terrestrial situation in mind. It was found that the partial sums of the spherical harmonic series for the potential (and gravity anomaly), evaluated below the surface of convergence, do not show signs of divergence until the truncation degree is relatively large. Also, Figure 8 suggests that the divergence problem may affect the geopotential series only if the truncation degree is 300 or greater. For the earth, the requirement of knowing the true value of the potential field at the surface is difficult to meet, even if, for the purpose of an ad hoc analysis, models are introduced to represent the earth's surface and gravity field.

Early works were based on modeling the earth's lithosphere by a volumetric density distribution of essentially constant value. In this and the present use of a surface layer density distribution, the true values of the modeled field can only be estimated, again, by a truncated (inner) series expansion. It was found that low degree comparisons of inner and outer series of the volumetric density model give unrealistically large values of the error. This result is attributable principally to the inadequacy of the choice of the model. Furthermore, since this model itself depends only marginally (through a crustal density of 2.67 g/cm^3 , etc.) on the actual characteristics of the earth's potential field, it was abandoned for a surface density layer model which could be defined (although not optimally) so as to yield a reasonable representation of the true potential field. This model does not represent exactly the earth's field at resolutions greater than 200 km, since random harmonic coefficients were generated to fill in the detail to a resolution of 67 km. However, the coefficients were forced to decay, with degree n , according to a degree variance model characteristic of the true gravity field. The main disadvantage of this density model is the inability to compute the true values of the potential on the surface to any desired accuracy. A model for which this is no problem consists of a sufficiently large number of point masses distributed globally just below the earth's surface (to ensure the divergence of the series), as well as deeper within (to generate long wavelength power). The difficulty with this model would be the numerical determination of the masses for a representative potential field.

The downward continuation errors depicted in Tables 3 through 7 are completely insignificant with respect to anticipated measurement accuracies of 1 mgal and 10 cm in the gravity anomaly and geoid undulation, respectively. For the anomaly the sum of the harmonics of the error up to degree 300 was found to be $0.3 - 0.5 \mu\text{gal}$ ($1 \mu\text{gal} = 10^{-3} \text{ mgal}$) near the equator, about $20 \mu\text{gal}$ in the midlatitudes, and $80 - 90 \mu\text{gal}$ in the polar regions. Similar minute values were obtained for the first 300 degrees of the error in the height anomalies: $0.3 - 0.5 \mu\text{m}$ ($1 \mu\text{m} = 10^{-6} \text{ m}$) in the low latitudes, about $70 \mu\text{m}$ in the midlatitudes, and approximately $400 \mu\text{m}$ near the poles. Of course, these numbers do not give the entire error since they exclude the contribution from degrees 301 to ∞ , representing a truncation effect, i.e., the neglect of terms of degree greater than \bar{n} of the inner series. We can expect the usual degree variance models to provide a fair estimate of this effect. This expectation is rather intuitive, based on the near sphericity of the earth's surface, the results

of section 2.1, and on the smallness of the values of Tables 3 and 4, but not founded on deductive reasoning; the same expectation may prove to be erroneous for the volumetric density model. Using the model (2.128), the RMS truncation error ($\bar{n}=300$) has values (for point estimates) of about 30 mgal and 36 cm, respectively. For the Gaussian smoothed fields (95% of the 300-th degree harmonic is filtered), the first 300 degrees of the gravity anomaly error approximately sum to 0.02 μ gal (equatorial region), 1.0 μ gal (midlatitudes), and 4.0 μ gal (near the poles), with respective values of 0.02 μ m, 3.0 μ m, and 20 μ m for the height anomaly. The RMS truncation effect is approximately 0.3 mgal and 0.7 cm, respectively. Therefore, the estimation of point or mean gravity anomalies and geoid undulations (height anomalies) using the outer series expansion to degree 300 anywhere on the earth's surface is practically unaffected by the divergence of the total series.

Throughout this exposition emphasis has been on the dissimilarity of partial sums of inner and outer series. For a constant radius $r_p = R_p$ greater than the bounding sphere radius R , the coefficients of the partial sum of the outer spherical harmonic series for the potential represent a portion of its spectrum on the sphere of radius R_p . Since the spheres of radius $r_p < R$ pass through the earth's interior, the coefficients of the inner series (constant r_p) cannot represent the spectrum of the exterior potential. Indeed, for the density layer model it is difficult to give an interpretation to these coefficients, which in any case vary as the point P moves on the earth's surface. By accepting the conclusion that the truncated outer series ($\bar{n} \leq 300$) can be used without concern for divergence anywhere on the earth's surface, we also cannot identify the outer harmonic components as spectral constituents of the potential (or gravity anomaly) on the surface. (Note that the harmonics should be evaluated on the actual surface of the earth, and not on some mean earth sphere.) Therefore, any evaluation of the outer series must be accompanied by an unambiguous statement regarding the quantity being estimated. For example, by introducing the Gaussian average, we attempt to eliminate, or filter, the high-degree information, so that the inner and outer series truncated at 300 are more nearly comparable.

A major part of this report was devoted to the development of ellipsoidal harmonic series, in particular, the transformation between ellipsoidal and spherical harmonic coefficients. Although the downward continuation error in ellipsoidal series is generally less than in spherical series, especially in the polar regions, there

seems to be no need in practice ($\bar{n} \leq 300$) to make the conversion for simple evaluations. On the other hand, because the spectral components of the potential on the earth's surface bear a closer resemblance to ellipsoidal harmonics than to spherical harmonics, the analysis of terrestrial data (including altimetry) is more correctly compared to (or combined with) the ellipsoidal spectrum. For example, the analysis of a global set of geoid undulations (in the ellipsoidal coordinate system (δ, λ)) yields harmonic coefficients which should be transformed according to (3.34), (3.35) before comparing them to potential coefficients derived from satellite data.

The expansions of the simulated surface and gravity field were restricted to terms of degree no greater than 300 because of limited computer storage capabilities, rather than a concern about excessive computer time. Obviously, for higher expansions of the potential, the error analysis must be redone since extrapolations on the basis of Table 5 are risky. In any new study of the downward continuation error one should endeavor to devise a density distribution (such as point masses) for which the potential function can be evaluated to any accuracy, thus allowing a more definitive assessment of the series divergence. Should the error ever prove to be relatively significant, it is recommended that corrections not be applied to spherical harmonic coefficients if the conversion to ellipsoidal harmonics eliminates the significance of the error.

The investigations in sections 2 and 3 have relied on approximate formulas for the gravity anomaly and geoid undulation (or height anomaly) in order to simplify their functional relationship to the disturbing potential. In section 4, corrections to these approximations were developed with the premise that the disturbing potential is a known quantity (e.g. in series form) and with a relative accuracy on the order of the square of the earth's flattening. These corrections should be applied to Δg , ζ whether they are evaluated using the spherical series (2.50), (2.58) or the ellipsoidal series (3.51), (3.53) (taking due account of the coordinate systems involved).

LIST OF REFERENCES

- Abromowitz, M., and I.A. Stegun, Handbook of Mathematical Functions, Dover Publications, Inc., New York, 1970.
- Arnold, K., "The Spherical-Harmonic Expansion of the Gravitational Potential of the Earth in the External Space and its Convergence," Gerlands Beitr. Geophysik, Leipzig, vol.87, no.2, pp.81-90, 1978.
- Arnold, K., "Picone's Theorem and the Convergence of the Expansion in Spherical Harmonics of the Gravitational Potential of the Earth in the External Space," Bollettino di Geofisica Teorica ed Applicata, vol.22, no.86, pp.95-103, 1980.
- Balmino, G., "Representation of the Earth Potential by Buried Masses," in The Use of Artificial Satellites for Geodesy, Geophysical Monograph 15, edited by S.W. Henriksen, et al., American Geophysical Union, Washington, D.C., pp.121-124, 1972.
- Balmino, G., K. Lambeck, and W.M. Kaula, "A Spherical Harmonic Analysis for the Earth's Topography," Journal of Geophysical Research, vol.78, no.2, pp.478-481, Jan 10., 1973.
- Bath, M., Spectral Analysis in Geophysics, seventh in the series of Developments in Solid Earth Geophysics, Elsevier Scientific Publishing Company, Amsterdam, 1974.
- Bowford, G., Geodesy, Clarendon Press, Oxford, 1971.
- Brovar, V.V., "Fundamental Harmonic Functions with a Singularity on a Segment and Solutions of Outer Boundary Problems," Geodesy and Aerophotogrammetry (translated from Russian by AGU), no.3, pp.150-155, 1964.
- Colombo, O.L., "Optimal Estimation from Data Regularly Sampled on a Sphere with Applications Geodesy," report no.291, Department of Geodetic Science and Surveying, The Ohio State University, 1979.

- Colombo, O.L., "Numerical Methods for Harmonic Analysis on the Sphere," report no.310, Department of Geodetic Science and Surveying, The Ohio State University, 1981.
- Cook, A.H., "The Determination of the External Gravity Field of the Earth from Observations of Artificial Satellites," Geophys. J.-R. Astr. Soc., vol.13, pp.297-312, 1967.
- Cushing, J.T., Applied Analytical Mathematics for Physical Sciences, John Wiley and Sons, Inc., New York, 1975.
- Ecker, E., "On the Spatial Convergence fo Spherical Harmonic Series," translation from German, DMAAC-TC-1849, St. Louis, MO, 1972.
- Gradshteyn, I.S. and I.M. Ryshik, Table of Integrals, Series, and Products, Academic Press, Inc., New York, 1980.
- Günter, N.M., Potential Theory and its Applications to Basic Problems of Mathematical Physics, Frederick Ungar Publishing Co., Inc., New York, 1967.
- Hajela, D.P., "Equal Area Blocks for the Representation of the Global Mean Gravity Anomaly Field," report no.224, Department of Geodetic Science and Surveying, The Ohio State University, 1975.
- Hajela, D.P., "Improved Procedures for the Recovery of 5 Mean Gravity Anomalies from ATS-6/GEOS-3 Satellite to Satellite Range-Rate Observations Using Least Squares Collocation," report no.276, Department of Geodetic Science and Surveying, The Ohio State University, 1978.
- Heiskanen, W.A. adn H. Moritz, Physical Geodesy, W.H. Freeman and Co., San Francisco, 1967.
- Hobson, E.W., The Theory of Spherical and Ellipsoidal Harmonics, Chelsea Publishing Company, New York, 1965.
- Hotine, M., Mathematical Geodesy, ESSA Monograph No. 2, U.S. Department of Commerce, Washington, D.C., 1969.
- Jekeli, C., "Alternative Methods to Smooth the Earth's Gravity Field," report of Department of Geodetic Science and Surveying, The Ohio State University, in press, 1981.

- Jung, K., "Figur der Erde," in Handbuch der Physik, edited by S. Flügge, vol.47, pp.534-639, 1956.
- Kellogg, O.D., Foundations of Potential Theory, reprint by Dover Publications, Inc., New York, 1953.
- Kholshevnikov, C., "On Convergence of an Asymmetrical Body Potential Expansion in Spherical Harmonics," Celestial Mechanics, vol.16, pp.45-60, 1977.
- Krarup, T., "A Contribution to the Mathematical Foundation of Physical Geodesy," Publ. no. 44, Danish Geodetic Institute, Copenhagen, 1969.
- Lembeck, K., "Methods and Geophysical Applications of Satellite Geodesy," Rep. Prog. Phys., vol.42, pp.547-628, 1979.
- Lerch, F.J., C.A. Wagner, S.M. Klosko, R.P. Belott, R.E. Laubscher, and W.A. Taylor, "Gravity Model Improvement Using GEOS-3 Altimetry (GEM 10A and 10B)," paper presented at the Annual Spring Meeting, American Geophysical Union, Miami, Florida, 1978.
- Levallois, J.J., "General Remarks on the Convergence of the expansion of the Earth Potential in Spherical Harmonics," translation from French, DMAAC-TC-1915, St. Louis, MO, 1973.
- Molodenskii, M.S., V.F. Ereneeov, and M.I. Yurkina, Methods for the Study of the External Gravitational Field and Figure of the Earth, translated from Russian, Israel Program for Scientific Translations, Jerusalem, 1962.
- Moritz, H., "Methods for Downward Continuation of Gravity," report no.67, Department of Geodetic Science and Surveying, The Ohio State University, 1966a.
- Moritz, H., "Linear Solutions of the Geodetic Boundary Value Problem," report no.79, Department of Geodetic Science and Surveying, The Ohio State University, 1966b.
- Moritz, H., "Precise Gravimetric Geodesy," report no.219, Department of Geodetic Science and Surveying, The Ohio State University, 1974.
- Moritz, H., "On the Convergence of the Spherical Harmonic Expansion for the geopotential at the Earth's Surface," Bolletino di Geodesia e Scienze Affini, no.2-3, pp.363-381, 1978.

- Moritz, H., Advanced Physical Geodesy, Abacus Press, Kent, 1980.
- Morrison, F., "Validity of the Expansion of the Potential Near the Surface of the Earth," proceedings of the Fourth Symposium of Mathematical Geodesy, Trieste, May 28-30, pp.95-106, 1969.
- Needham, J., "The Formation and Evaluation of Detailed Geopotential Models Based on Point Masses," report no.149, Department of Geodetic Science and Surveying, The Ohio State University, 1970.
- Neumann, J., "Entwicklung der im Elliptischen Coordinaten Ausgedrückten Reciproken Entfernung Zweier Punkte in Reihen,....," Journal für die Reine und Angewandte Mathematik, by A.L. Grelle, vol.37, pp.21-50, 1848.
- NRC, "Applications of a Dedicated Gravitational Satellite Mission," National Academy of Sciences, Washington, D.C., 1979.
- Paul, M.K., "Recurrence Relations for Integrals of Associated Legendre Functions," Bulletin Geodesique, vol.52, pp.177-190, 1978.
- Pellinen, L.P., "A Method for Expanding the Gravity Potential of the Earth in Spherical Harmonics," translated from Russian, ACIC-TC-1282, NTIS: AD-661819, Moscow, 1966.
- Petrovskaya, M.S., "Upward and Downward Continuations in the Geopotential Determination," Bulletin Geodesique, vol.53, pp.259-271, 1979.
- Rapp, R.H., "A Global 1°x1° Anomaly Field Combining Satellite, GEOS-3 Altimeter and Terrestrial Anomaly Data," report no.278, Department of Geodetic Science and Surveying, The Ohio State University, 1978.
- Rapp, R.H., "Potential Coefficient and Anomaly Degree Variance Modelling Revisited," report no.293, Department of Geodetic Science and Surveying, The Ohio State University, 1979.
- Reed, G.B., "Applications to Kinematical Geodesy for Determining the Short Wave Length Components of the Gravity Field by Satellite Gradiometry," report no.201, Department of Geodetic Science and Surveying, The Ohio State University, 1973.

- Rummel, R., "Determination of Short-Wavelength Components of the Gravity Field by Satellite to Satellite Tracking or Satellite Gradiometry, - An Attempt to an Identification of Problem Areas," Manuscripta Geodaetica, vol.4, pp.107-148, 1979.
- Rummel, R., "Geoid Heights, Geoid Height Differences, and Mean Gravity Anomalies from "Low-Low Satellite to Satellite Tracking - An Error Analysis," report no.306, Department of Geodetic Science and Surveying, The Ohio State University, 1980.
- Rummel, R., K.-P. Schwarz, and M. Gerstl, "Least Squares Collocation and Regularization," Bulletin Geodesique, vol.53, pp.343-361, 1979.
- Savrov, L.A., "Gravity Anomaly Expansion in Ellipsoidal Lamé Functions," English translation, DMAAC-TC-2008, St. Louis, MO, 1974.
- Schwarz, K.-P., "Investigations on the Downward Continuation of Aerial Gravity Data," report no.204, Department of Geodetic Science and Surveying, The Ohio State U., 1973.
- Shebalin, J.V., "The Determination of Surface Harmonic Expansion Coefficients from Mean Gravity Anomalies by Orthogonal Collocation," Journal of Geophysical Research, vol.85, no.B4, pp.1809-1813, April 10, 1980.
- Sjöberg, L., "On the Errors of Spherical Harmonic Developments of Gravity at the Surface of the Earth," report no.257, Department of Geodetic Science and Surveying, The Ohio State University, 1977.
- Sjöberg, L., "On the Convergence Problem for the Spherical Harmonic Expansion of the Geopotential at the Surface of the Earth," Bollettino di Geodesia e Scienze Affini, vol.39, no.3, pp.261-270, 1980.
- Thikonov, A.N. and V.Y. Arsenin, Solutions of Ill-Posed Problems, V.H. Winston and Sons, Washington, D.C., 1977.
- Tscherning, C.C. and R.H. Rapp, "Closed Covariance Expressions for Gravity Anomalies, Geoid Undulations, and Deflections of the Vertical Implied by Anomaly Degree Variance Models," report no.208, Department of Geodetic Science and Surveying, The Ohio State University, 1974.

Walsh, J.L., "The Approximation of Harmonic Functions by Harmonic Polynomials and by Harmonic Rational Functions," Bull. Amer. Math. Soc., vol.35, pp.499-544, 1929.

Walter, H.G., "Association of Spherical and Ellipsoidal Gravity Coefficients of the Earth's Potential," Celestial Mechanics, vol.2, pp.389-397, 1970.

Wermer, J., Potential Theory, Lecture Notes in Mathematics, no.408, Springer Verlag, Berlin, 1974.

APPENDIXES

A. Convergence and Divergence Conjectures

The "proof of convergence" by Arnold (1978) can be outlined as follows. It is well known that any reasonably well behaved function (not necessarily continuous) on a surface is expandable as a series of surface spherical harmonic functions. Instead, however, one may ask whether the set of solid spherical harmonics

$$Z_{nm} = \frac{1}{r^{n+1}} \bar{Y}_{nm}(\theta, \lambda) \quad (A.1)$$

considered as surface functions of two variables θ, λ (i.e. $r=r(\theta, \lambda)$) is also a complete set for functions defined on the surface. In this case, the series for the surface potential

$$V(\theta, \lambda) = \sum_{n=0}^{\infty} \sum_{m=-n}^n \frac{v_{nm}}{r^{n+1}} \bar{Y}_{nm}(\theta, \lambda) \quad (A.2)$$

would be a uniformly convergent series everywhere on the surface. Consider now the monotonically decreasing sequence r^{n+1}/r'^{n+1} , $r' > r$, which is, moreover, bounded. Hence Abel's convergence criterion can be applied to claim the convergence of

$$V(r', \theta, \lambda) = \sum_{n=0}^{\infty} \sum_{m=-n}^n \frac{v_{nm}}{r'^{n+1}} \bar{Y}_{nm}(\theta, \lambda) \quad (A.3)$$

for every $r' > r$. Since the function $V(r', \theta, \lambda)$ thus defined is harmonic and satisfies the boundary values, by the uniqueness of the boundary-value problem, V must be earth's potential. Furthermore, by the uniqueness of the

spherical harmonic expansion of the potential, the above series coincides with the series that would be determined on the bounding sphere. Thus, to prove convergence of the spherical harmonic series everywhere on and above the earth's surface, indeed everywhere above the Bjerhammar sphere, it is enough to prove the completeness of the functions (A.1). Arnold failed here as his "proofs" of completeness rely on the assumed truth of the conjecture. In a more recent paper (Arnold, 1980), the completeness of the functions (A.1) is supposed to be proved by showing that there exists no function ρ such that

$$\iint_{\sigma} \rho^2 d\sigma > 0 \quad (\text{A.4})$$

and such that

$$\iint_{\sigma} \rho Z_{nm} d\sigma = 0, \quad \text{all } n, m \quad (\text{A.5})$$

But this is a necessary and sufficient condition for completeness of orthogonal functions: the Z_{nm} are clearly not orthogonal and the proof fails again.

A "proof of divergence" of the potential series at the earth's surface was presented by Morrison (1970) under the assumption that the zonal coefficients do not decay, in magnitude, faster than some fixed negative power of the degree n . However, the "proof" also relies on the erroneous statement that the spherical harmonic series diverges if its subseries of zonals diverges (the latter was shown for the assumed coefficient decay). The fallacy of this argument is easily demonstrated by the example of the alternating series

$$\sum_{n=1}^{\infty} \frac{(-1)^{n+1}}{n} \quad (\text{A.6})$$

which converges (to the value $\ln 2$), but the subseries of even terms only, or odd terms only, by itself diverges.

B. Series Expansions for the Serrated Ellipsoid

For points P below the bounding sphere, the serrated, homogeneous ellipsoid is decomposed into regions for which $r_p > r_{si}$ and $r_p < r_{si}$. Substituting the series (2.7) and (2.8) into (2.24), the potential is then expressible as a convergent series:

$$V_p = \kappa \chi r_p \sum_{n=0}^{\infty} \sum_{i=0}^{2N-1} \int_0^{2\pi} \int_{\theta_i}^{\theta_{i+1}} \int_0^{\bar{r}_i} \left(\frac{r}{r_p}\right)^{n+2} dr + \int_{\bar{r}_i}^{r_{si}} \left(\frac{r_p}{r}\right)^{n-1} dr \big] P_n(\cos \psi) d\sigma \quad (\text{B.1})$$

where $\bar{r}_i = \min(r_p, r_{si})$; if $r_p > r_{si}$, then the second integral with respect to r vanishes. Equation (B.1) readily converts to

$$V_p = 2\kappa \chi r_p \sum_{\substack{n=0 \\ n \text{ even}}}^{\infty} \left[\sum_{i=0}^j \int_0^{2\pi} \int_{\theta_i}^{\theta_{i+1}} \int_0^{r_{si}} \left(\frac{r}{r_p}\right)^{n+2} dr P_n(\cos \psi) d\sigma + \sum_{i=j+1}^{N-1} \int_0^{2\pi} \int_{\theta_i}^{\theta_{i+1}} \left[\int_0^{r_p} \left(\frac{r}{r_p}\right)^{n+2} dr + \int_{r_p}^{r_{si}} \left(\frac{r_p}{r}\right)^{n-1} dr \right] \cdot P_n(\cos \psi) d\sigma \right] \quad (\text{B.2})$$

where the equatorial symmetry has been invoked (only even zonals appear in the series) and $r_{si} < r_p < r_{si+1}$; if $r_p > r_{si}$ for all i , then $j=N-1$. Performing the integrations with respect to r and using

$$\int_0^{2\pi} \int_{\theta_i}^{\theta_{i+1}} P_n(\cos \psi) d\sigma = \frac{1}{2n+1} \sum_{m=-n}^n \int_0^{2\pi} \int_{\theta_i}^{\theta_{i+1}} \bar{Y}_{nm}(\theta, \lambda) d\sigma \cdot \bar{Y}_{nm}(\theta_p, \lambda_p) \quad (\text{B.3})$$

$$= 2\pi P_n(\cos \theta_p) \int_{\theta_i}^{\theta_{i+1}} P_n(\cos \theta) \sin \theta d\theta$$

we obtain

$$\begin{aligned}
 V_p = & 4\pi\kappa\chi r_p^2 \sum_{\substack{n=0 \\ n \text{ even}}}^{\infty} \frac{1}{n+3} \frac{1}{2n+1} \left[\sum_{i=0}^j \left(\frac{r_{si}}{r_p} \right)^{n+3} \mathcal{Q}_{ni} \right] P_n(\cos\theta_p) + \\
 & + 4\pi\kappa\chi r_p^2 \sum_{\substack{n=0 \\ n \neq 2 \\ n \text{ even}}}^{\infty} \frac{1}{2n+1} \left[\sum_{i=j+1}^{N-1} \left(\frac{2n+1}{(n+3)(n-2)} - \frac{1}{n-2} \left(\frac{r_p}{r_{si}} \right)^{n-2} \right) \mathcal{Q}_{ni} \right] \\
 & P_n(\cos\theta_p) + \quad (B.4)
 \end{aligned}$$

$$+ 4\pi\kappa\chi r_p^2 \frac{1}{5} \sum_{i=j+1}^{N-1} \left(\frac{1}{5} + \ln \frac{r_{si}}{r_p} \right) \mathcal{Q}_{2i} P_2(\cos\theta_p)$$

where (using equation (2.59) of (Hobson, 1965, p.33))

$$\begin{aligned}
 \mathcal{Q}_{ni} &= (2n+1) \int_{\theta_i}^{\theta_i+1} P_n(\cos\theta) \sin\theta d\theta \\
 &= \begin{cases} P_{n+1}(\cos\theta_i) - P_{n-1}(\cos\theta_i) - P_{n+1}(\cos\theta_{i+1}) + & (B.5) \\ \quad + P_{n-1}(\cos\theta_{i+1}), & n \geq 1 \\ P_1(\cos\theta_i) - P_1(\cos\theta_{i+1}), & n = 0 \end{cases}
 \end{aligned}$$

As reference potential, we may use the zero and second degree terms:

$$U_p = \sum_{n=0,2} 4\pi\kappa\chi r_p^2 \frac{1}{n+3} \frac{1}{2n+1} \left(\sum_{i=0}^{N-1} \left(\frac{r_{si}}{r_p} \right)^{n+3} \mathcal{Q}_{ni} \right) P_n(\cos\theta_p) \quad (B.6)$$

Then the disturbing potential becomes for points P outside the bounding sphere:

$$\begin{aligned}
 T_p &= V_p - U_p \\
 &= 4\pi\kappa\chi r_p^2 \sum_{\substack{n=4 \\ n \text{ even}}}^{\infty} \frac{1}{n+3} \frac{1}{2n+1} \left(\sum_{i=0}^{N-1} \left(\frac{r_{si}}{r_p} \right)^{n+3} \mathcal{Q}_{ni} \right) P_n(\cos\theta_p) \quad (B.7)
 \end{aligned}$$

and for points P below the bounding sphere:

$$\begin{aligned}
 T_p = & 4\pi\kappa\chi r_p^2 \left(\sum_{\substack{n=4 \\ n \text{ even}}}^{\infty} \frac{1}{n+3} \frac{1}{2n+1} \left(\sum_{i=0}^j \left(\frac{r_{si}}{r_p} \right)^{n+3} \rho_{ni} \right) P_n(\cos\theta_p) + \right. \\
 & + \sum_{\substack{n=0 \\ n \neq 2 \\ n \text{ even}}}^{\infty} \frac{1}{2n+1} \left[\sum_{i=j+1}^{N-1} \left(\frac{2n+1}{(n+3)(n-2)} - \frac{1}{n-2} \left(\frac{r_p}{r_{si}} \right)^{n-2} \right) \rho_{ni} \right] \cdot \\
 & \cdot P_n(\cos\theta_p) + \\
 & - \sum_{i=j+1}^{N-1} \left(\frac{r_{si}}{r_p} \right)^3 \rho_{0i} + \frac{1}{5} \sum_{i=j+1}^{N-1} \left[\frac{1}{5} + \ln \frac{r_{si}}{r_p} - \frac{1}{5} \left(\frac{r_{si}}{r_p} \right)^5 \right] \cdot \\
 & \cdot \rho_{1i} P_2(\cos\theta_p) \Big) \quad (B.8)
 \end{aligned}$$

Using the definition of the gravity anomaly (2.42), the corresponding series are readily found to be

$$\begin{aligned}
 \Delta g_p = & 4\pi\kappa\chi r_p \sum_{\substack{n=4 \\ n \text{ even}}}^{\infty} \frac{n-1}{(n+3)(2n+1)} \left[\sum_{i=0}^{N-1} \left(\frac{r_{si}}{r_p} \right)^{n+3} \rho_{ni} \right] \cdot \\
 & \cdot P_n(\cos\theta_p), \quad r_p > R \quad (B.9)
 \end{aligned}$$

and for $r_p < R$

$$\begin{aligned}
 \Delta g_p = & 4\pi\kappa\chi r_p \left(\sum_{\substack{n=4 \\ n \text{ even}}}^{\infty} \frac{n-1}{(n+3)(2n+1)} \left[\sum_{i=0}^j \left(\frac{r_{si}}{r_p} \right)^{n+3} \rho_{ni} \right] P_n(\cos\theta_p) + \right. \\
 & + \sum_{\substack{n=0 \\ n \neq 2 \\ n \text{ even}}}^{\infty} \frac{1}{2n+1} \left[\sum_{i=j+1}^{N-1} \left(\frac{n+2}{n-2} \left(\frac{r_p}{r_{si}} \right)^{n-2} - \frac{4(2n+1)}{(n+3)(n-2)} \right) \rho_{ni} \right] \cdot \\
 & \cdot P_n(\cos\theta_p) + \\
 & + \frac{1}{3} \sum_{i=j+1}^{N-1} \left(\frac{r_{si}}{r_p} \right)^3 \rho_{0i} + \frac{1}{5} \sum_{i=j+1}^{N-1} \left[\frac{1}{5} - 4 \ln \frac{r_{si}}{r_p} - \frac{1}{5} \left(\frac{r_{si}}{r_p} \right)^5 \right] \cdot \\
 & \cdot \rho_{1i} P_2(\cos\theta_p) \Big) \quad (B.10)
 \end{aligned}$$